Extracellular polymeric substances involved in adhesion and biofilm formation by *Sulfobacillus thermosulfidooxidans*

Dissertation

zur Erlangung des akademischen Grades eines

Doktors der Naturwissenschaften

– Dr. rer. nat. –

vorgelegt von

Qian Li

geboren in Hunan, China

Biofilm Centre, Fakultät für Chemie

der

Universität Duisburg-Essen

2017

Die vorliegende Arbeit wurde im Zeitraum von Januar 2013 bis April 2017 im Arbeitskreis von Prof. Dr. Wolfgang Sand im Biofilm Centre der Fakultät für Chemie an der Universität Duisburg-Essen durchgeführt.

Tag der Disputation: 06.10.2017

Gutachter:	Prof. Dr. Wolfgang Sand
	Prof. Dr. Bettina Siebers
Vorsitzender:	Prof. Dr. André H. Gröschel

The results obtained during the promotion are partly in the following original publications published or in press:

Q. Li, W. Sand, R. Zhang; Enhancement of Biofilm Formation on Pyrite by *Sulfobacillus thermosulfidooxidans*; Minerals; 2016, 6(3), 71-71.

Q. Li, W. Sand; Mechanical and chemical studies on EPS from *Sulfobacillus thermosulfidooxidans*: from planktonic to biofilm cells; Colloids and Surfaces B: Biointerfaces, 2017, 153, 34-40.

Q. Li, W. Sand; Quantification of cell-substratum interactions by atomic force microscopy; Colloids and Surfaces B: Biointerfaces, 2017.

Contents

List of Abbreviations

AFM	Atomic force microscopy
AHLs	N-acyl homoserine lactones
AMD	Acid mine drainage
ATR-FTIR	Attenuated Total Reflection-Fourier Transmission Infra-Red spectroscopy
CLSM	Confocal laser scanning microscopy
DSMZ	Deutsche Stammsammlung von Mikroorganismen und Zellkulturen
EFM	Epifluorescence microscopy
EPS	Extracellular polymeric substances
MAC	Mackintosh basal salt medium
MS	Metal sulfides
PEI	Polyethyleneimine
PLL	Poly-L-lysine
QS	Quorum sensing
SEM/EDS	Scanning electron microscopy/energy dispersive X-ray spectroscopy

Abstract

Bioleaching is the mobilization of metal cations from insoluble ores by microorganisms. Bacteria first attach to minerals and then form biofilms, which can initiate and enhance bioleaching. Extracellular polymeric substances (EPS) play a crucial role during the whole process. Bacterial adhesion and biofilm formation are key steps to prevent environmental problems called acid mine drainage or to improve leaching efficiency in industry. Thus, profound investigations of EPS involved in bacterial adhesion and biofilm formation are crucial in order to guide the leaching process in one or the other direction.

The Gram-positive bacterium *Sulfobacillus thermosulfidooxidans* DSM 9293^{T} was chosen as the research object. The bacterium cannot form biofilms on pyrite. However, regularly exchanging exhausted medium with fresh medium leads to a continuous biofilm development on pyrite by *S. thermosulfidooxidans*. By this way multiply layered biofilms were observed on pyrite slices, while only monolayered biofilms were visible on pyrite grains. Meanwhile biofilm formation by *S. thermosulfidooxidans* on pyrite could also be observed just in the presence of *Leptospirillum ferriphilum*. Other strategies tested in this study to enhance biofilm formation, like adjusting the initial pH, supplementing an extra energy source or additional doses of ferric ions show no positive effect.

Under biofilm favouring conditions the attachment and biofilm formation

by *S. thermosulfidooxidans* were followed during pyrite leaching. The results indicate that a slimy and soft EPS matrix heterogeneously accumulated on the mineral surface inducing further bacterial adhesion and forming a robust biofilm. After attaching to the pyrite surface the cells started to change the composition of their EPS. Huge amounts of humic substances were detected in the biofilm EPS.

A new technique based on an atomic force microscope (AFM) equipped with a pyrite-/chalcopyrite-modified cantilever instead of the use of silicon nitrides types was prove to be useful for quantifying the real interaction forces between planktonic cells or biofilms and the substrata. The force measurements were achieved under the natural living conditions of the bacteria without any artefact resulting from the use of denaturing chemicals such as glutaraldehyde which is often applied to study the adhesion of *S. thermosulfidooxidans*. The results illustrate that planktonic cells of both pyrite- and sulfur-grown species of *S. thermosulfidooxidans* show more affinity to pyrite than to chalcopyrite (2 nN versus 0.13 nN). However, biofilm cells show low affinity to either pyrite or chalcopyrite. The EPS collected from planktonic cells of *S. thermosulfidooxidans* exhibit a high content of proteins, while the EPS of biofilm cells show a low content of proteins indicating that these polymers play an important role in adhesion.

1. Introduction

1.1 Bioleaching

1.1.1 Definition and mechanism of bioleaching

Bioleaching is defined as the mobilization of metal ions from insoluble metal sulphides, such as pyrite (FeS_2), arsenopyrite (FeAsS), chalcopyrite ($CuFeS_2$) and marcasite (FeS_2), by biological oxidation and complexation [1]. Since the time when the first leaching bacterium was isolated and identified [2, 3], several hypotheses about mineral oxidization mechanisms were proposed and discussed finally leading to a direct and an indirect mechanism [4]. The direct mechanism suggests microorganisms that dissolve minerals by means of intimate cell contact via enzymes and oxygen, while the indirect mechanism assumes the mineral dissolution to be achieved by the action of ferric ions and that microorganisms are only responsible for the regeneration of the strong oxidant from dissolved ferrous ions. The indirect mechanism does not require microbial attachment. This long-standing debate was finally ended by Sand et. al [5], in which the direct mechanism is proved to be inexistent. The paper demonstrates two different indirect oxidation mechanisms together with a special focus on the pivotal role of extracellular polymeric substances (EPS). This work is the origin of the nowadays well accepted mechanism that bioleaching is performed by microorganisms via the thiosulfate or the polysulfide pathway in a contact or a non-contact mode [6].

Metal sulfides can be classified into acid soluble and acid insoluble according to their solubility in acid. The representative acid insoluble metal sulfides are molybdenite, tungstenite and pyrite, whereas sphalerite, chalcopyrite and galena belong to the acid soluble metal sulfides. In the case of acid insoluble metal sulfides, the valence bands of metal and sulfur atoms are only derived from orbitals of metal atoms and they do not contribute to the bonding between the metal and the sulfur moiety of the mineral. Thus, only oxidizing reagents like ferric ion can attack and break this bonding. While in the case of acid soluble metal sulfides, the valence bands are derived from both orbitals of metal and sulfur atoms. Except for oxidizing reagents like ferric ions, protons can also remove electrons from the valence band and, therefore, cause a break of the bonds between the metal and the sulfur moiety of the metal sulfide.

The thiosulfate mechanism is valid for acid insoluble metal sulfides. This mechanism is exclusively based on the oxidative attack of ferric ions and the main sulfur intermediate is thiosulfate. The following simplified equation describes how bioleaching performs in this mechanism:

$$MS + 6\ Fe^{3+} + 3\ H_2O \rightarrow S_2O_3^{2-} + 7\ M^{2+} + 6\ H^{+} \quad (1)$$

Thiosulfate is unstable in acidic ferric ions containing solution. Within seconds it is attacked by ferric ions and degrades into tetrathionate:

$$2S_2O_3^{2-} + 2\ Fe^{3+} \rightarrow 2\ Fe^{2+} + S_4O_6^{2-} \quad (2)$$

Tetrathionate hydrolyses to disulfane-monosulfonic acid and sulfate:

$$S_4O_6^{2-} + H_2O \rightarrow HSSSO_3^- + SO_4^{2-} + H^+ \quad (3)$$

Based on this highly reactive compound several reactions occur under formation of elemental sulfur, thiosulfate, trithionate or pentathionate:

$$S_3O_3^{2-} + S_2O_3^{2-} + 0.5\ O_2 + 2\ H^+ \rightarrow S_5O_6^{2-} + H_2O \quad (4)$$

$$S_3O_3^{2-} + S_4O_6^{2-} \rightarrow S_2O_3^{2-} + S_5O_6^{2-} \quad (5)$$

$$S_3O_3^{2-} + 1.5\ O_2 \rightarrow S_3O_6^{2-} \quad (6)$$

$$4\ S_3O_3^{2-} \rightarrow S_8 + 4\ SO_3^{2-} \quad (7)$$

The polysulfide mechanism applies to acid soluble metal sulfides and the dissolution is started by proton attack and a consecutive oxidation of H_2S by ferric ions:

$$MS + 2\ H^+ \rightarrow M^{2+} + H_2S \quad (8)$$

$$H_2S + Fe^{3+} \rightarrow H_2S^{*+} + Fe^{2+} \quad (9)$$

The radical H_2S^{*+} may also be formed by an attack of ferric ions on the metal sulfides without intermediary occurring H_2S:

$$MS + Fe^{3+} + 2\ H^+ \rightarrow M^{2+} + H_2S^{*+} + Fe^{2+} \quad (10)$$

By dissociation of the strong acid H_2S^{*+}, the radical HS^* occurs:

$$H_2S^{*+} + H_2O \rightarrow H_3O^+ + HS^* \quad (11)$$

Two HS^* radicals react to a disulfide:

$$2\ HS^* \rightarrow H_2S_2 \quad (12)$$

The disulfide is oxidized by ferric ions or HS^* radicals:

$$H_2S_2 + Fe^{3+} \rightarrow H_2S_2^{*+} + Fe^{2+} \quad (13)$$

$$H_2S_2 + HS^* \rightarrow HS_2^* + H_2S \quad (14)$$

Then tetrasulfide or trisulfide were formed by dimerization of two HS^{2*} or by the reaction of HS_2^* with HS^* radicals, respectively. Chain elongation of the polysulfides proceed by analogous reactions. Under acidic conditions, polysulfides decompose to elemental sulfur mainly in the form of S_8 rings:

$$H_2S_9 \rightarrow H_2S + S_8 \quad (15)$$

For both mechanisms, the role of microorganisms is to oxidize the produced ferrous ions or/and the inorganic sulfur compounds. The reactions are as follows:

$$14\ Fe^{2+} + 3.5\ O_2 + 14\ H^+ \rightarrow 14\ Fe^{3+} + 7\ H_2O \quad (16)$$

$$S_2O_3^{2-} + 2\ O_2 + H_2O \rightarrow 2\ SO_4^{2-} + 2\ H^+ \quad (17)$$

$$0.125\ S_8 + 1.5\ O_2 + H_2O \rightarrow SO_4^{2-} + 2\ H^+ \quad (18)$$

The regenerated ferric ions enter the reaction cycle again. Sulfuric acid, oxidized from inorganic sulfur compounds, keeps the iron ions in the ferric state. Fig. 1 summarizes the reaction pathways of the thiosulfate or the polysulfide leaching mechanism. Most of the microorganisms attach to surfaces and live in biofilms besides some planktonic cells. The latter perform leaching in non-contact mode, while biofilm cells perform leaching in contact mode. After an initial stage of cell adhesion EPS are produced increasingly. Thus, contact leaching occurs in a micro-space between the EPS and mineral surface. The leaching rate may speed up

because of a high concentration of ferric ions complexed in the EPS [7]. Fig. 2 shows a simplified model of the contact leaching mechanism.

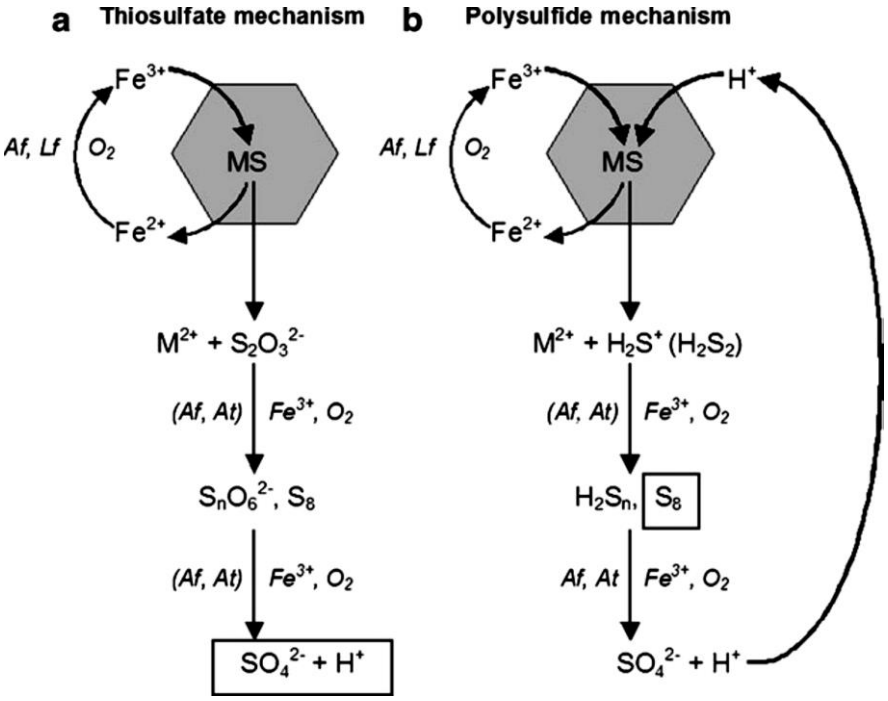

Fig. 1. Scheme of bioleaching mechanism. MS= metal sulfide, M^{2+}= metal cation, *Af*, *Acidithiobacillus ferrooxidans*; *Lf*, *Leptospirillum ferrooxidans*; *At*, *A. thiooxidans* (modified from Schippers and Sand, 1999 [8]).

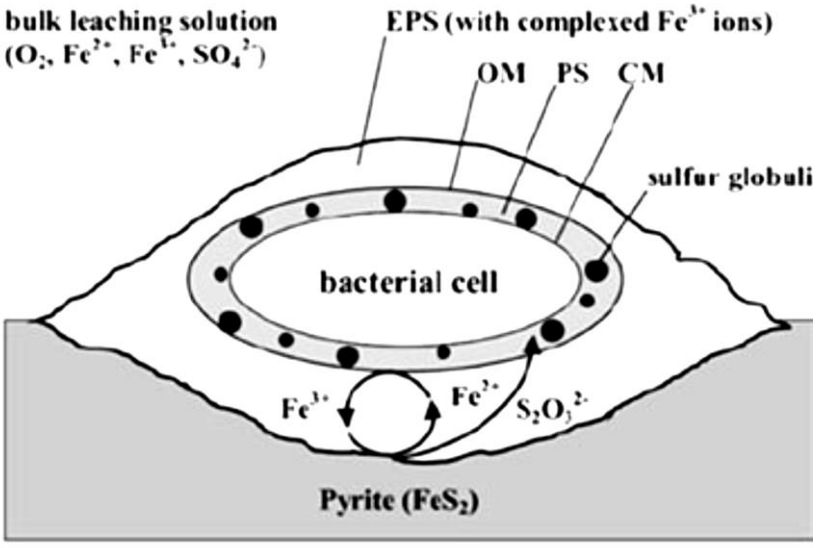

Fig. 2. Model of contact leaching of pyrite catalysed by a cell of *A. ferrooxidans* (modified from Sand et al., 1995 [9]). CM= cytoplasmic membrane, PS= periplasmic space, OM= outer membrane.

1.1.2 Associated microorganisms in bioleaching

Microbiological degradation of minerals began with the appearance of life on Earth as a product of the interacting evolution of biosphere, atmosphere, hydrosphere and lithosphere. Acid mine drainage (AMD), which is known as a serious natural environmental problem, is a result of bioleaching [10]. However, the proof of sulfuric acid and metal ions in AMD was considered as the result of chemical reactions till Colmer and Hinkle isolated two unidentified bacteria from AMD sites and suggested the important role of microorganisms in AMD in 1947 [2]. Starting from this discovery more and more bacteria or archaea were isolated and identified. These microorganisms have several physiological characteristics in common. They are chemolithoautotrophs and able to use ferrous iron and/or reduced inorganic sulfur as electron donors. They are acidophilic and thrive usually in a pH range of 1.5-2.0. They generally grow faster under aerobic conditions than under anaerobic conditions. They fix CO_2 and an extra small amount of carbon source like yeast extract is needed for less-efficient CO_2-fixing species [11]. Based on the temperature preferences the microorganisms can be divided into three groups: mesophiles (T_{opt} ca. 20-40^oC), moderate thermophiles (T_{opt} ca. 40-60^oC) and extreme thermophiles (T_{opt} >60^oC) [12]. The group of mesophiles are dominantly rod-shaped, Gram-negative eubacteria such as *A. ferrooxidans, A. thiooxidans* and *L. ferrooxidans*. Archaea and eubacteria (the majority are Gram-positive) comprise the group of moderate thermophiles. *Sulfobacillus*

thermosulfidooxidans, *A. caldus* and *L. ferriphilum* are some representative microorganisms. The group of extreme thermophiles exclusively consists of archaea such as *Sulfolobus metallicus*, *Acidianus brierleyi* and *Sulfolobus shibitae*.

In this study, the focus is placed on the genus *Sulfobacillus*, which was first reported by Golovacheva and Karavajko in 1978 [13]. Until now there are five species classified for this genus based on phylogenetic and physiological characteristics: *S. thermosulfidooxidans* [13], *S. acidophilus* [14], *S. thermotolerans* [15], *S. sibiricus* [16] and *S. benefaciens* [17]. A detailed comparison of phenotypic characteristics of *Sulfobacillus* species is listed in Table 1. Among them *S. thermosulfidooxidans* is the most studied species. For the present work strain DSM 9293^T of *S. thermosulfidooxidans* was selected. The genus *Sulfobacillus* is Gram-positive, generally non-motile, rod shaped, endospore-forming and a moderately thermophilic acidophile (T_{opt} ca. 38.5-55°C, T_{max} ca. 60 °C; pH_{opt} ca. 1.5-2.4). The bacteria exhibit a versatile metabolism and can grow autotrophically (e.g. on ferrous iron, reduced inorganic sulfur compounds such as tetrathionate, thiosulfate and elemental sulfur, as well as sulfide minerals), heterotrophically (e.g. on yeast extracts), or mixotrophically (e.g. on both ferrous iron or reduced sulfur and yeast extracts, both CO_2 and yeast extracts are used as carbon sources). Strains of *Sulfobacillus* were isolated from acidic environments associated with mineral deposits and

ores, mineral processing mills and acidic geothermal areas, so they are used for optimization of microbial communities in industrial bioleaching processes [18].

Table 1 Characteristics of strains of *Sulfobacillus* species.

Characteristic	1	2	3	4	5
Cell size (μm) (length x width)	0.8-1.2 x 1.5-4.5	0.6-0.8 x 1-3.0	0.5-0.8 x 3.0-5.0	0.7-1.1 x 1.0-3.0	2.5±0.5 x 0.6±0.05
Growth pH range (optimum)	1.2-2.4 (2.0)	1.5-5.5 (1.7-2.4)	(2.0)	1.1-2.6 (2.0)	0.8-2.2 (1.5)
Growth temperature (optimum)(^{o}C)	20-60 (40)	20-60 (50-55)	(45-50)	17-60 (55)	30-47 (38-39)
DNA G+C content (mol%)	48.2±0.5	47.2-47.5	56±1	48.2±0.2	50.6±0.2
Chemolithotrophic growth with: Fe^{2+}	+	+	+	+	+
S^{o}	+	+	+	+	+
Tetrathionate	+	+	ND	+	+
Sulfide minerals	+	+	+	+	+
Utilization of: Malate	+	ND	ND	ND	ND
Fructose	+	+	+	ND	+
Glucose	+	+	+	ND	+
Sucrose	+	+	+	ND	ND
Glutathione (reduced)	+	+	ND	ND	ND
Casein	ND	+	ND	ND	ND
Trehalose	ND	+	ND	ND	ND
Mannose	ND	+	ND	ND	+
Raffinose	ND	+	ND	ND	ND
Glutamate	ND	+	ND	ND	+
Ribose	ND	ND	+	ND	+
Galactose	ND	ND	ND	ND	+
Minimum generation time (h)	2.0(Fe^{2+}); 1.8 (S^{o})	2.5(Fe^{2+}); 6 (S^{o})	3.5(Fe^{2+}); 6.8(yeast extracts)	1.4(Fe^{2+});3.5(S^{o})	3.1(Fe^{2+})
Anaerobic growth with ferric iron as electron acceptor	ND	+	+	ND	+

+ growth, *ND* indicates not determined. Strains include: 1. *S. thermotolerans* Krl^{T} [15]; 2. *S. thermosulfidooxidans* DSM 9293^{T} [13]; 3. *S. acidophilus* NAL^{T} [14]; 4. *S. sibiricus* N1^{T} [16]; 5. *S. benefaciens* BRGM2^{T} [17]. All cells are rod shaped and spore forming and grow on yeast extracts.

1.2 EPS involved microbial adhesion and biofilm formation

Microorganisms are generally living in one of two life style: planktonic, freely swimming in bulk solution, or sessile, as a unit attached to a surface or within the confines of a biofilm. Ubiquitously in aquatic environments microorganisms attach to substrata and, subsequently, form biofilms. Biofilms are defined as aggregates of microorganisms embedded in a self-produced matrix of EPS which make the microorganisms adherent to each other and/or a surface. EPS are mainly composed of polysaccharides, proteins, nucleic acids and lipids [19]. Biofilms account for the phenomenal ecological success of the microorganisms. Firstly, EPS provide protection from environmental stress such as UV radiation, pH shifts, osmotic shock, hunger and desiccation [20]. Secondly, the highly permeable water channels within the biofilm allow the exchange of nutrients and metabolites with the environment, thereby enhancing nutrient availability and removal of metabolites [21]. Lastly, biofilms provide a possibility of gene transfer within or between populations by conjugation [22]. To form a biofilm the cells have to go through five stages [23]. The first stage addresses the initial attachment of cells to the surface. Physicochemical interactions and cell appendages such as flagella and pili play important roles in this stage [24-26]. Driven by chemotaxis flagella bring a bacterium in reach of a surface and pili aroused twitching allows the bacterium to move along the surface, because of hydrophobic

components and chemical functional groups in EPS physicochemical interactions, such as hydrogen bonding, hydrophobic and electrostatic forces, enable the bacterium to attach on the surface. After the initial adhesion, the cells will successively enter the next four stages: production of EPS resulting in more firmly adhered “irreversible” attachment, early development of biofilm architecture, maturation of biofilm architecture and dispersion of single cells from the biofilm (Fig. 3).

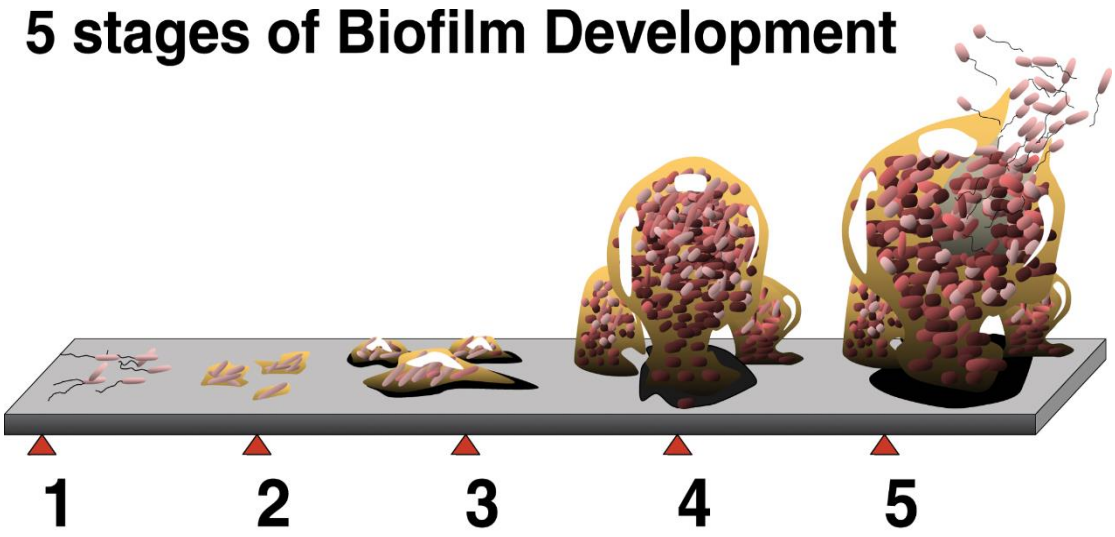

Fig. 3. Diagram showing the development of a biofilm as a five-stage process (modified from Monroe, 2007 [27]). Stage 1: initial attachment. Stage 2: irreversible attachment. Stage 3: early development of biofilm architecture. Stage 4: maturation of biofilm architecture. Stage 5: dispersion of single cells from the biofilm.

1.2.1 Attachment of acidophiles to surfaces

A simple way to investigate adhesion of acidophiles to a mineral surface is directly counting the cell number of planktonic cells and by this way to extrapolate to the number of adhered cells. Based on this method Ohmura et al. [28] found out that the adhesion of acidophiles is mineral-selective. In their study adhesion of *A. ferrooxidans* and *Escherichia coli* to four

minerals were followed and it was found that ferrous iron-grown *A. ferrooxidans* could recognize the reduced iron in minerals and selectively adhered to iron contained minerals. Ghauri et al. [29] checked sixteen strains of acidophilic bacteria for adherence to pyrite, glass beads or ferric hydroxysulfates. According to their results, the acidophiles attached more readily to pyrite than to the other substrata, and this kind of adherence differences were apparent between different species, even between different strains of the same species. Gehrke et al. [7] attributed this selective adhesion to the growth substrate which influences the chemical composition of EPS. In their work EPS composition of different energy-grown *A. ferrooxidans* as well as their attachment to different substrata were investigated. They pointed out that EPS was a prerequisite for an attachment and its composition decided microbial preference. Glucuronic acids in EPS could complex ferric ions, rendering the cell surface positively charged, and then the cells were attracted by negatively charged pyrite in salt solution at low pH. The glucuronic acids only largely existed in the EPS of ferrous iron-grown cells. For sulfur-grown cells more than half of their EPS were composed by lipids, then strong hydrophobic forces dominated the attachment to hydrophobic substrata such as sulfur. Thus, they concluded that sulfur-grown cells preferred to attach to hydrophobic surfaces, ferrous iron-grown cells adhered exclusively to negatively charged substrata and pyrite-grown cells accepted both substrata. Noël et

al. [30] found that such preferences could be revoked. Specifically, *L. ferriphilum*, as a precolonizer on pyrite, can help the sulfur oxidizer *A. caldus* attach to pyrite. The latter cannot attach to pyrite by its own. By monitoring the adhesion of *A. thiooxidans* to alive or dead biofilms of iron-oxidizer (*A. ferrooxidans* and *L. ferrooxidans*) pre-colonized pyrite, it was noticed that *A. thiooxidans* could only benefit from the living biofilms and cell-cell communication played a pivotal role in this context [31]. With the help of atomic force microscopy (AFM) the preference of bacteria to minerals can be quantified by measuring the adhesion force. The adhesion forces between acidophiles and metal sulfides are in the range of 0.6-1.1 nN [32-35]. It has been proven successfully that cells of *A. ferrooxidans*, *A. thiooxidans* or *L. ferrooxidans* show selective adhesion to chalcopyrite because the measured adhesion forces of the three strains to chalcopyrite were 0.8470, 0.8437 and 1.0426 nN, respectively [32].

1.2.2 Biofilms of acidophiles

Localization of attached acidophiles and their development on a mineral surface occurs not randomly but oriented. Steps and non-crystallographic features such as scratches, microcracks and grooves are the preferred sites. Cells attached to these high-energy sites were observed either in environment in situ [36] or in lab experiments [30, 37]. Edwards et. al [38] found that these sites were not always orienting cell attachment because attachment of *A. caldus* was not correlated with visible polished scratches.

They observed that the cell orientation coincided with etching pit edges and secondary sulfur minerals that developed during mineral degradation. This immediately suggests that acidophiles chemotactically select the optimal site for chemoautotrophic growth on the mineral surface. Further on, cell motility seems to be a prerequisite for this mode of cell adherence, as preferential attachment sites or cell orientation cannot be observed in case of non-motile microorganisms such as *S. thermosulfidooxidans* [39]. Acidophiles generally form monolayered biofilms on metal sulfides [36, 37]. This type of biofilm is favoured under bioleaching conditions, because most acidophiles are aerobic microorganisms. Formation of a monolayered biofilm is good for diffusion of oxygen to the cell surface. In addition it is more efficient for exchanging metabolic wastes and nutrition by monolayered biofilms. Biofilm formation processes are controlled by quorum sensing (QS) mechanisms and the identified QS molecules of the N-acylhomoserine lactone type (AHLs) can positively regulate biofilm formation by Gram-negative leaching bacteria such as *A. ferrooxidans* and *A. thiooxidans* on mineral surfaces [40-42]. The cell-cell communication may not only occur within communities of the same strain, it also exists between different species or genera and even between bacteria and archaea. Investigations of microbial communities in AMD show that the biofilms are not composed by single bacteria but composed by bacteria from different genus and archaea [43, 44].

1.2.3 Extracellular polymeric substances of acidophiles

EPS play a crucial role in the processes of adhesion to and biofilm formation on metal sulfides by acidophiles. EPS are mainly composed of polysaccharides, proteins, lipids and glucuronic acids, but the composition, as mentioned before, could be modified by growth substrata [7]. Solid substrata stimulate EPS secretion. Planktonic cells grown on solid substratum, in case of *A. ferrooxidans*, produce 5 to 13 times more EPS than the cells grown on soluble substratum. Sessile cells of *A. ferrooxidans* excrete 35 to 87 times more EPS than their planktonic cells [7, 37]. EPS is a prerequisite for microbial adhesion. It was reported that after EPS removal both the adhesion forces between acidophiles and metal sulfides and the number of attached cell were decreasing dramatically [32, 35]. The number of attached cells was reduced even by a factor of more than 3 [37]. EPS secretion increases as soon as the cells have attached on a surface. Zeng et al. [45] followed the biofilm formation by moderate thermophiles and found that after attaching on chalcopyrite the cells began to produce EPS and 10 days later the attached cells were fully covered by EPS. Meanwhile, the proportion of each EPS fraction changed during bioleaching. It is also found that under poor conditions such as phosphate limited growth conditions, EPS expression by *A. ferrooxidans* could be enhanced [46]. By applying fluorescently labelled lectins EPS can be visible even under in situ conditions [46]. Lectins are proteins or

glycoproteins capable of binding reversibly and specifically to carbohydrates without altering their structures. Because the glycoconjugates in EPS are different among acidophiles, lectins can even be used to distinguish the cells in a mixed biofilm [47].

1.3 Atomic force microscopy

The application of AFM to measure extremely small forces and to scan surface structures on the atomic scale was first introduced by Binnig in 1986 [48]. Unlike other techniques, AFM consists of a mechanical device and the cantilever is the most critical part. The cantilever is a plate spring with one end fixed on a holder and another end carrying a sharp tip. The tip is brought into contact with and moved across a sample surface. Movement and deflection of the cantilever during scanning are recorded and then converted into an electrical signal to produce an image. The deflection is recorded by focusing a laser beam on the free end of the cantilever and detecting the position of the reflected beam via a position sensitive photodiode. According to the deflection of the cantilever by applying Hooke's Law the interactions between the tip and the sample can be quantified. The sensitivity of the AFM is in the piconewton range (10^{-12} N). Thus, except force measurement AFM owns other unique advantages in term of imaging (Fig. 4). For instance, there are no special requirements for sample treatment and it can produce atomic resolution images of both conductors and non-conductors either in air or in aqueous solutions. There

are two modes, known as contact and intermittent contact mode, for imaging. In contact mode, the tip is moved into contact with a sample surface and they keep contacting during the whole scanning process. The sample height is adjusted to keep the deflection of the cantilever constant using a feedback loop. A topographic image is obtained by giving calibrated height information about the sample relief. At the same time a vertical deflection image, which reveals surface details of corrugated sample, is yielded by employing the error signal. In intermittent contact mode (tapping mode), the cantilever oscillates at a given frequency and the tip only touches the sample surface at the end of its downward movement. The reduction in oscillation amplitude here is the feedback control signal and it is used to measure the topography of the surface. Compared with the contact mode, the lateral forces produced in the intermittent mode during scanning are much more smaller. Therefore, the risk of measuring artefacts from surface damages is minimized.

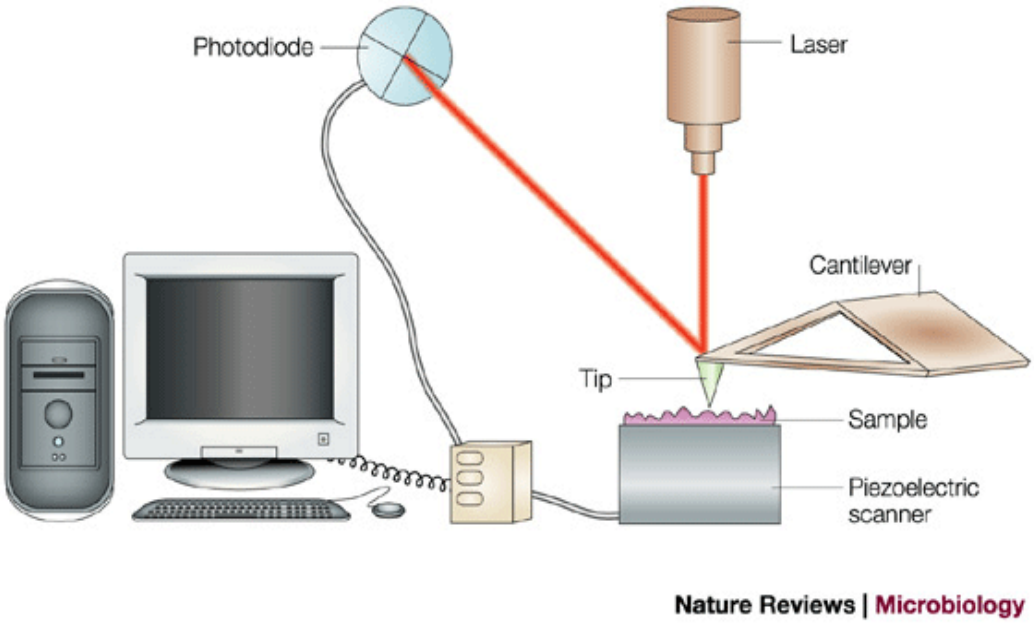

Fig. 4 Schematic diagram of a common setup of an AFM (from Dufrêne, 2004 [49]). The sample is mounted on a stage that can move in the x, y and z directions by using a piezoelectric scanner. The deflection of the cantilever in response to interactions at the tip is detected by an optical lever, in which the movements of a laser reflected off the cantilever are detected by a split-segment photodiode. The deflection data are passed to a computer controller that provides appropriate feedback to the stage and collects data. The essential elements of an AFM are: a probe (tip) attached to a spring (cantilever); a means of measuring deflections of the spring (optical lever and split-segment photodiode); a sample; and a means for moving the sample and tip relative to each other (piezoelectric scanner). Deflections of the cantilever are then used to measure interactions between the tip and the sample.

1.3.1 AFM for imaging

Shortly after the invention of AFM this technique started to be applied for imaging various biological samples, including biological molecules such as proteins, cells and biofilms, in their native environment or under defined laboratory conditions [50-53]. Because there is no strict requirement for sample preparation, the sample can be scanned in its native state and lots of research was done contributing to many biologic discoveries. Due to the

high sensitivity AFM provides precise data on the surface ultrastructure of biological samples. The AFM images clearly show that the surface of dormant spores of *Phanerochaete chrysosporium* is uniformly covered with rodlets, while its germinating spores have a very smooth surface partially covered with rough granular structures [54]. By changing the pH of the buffer solution, Müller et al. [51] found that the height of the purple membranes is pH dependent, since the height decreased from 5.6 nm to 5.1 nm, if the pH was adjusted from 10.5 to 4. AFM is an excellent tool for monitoring function related conformational changes. The extracellular porin surface of *E. coli* was shown to be existing in two conformations, which explained the two open-channel configurations of *E. coli* porins [52]. AFM is also used for recording dynamic changes on the surfaces of living single cells. Ahimou et al. [55] monitored enzyme digestion of the cell wall of *Saccharomyces cerevisiae* within 60 min. The results showed that protease caused a progressive increase of surface roughness and large depressions surrounded by protruding edges were formed. Yamashita et al. [56] visualised that the outer membrane of a magnetotactic spirillum was covered with a net-like structure comprising holes and the holes in the net-like structure slowly diffused in the cell surface. Except recording dynamic changes on bacterial surfaces, AFM also captured the cell growth and the formation of the septum of *E. coli* in nutrient medium [57]. AFM is a useful tool for investigating topographic and morphological features of biofilms

on opaque materials. One of the earliest AFM application to image biofilms was performed by Bremer et al. [58]. Their AFM images revealed that the biofilms were heterogeneous both in depth and in distribution, meanwhile they were associated with corrosion pits on the copper surface. After removal of the biofilms, the corrosion pit could be measured [39].

1.3.2 AFM for quantifying adhesion

AFM is a powerful technique to detect and measure adhesion events between the AFM tip and a surface or two sample surfaces. In the latter case one sample needs to be immobilized on the AFM tip. The force is collected from a force curve which records the AFM cantilever deflections when the cantilever is approaching to and retracting from the sample surface. The deflection of the cantilever can be converted into force by using Hooke's law: $F = kd$, where k is the cantilever spring constant and d is the cantilever deflection. The cantilever spring constant needs to be determined before and after force measurement, because it may differ from the one given by the manufacturer.

A complete force curve comprises an approach curve and a retraction curve. Upon the force curve every interaction happening between the two surfaces can be detected and one can also check the reacting distance. When the cantilever is far apart from the surface, the force experienced by the cantilever is zero. As the cantilever approaches the surface, the cantilever bends upwards owing to repulsive forces. The repulsion may

come from electrostatic, hydration or steric forces. The repulsive forces increase until the tip jumps into contact with the surface when the gradient of attractive forces exceeds the spring constant and the gradient of repulsive forces. If the approach happens between two hard surfaces in the absence of any long-range interactions, there will be a small downward deflection shown in the approach curve prior to contact. After contact the cantilever retracts from the surface, thus a retraction curve follows the approach curve and there is often hysteresis. The hysteresis is due to adhesion, which is reflected in the retraction curve as a deflection below the zero-deflection line. The reason of adhesion can vary depending on the sample and environment. In general, the adhesion in air partly results from capillary forces, because a layer of water absorbed on the sample surface wicks up the tip and forms a connection between the tip and the sample [59]. Van der Waals forces also make contribution to the adhesion and it requires a large force to overcome the forces between the tip and the sample [60]. In fluid, the adhesion becomes complicated because more forces such as hydrogen bonding, hydrophobic, electrostatic and van der Waals forces may get involved. For biological samples, other forces such as forces from molecular recognition may also need to be considered [61]. The cantilever continues retracting from the surface and when its deflection forces overcome the adhesion, the tip will jump-off from the surface resetting the cantilever to the zero-deflection line. The hysteresis and jump-off event are

shown as a smooth negative deflection in the retraction curve, but in case of a biological sample a saw-tooth pattern can be observed due to the breakages of multiple polymer molecules binding with the tip [59, 61].

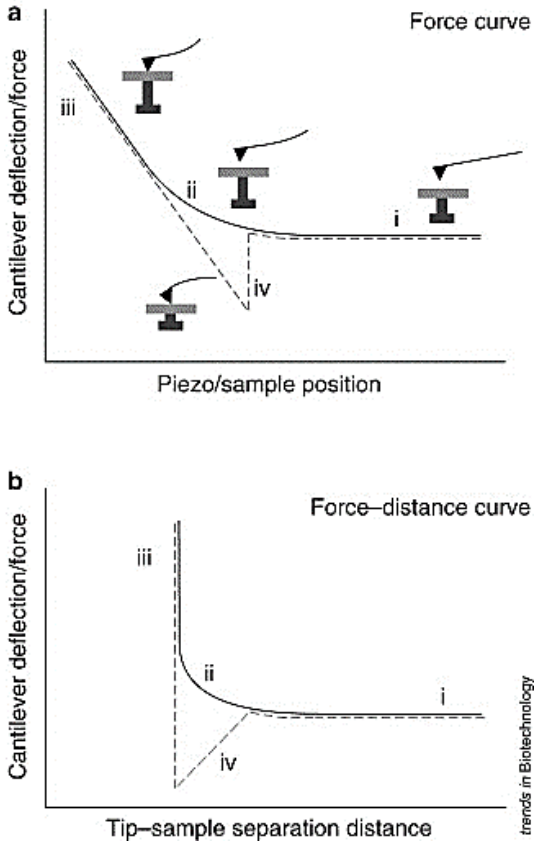

Fig. 5. Components of a force curve. (a) Uncorrected force curve. (b) Corrected force curve. (a, b) As the stage extends and retracts, the tip-sample separation distance decreases and then increases, and the tip-sample interaction force changes accordingly. A complete force curve contains both the approaching (solid) and retracting (dashed) portions. There are five regions of interest in a typical force curve. At the beginning of the curve (i), the tip is far from the sample, and there is no interaction and no cantilever deflection (zero-deflection line). As the stage extends and brings the sample closer to the tip, long- and short-range tip-sample interactions cause the cantilever to deflect (ii); here, a long-range repulsive interaction is shown. When the tip contacts the surface, the stage movement and cantilever deflection become coupled, which appears in the curve as a straight line (iii); this is sometimes called the contact line. At maximal deflection, the stage stops advancing and begins to retract. The retract curve can display hysteresis (iv) owing to a variety of tip-sample interactions, the most common of which is an adhesive force before the sample pulls away from the tip. The tip may then experience long-range interactions before the tip-sample separation distance is large enough for the cantilever to return to zero deflection (from Heinz and Hoh, 1999 [59]).

Microbial adhesion is the first step of biofilm formation and it is of major interest in biotechnology, environmental sciences and medicine. AFM with the force measurement function helps scientists to quantify and evaluate the effects of environment, cellular surface molecular structure and composition on adhesion, thereby making contributions to shed light on the mechanism of cell adhesion. Razatos et al. [62] compared the interactions between the AFM tip and *E. coli* or its mutants and found that adhesion force was affected by the length of core lipopolysaccharide molecules on *E. coli* cell surface and by the production of the capsular polysaccharide, colanic acid. Chandraprabha et al. [63] probed interactions between AFM tip and *A. ferrooxidans* under various conditions. Their results showed that pH, ionic strength and surface biopolymers had effects on adhesion. In order to investigate more detailed for specific information on the interactions between two objects, the AFM cantilever can also be modified. By immobilizing *Shewanella* on an AFM cantilever Lower et al. [64] obtained a cell probe and they used this cell probe to measure the interactions between the cell probe and a mineral surface. The results indicated that the bacteria could recognize the mineral surface because of the increased adhesion force due to an extended contact time. To have a better understanding on the interactions between proteins and their binding to specific ligands and membrane surfaces, Thormann et al. [65] modified an AFM cantilever with lung surfactant protein D and measured its

interactions with various carbohydrates. AFM can also do continuous force measurements across a surface. In this case the adhesion force values are collected from the recorded force curves and converted to a colour signal according to the magnitude to produce an image. The obtained image is a so called force mapping image or force-volume image and it shows the force distributions on the surface (Fig. 6). It is possible to detect, locate and real-time monitor the reacting area on a surface by using the force mapping mode. Alsteens et al. [66] scanned *E. coli* infected by His-tagged phages by Ni^{2+}-NTA groups modified tip in force mapping mode. They found the adhesion events were organized into nanodomains in the septum regions, thereby suggesting that these domains are the assembling machinery location for the phage. AFM with force measuring function can be applied in the medical field to evaluate the risk for diseases. Guedes et. al [67] found that the interaction between fibrinogen and erythrocytes is modified in chronic heart failure patients: ischaemic patients showed increased fibrinogen-erythrocyte binding forces compared with non-ischaemic patients. The patients with an increased binding force initially were hospitalized more frequently. The results illustrate that force measurement by AFM can be used to identify patients with increased risk for cardiovascular diseases.

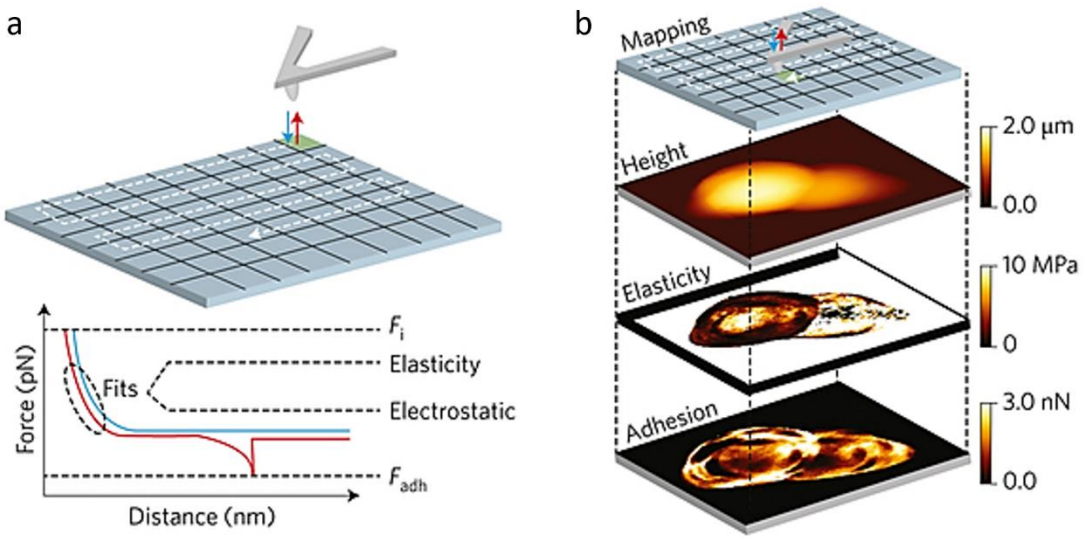

Fig. 6. Force-distance curve-based AFM. a, Force-distance curve-based AFM imaging records pixel-by-pixel force-distance curves while contouring the sample topography. Parameters, such as the tip-sample adhesion force F_{adh} or elastic and electrostatic properties of the sample, are extracted by fitting the curve. Parameters can be displayed as coloured maps and correlated to the topography. b, Example of multiparametric force-distance curve-based AFM imaging of the elasticity and adhesion of two dividing cells of *Staphylococcus aureus* (from Dufrêne et al., 2017 [68]).

1.3.3 AFM for investigating nanomechanical properties

By relating an applied force to the indentation depth as the tip is pushed onto a sample, the nanomechanical properties of a sample can be evaluated. In this case the approach curve depicts the applied force to the cantilever versus the vertical deformation of the sample. A particularly crucial information implied in this curve is the contact point where the tip comes in contact with the sample surface. If the sample is non-deformable, then the tip will not continue its descent after it contacts with the sample, and the bending of the cantilever will be equal to its vertical displacement. However, if the sample is soft and deformable, then after contact the tip will indent and the bending of the cantilever becomes lower than its vertical

displacement. The indentation is shown as a non-linear progress of the approach curve. Although long-range forces such as electrostatic forces also give rise to a non-linear curve, the characteristic problem can be diminished by adjusting the physicochemical conditions like ionic strength and pH. However, most of the studies were done by ignoring the contributions from these forces [69]. Both cases of non-deformable and deformable samples are demonstrated in Fig. 7.

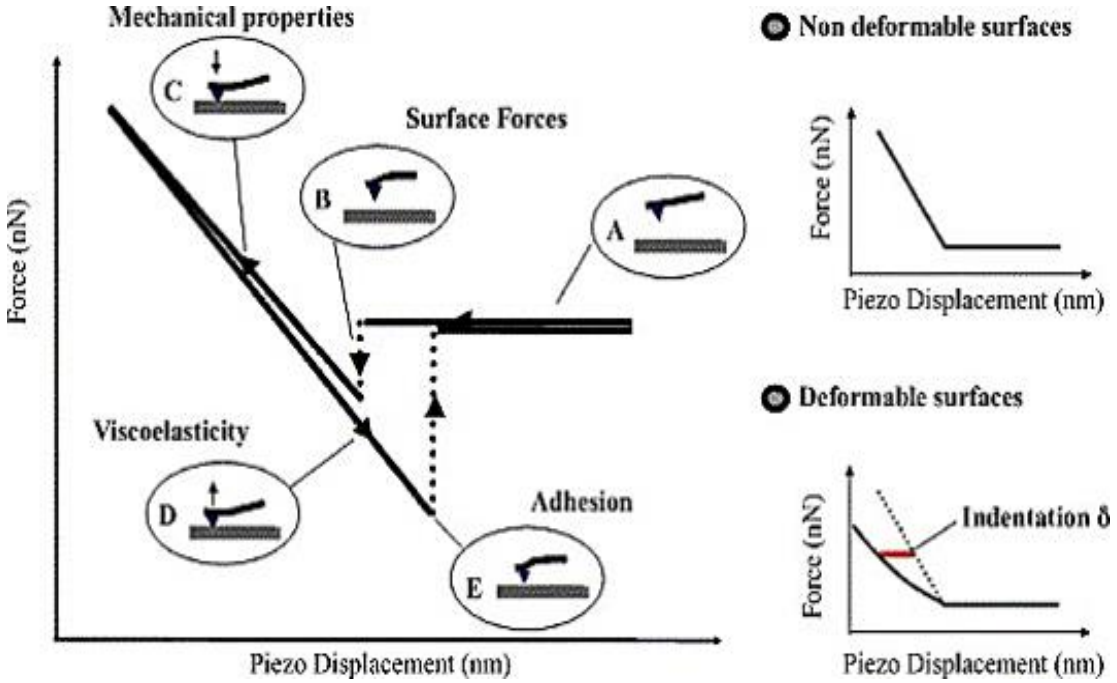

Fig. 7. Schematic diagram of a typical force curve for a non-deformable surface with attractive forces between the AFM tip and the sample (Left). The two ideal diagrams on the right show the approach force curves for non-deformable (top) and deformable (bottom) samples in the absence of surface forces (from Gaboriaud and Dufrêne, 2007 [69]).

Deformation under stress is a mechanical property of a material called elasticity, and it can be evaluated by Young's modulus. The higher the value of Young's modulus, the stiffer is the material. The numerical value of Young's modulus is obtained by applying theoretical models. Hertz

model and Sneddon model are the most used ones. These two models should be chosen according to the shape of the AFM tip. The AFM tips have a four-sided pyramidal shape and their very end can be modelled by a cone or a paraboloid. Hertz model is for paraboloidal tip, while Sneddon model is applied for conical tip. In case of paraboloidal tips the indentation depth (δ) and the applied force (F) are connected through the following formula:

$$F = \frac{4\mathrm{E}\sqrt{R}}{3(1-\mu^2)}\delta^{1.5}$$

In case of conical tips they are connected through

$$F = \frac{2\mathrm{E}}{\pi(1-\mu^2)}\tan(\alpha)\delta^2$$

where E is the Young's modulus, R is the radius of curvature of the paraboloidal tip and α is half-angle of the conical tip. δ is the Poisson ratio of the sample (ranging from 0 to 0.5), which reflects the compressibility of the sample. Its maximal value corresponds to an incompressible material. A value of 0.5 is usually assumed for cells.

An AFM equipped with the elasticity analysing function has widened the horizon of the fundamental mechanisms of cellular processes and many exciting results have been reported. E.g. heat-sterilized cells present a Young's modulus twice as high as that of healthy bacteria [70]. An elasticity map, produced in force mapping mode (Fig. 6), showed that the bacterial membrane is not mechanically uniform, but contains stiffer areas,

which might be associated with bacterial nucleoids [71]. Also from elasticity maps, it is found that bacteriophages were preferentially detected in soft regions of bacteria and these regions generally surrounded by much stiffer cell wall properties [66]. Ungureanu et. al [72] quantified the changes in the neuronal membrane elasticity induced by treatment with two amyloid-beta isoforms which are responsible for several neurotoxic mechanisms relevant to the pathology of Alzheimer's disease. They found that after a short time incubation with the two amyloid-beta species there were changes in the elasticity of young, mature and aged neurons. This finding illustrates that changes in neuronal membrane elasticity might directly induce functional changes related to neurodegeneration.

2. Aims of this work

To the best of our knowledge until today only few studies shed light on the role of EPS involved in adhesion and biofilms of Gram-positive acidophiles during bioleaching of metal sulfides. Cell adhesion to a mineral surface can initiate bioleaching and subsequently biofilms can enhance bioleaching. EPS play an important role in these processes. Thus, analysis of EPS composition as well as quantification of the adhesion force between the cells and the minerals should contribute to a better understanding of the bioleaching process.

The present work is focused on the relationship between adhesion forces and EPS formation by establishing a method to precisely measure the interactions between bacteria and metal sulfides under almost in situ conditions, as well as by chemical and mechanical analysis of EPS collected from both leaching species of planktonic cells and biofilms. For this the Gram-positive bacterium *S. thermosulfidooxidans* DSM 9293^{T} was chosen.

The study mainly aims to investigate the following questions:

1. How do bacterial surface compounds chemically and mechanically change during the bacterial transition from the planktonic to the biofilm state, when growing on pyrite or sulfur?

2. How can one measure the interactions between bacteria and minerals under almost in situ conditions without denaturing the bacterial surfaces?

And how strong are the forces?

3. Materials and methods

3.1 Strain and cultivation

S. thermosulfidooxidans DSM 9293^T was obtained from the culture collection of the department of Aquatic Biotechnology, Biofilm Centre, University of Duisburg-Essen. The culture was original purchased from Deutsche Sammlung von Mikroorganismen und Zellkulturen (DSMZ), Germany. The strain was cultivated in Mackintosh basal salt medium (MAC) [73] containing 0.02% yeast extract with an initial pH of 2.5. 2% (m/v) pyrite grains or 1 g/L (m/v) elemental sulfur was supplemented as energy source. Cells were cultivated aerobically at 45 ^oC either in Erlenmeyer flasks on a rotary shaker at 140 rpm or in 5 L bottles with aeration (sterile air, ~15 L/h) and agitation at 180 rpm by magnet stirring.

3.2 Preparation of substratum

Pyrite slices were cut off from pyrite cubes with a size of 1 cm x 1 cm x 1 cm (Museum grade, Freiberg, Germany). These pyrite cubes were naturally crystallized, and their six sides were smooth and shiny. After cutting, slices with one shiny side and one rough side were obtained, and this study only focused on the shiny side. Rest of the pyrite was ground and by applying wet-sieving pyrite grains with a size of 100–200 µm were obtained. To sterilize the pyrite grains and slices, they were first boiled with 6 N HCl for 30 minutes. After that they were rinsed with deionized water till pH neutrality and then washed twice with acetone to remove oxidation

products. After drying in a fume hood, a final sterilization was performed under nitrogen atmosphere at 120 °C overnight [74].

To produce sulfur prills, sulfur powder (Carl Roth, Germany) was molten in a glass beaker at 300 °C and then poured into cold deionized water with an agitation of 250 rpm. Sulfur prills with a diameter of 1-3 mm were then obtained. To produce sulfur slices, the molten sulfur was poured on glass plates first. After its solidification, sulfur slices with a size of 1 cm x 1 cm x 2 mm were obtained by manually cutting the sulfur layer. Both sulfur prills and slices were autoclaved at 110 °C for 90 minutes for sterilization.

3.3 Cell number, pH and iron determination

The planktonic cell density was determined by direct counting with a Thoma counting chamber (Assistant, Germany) under a light microscope (Leica DMLS, Wetzlar GmbH) in phase contrast mode with a magnification of 400 times.

The pH was determined with a digital pH meter (Model pH 537, WTW, inLab® 422 Combination Semi-micro pH Electrode, Mettler Toledo).

Ferrous and total iron ions were quantified by the following procedures described by Tamura [75]. The principle is that ferrous ions complex 1,10-Phenanthroline. The complexes have a red colour and can be measured spectrophotometrically at 492 nm. Subsequently the total iron can be quantified by adding hydroxylamine which can reduce ferric ions to ferrous

ions. The samples were measured in triplicate within microtiter plates with a UV-Vis spectrophotometer (TECAN, Infinite pro® 200).

3.4 Strategies for enhancing biofilm formation

Different initial medium pH were adjusted with 1 M H_2SO_4 or KOH. 10 mM ferric chloride, 50 mM potassium tetrathionate or sodium thiosulfate were prepared as standard solutions and sterilized by filtration. Phosphate starvation was tested by using phosphate free MAC medium. Medium replacement was performed by exchanging fresh MAC medium containing 0.02% yeast extract with exhausted medium every two days. The experiments were conducted in 300 mL flasks with 3% pyrite in 150 mL MAC medium. The initial cell density for all experiments was 2×10^8 cells/mL. All assays were done in triplicate.

3.5 Pre-colonization and leachate experiments

Pyrite grains (50-100 µm) were incubated at 2% with 10^8 cells/mL of iron-grown *L. ferriphilum* DSM 14647 in 50 mL MAC medium for 24 hours. Afterwards, for pre-colonization experiments, the culture supernatants were discarded and the pyrite (with attached cells) was washed three times with fresh MAC medium. To elucidate, whether living biofilms may influence further pyrite colonization, one set of pre-colonized pyrite grains were incubated at 100°C for 2 hours to heat-inactivate the biofilms. After washing, sulfur-grown *S. thermosulfidooxidans* cells were added to all flasks filled with 50 ml fresh medium containing 0.02% yeast extract. The

final cell density was 10^8 cells/mL. For this experiment, several controls were used. One control was named as mixed culture: $5x10^7$ cells/mL of sulfur-grown *S. thermosulfidooxidans* cells and $5x10^7$ cells/mL of iron-grown *L. ferriphilum* cells were inoculated to 2% clean pyrite. One control was named as *L. ferriphilum*: leaching was only performed by one day old biofilms of *L. ferriphilum*. One control was named as *S. thermosulfidooxidans*: 10^8 cells/mL of *S. thermosulfidooxidans* were inoculated with clean pyrite.

For leachate experiments, the culture supernatants of *L. ferriphilum* were collected and filtered through a filter with a pore size of 0.22 µm. Afterwards, pyrite-grown cells of *S. thermosulfidooxidans* were inoculated to the filtered leachate with a final concentration of 10^8 cells/mL. 2% fresh pyrite were then added to all the flasks. Considering the importance of ferric ions for leaching, one batch of experiment was set as control in which the same amount of iron detected in the leachate was added to the fresh medium and then inoculated with cells of *S. thermosulfidooxidans*. The added iron was ferric chloride.

3.6 EPS extraction and analysis

A sodic ion exchange resin Dowex Marathon C (Sigma-Aldrich) was used for extracting EPS from the cells/biofilms. In the case of the planktonic cells, 5 L stationary phase culture were harvested by centrifugation at 11270 g for 10 min. After washing with sterile MilliQ water the cells were

suspended in resin pulp with a ratio of 30 g resin/g cell weight. In the case of the biofilms, the pyrite grains or sulfur prills were collected. After washing the pyrite grains or sulfur prills were mixed with the resin in a same volume. Both extractions were performed at 4 ^{o}C, 600 rpm for 1.5 h. After extraction the supernatant was first centrifuged and then filtered through a filter with a pore size of 0.22 µm. Dialysis followed using a cellulose membrane of 3500 MWCO. First it was done in running deionised water overnight and then in MilliQ water for 2 h at 4 ^{o}C with changing the water every half hour. The obtained EPS solutions were divided in two parts: one was used for analysis; the other was freeze-dried to obtain the dry weight of the EPS.

The amount of polysaccharide was determined by the protocol of Dubois [76]. Briefly, polysaccharides give an orange-yellow colour, if treated with phenol and concentrated sulfuric acid. The content of humic substance and the content of protein were determined and corrected according to modified Lowry method [77]. The method is based on the appearance of a chromogen: proteins react with the Folin phenol reagent after alkaline copper treatment. When $CuSO_4$ is omitted, the colour development is due to humic substance and chromogenic amino acids. Without $CuSO_4$ the colour developed by bovine serum albumin decreased to 20%, but no decrease was observed for humic substance. Thus, the measured wave lengths for protein and humic substance should be corrected to remove the

mutual interference of each other. Glucuronic acid was quantified by the assay described by Blumenkrantz and Asboe-Hansen [78]. This method is based upon the appearance of a chromogen, if uronic acid and meta-hydroxydiphenyl are heated to 100 ^{o}C in concentrated sulfuric acid/tetraborate.

Fourier transform infrared spectroscopy (FTIR) was also applied for analysis of the EPS composition and the freeze-dried EPS sample was used. The IR spectra were recorded on a FT-IR 430 spectrometer from Jasco with a Pike MIRacle ATR sampling accessory. Bands were quoted in cm^{-1}. The baseline shift of blank spectra was corrected by Spectra Manager (JASCO, Japan). Two measurements were done for each sample and the spectral peak shifted no more than 1 cm^{-1}.

3.7 Atomic force microscopy and epifluorescence microscopy instrumentation and performance

A NanoWizard II atomic force microscope (JPK Instruments, Berlin, Germany) combined with an upright epifluorescence microscope (Axio Imager A1m, Zeiss, Germany) as a BioMaterial workstation (JPK Instruments) were used to locate and scan cells or biofilms. The BioMaterial workstation allows to transfer the samples between the atomic force microscope and the epifluorescence microscope, giving same positions for both microscopes [79]. In this study, planktonic cells and biofilms, stained with 6 µM SYTO 9, were at first observed under the

epifluorescence microscope and then transferred to the atomic force microscope for scanning and force and elasticity measurements. A CSC38/NO AL (Mikromasch, Tallinn, Estonia) probe was used and cantilever B with the following parameters was chosen for scanning and measuring: length, 350 μm; width, 32.5 μm; thickness, 1.0 μm; resonance frequency, 10 kHz; shape, cone with a full cone angle of 40°; and force constant, 0.03 N/m. Before the experiments the cantilevers were immersed in Piranha solution for 10 min and then washed with sterile MilliQ water. All AFM operations were performed in MAC medium at pH 2.5 at room temperature. The sensitivity of the optical lever system and the cantilever spring constant were calibrated in liquid prior to each experiment. The spring constant for each cantilever was compatible with the manufacturer's specifications.

For AFM imaging, contact mode was applied. The applied setpoint was below 1 nN and the scan rate ranged from 0.1 to 0.5 Hz. Force mapping mode was performed to obtain force map images, which were obtained as matrices of 64 x 64 force-distance curves on a defined surface area. Two separate pyrite coupons were measured. Before the measurements the cantilever was immersed in the medium over the samples for 30 min to be equilibrated. All force-distance curves were recorded with an applied force of 800 pN, using a constant approach and retraction speed of 2 μm/s. The relative elasticity map of the sample is computed from the force-distance

curves via Hertz model and Young's modulus was used to quantify the stiffness of the sample.

3.8 Preparation of pyrite-/chalcopyrite-modified cantilever

The probes for the force measurements were prepared by attaching small pyrite particles (size range 5-10 µm) to tipless AFM cantilevers (type NP-O, Bruker, California). The procedure was carried out in a Dimension D3100 AFM system (Bruker, California). A small amount of two-component epoxy glue (Araldite, Selleys, Australia) was spread on a glass slide to form small droplets. The AFM was then used to approach the tipless cantilever to a small glue droplet and dip the end of the cantilever into the glue. Subsequently, the scanner was withdrawn and the probe was moved to the particle to be attached to the tip of the cantilever. The instrument was then engaged in Contact Mode AFM with the tip of the cantilever directly on the selected particles. After a 10 second waiting period, the scanner was withdrawn and the freshly prepared pyrite AFM probe set aside for the glue to fully cure.

3.9 Immobilization of cells on glass slides

For immobilization of planktonic cells, a glass slide was chosen as substratum. The glass slides were washed with Piranha solution and rinsed with sterile MilliQ water. After cleaning a drop of 0.01% poly-L-lysine (PLL; M.W. 150-300 K; Sigma) or 1% polyethyleneimine (PEI; M.W. 1200; Alfa Aesar) was placed on one side of a glass slide and incubated for

4 h. After rinsing with sterile MilliQ water the glass slide can be used for immobilization of cells. The bacteria were harvested in exponential phase by centrifugation at 11270 g for 10 min. After washing with sterile MAC medium and MilliQ water, one drop of a highly concentrated cell suspension was placed on a PLL- or PEI-coated glass slide. Afterwards, the glass slide was incubated at 4 ^{o}C for 3 h and gently rinsed with sterile MilliQ water to remove loosely attached cells. For immobilizing cells by glutaraldehyde (M.W. 100.12; Sigma) the glass slides with one drop of 25% glutaraldehyde were incubated overnight and then washed with MilliQ water. Afterwards, one drop of cell suspension was placed on the glass slide and the cells were further treated with a drop of 2.5% glutaraldehyde at 4^{o}C. After 2 h the glass slide was rinsed with MilliQ water.

4.0 Scanning electron microscopy/energy dispersive X-ray spectroscopy

SEM/EDS was used to analyse pyrite surface as well as the biofilm grown on it. Pyrite slices with 3 months old biofilms were first taken out from Erlenmeyer flasks with a tweezer under sterile conditions. Then they were rinsed with sterile MilliQ water five times. After drying under N_2 atmosphere, SEM and EDX measurements were performed on an FEI QUANTA 400 microscope equipped with a tungsten filament gun and an EDAX EDX detector.

4.1 Confocal laser scanning microscopy

A laser scanning module (LSM 510 Carl Zeiss® Jena) combined with an inverted Axiovert100 M BP microscope (Zeiss®) was used for biofilm visualization. Mosaix mode was especially applied for visualizing biofilm development on pyrite slices. This software can provide information in one image by integrating several images. In this study 25 (5×5) images were integrated.

4. Results

4.1 Attachment and biofilm formation on pyrite by *S. thermosulfidooxidans*

Fig. 8 A shows how the number of attached cells of *S. thermosulfidooxidans* changed on pyrite grains as a function of time. According to the figure, around 13% of total inoculated cells attached to the pyrite in the first 10 minutes. In the next 100 minutes the attached cells gradually increased to 27% and the amount of attached cells levelled off until the end of the experiments. This number indicates a poor attachment of *S. thermosulfidooxidans* to pyrite. Fig. 8 B, C and D are the EFM images, which give a direct visualization on the changes of attached cells of *S. thermosulfidooxidans* on pyrite grains within 40 days. It can be seen that after 1 day of incubation a few cells were visualized on pyrite surfaces and their distribution was heterogeneous (Fig. 8 B). However, after 20 days of incubation it became difficult to detect attached cells (Fig. 8 C) and after 40 days no attached cells were visible (Fig. 8 D). The same results were obtained, when pyrite slices were used as substratum (Fig. 9). Although there were many cells or big cell clusters on the surface after 1 day of incubation, cells had disappeared after 14 days of incubation.

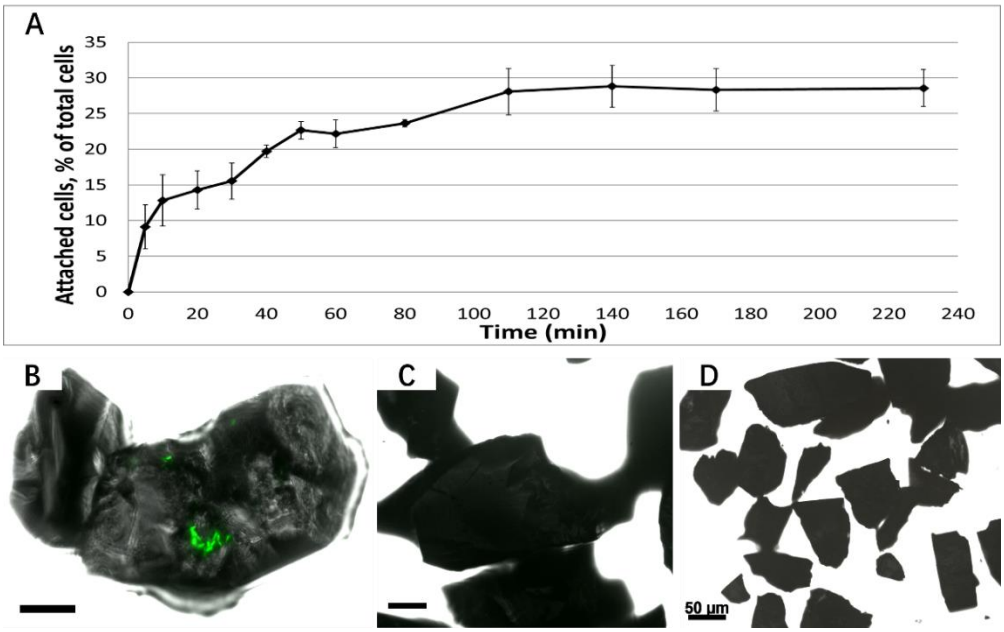

Fig. 8. Amount of attached cells of *S. thermosulfiooxidans* to pyrite grains within 4 h (A) and their biofilm development on pyrite grains after 1 day (B), 20 days (C) and 40 days (D) of incubation under 45°C in MAC medium with 0.02% yeast extract addition. B, C and D are EFM images and green signal indicate cells. Scale bar, 20 µm.

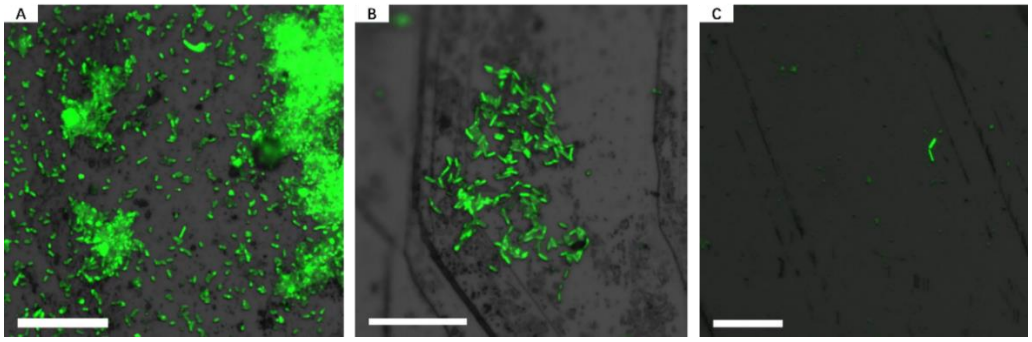

Fig. 9. Biofilms of *S. thermosulfiooxidans* on a pyrite slice after 1 day (A), 7 days (B) and 14 days (C) of incubation under 45°C in MAC medium with 0.02% yeast extract addition. A, B and C are EFM images and green signals indicate cells. Scale bar, 20 µm.

4.2 Effects of different strategies on enhancement of biofilm formation on pyrite by *S. thermosulfidooxidans*

Fig. 10 shows the attached cells of *S. thermosulfidooxidans* on a pyrite surface after one week of incubation under different conditions. Fig. 10 A and B show, how the biofilms of *S. thermosulfidooxidans* developed on

pyrite surfaces with an initial pH of 1.5 or 3.5, respectively. The EFM images indicate that no cells were attached on pyrite grains either at pH 1.5 or 3.5. Although some green dots on pyrite surface were detectable, when cells were grown at pH 1.5, these dots were most likely not cells as indicated by shape and size. Fig. 10 C and D show, how the biofilms developed with 2 mM tetrathionate or thiosulfate as extra energy source, respectively. No cell signals can be observed in the images, which illustrates that neither of them showed a positive effect on biofilm formation. Ferric ions also did not help *S. thermosulfidooxidans* to colonize on pyrite surfaces, as it is revealed by Fig. 10 E. No well-formed biofilms exist on the pyrite surfaces and only a few single cells occur as shown in Fig. 10 F. This indicates that phosphate starvation does not significantly enhance biofilm formation.

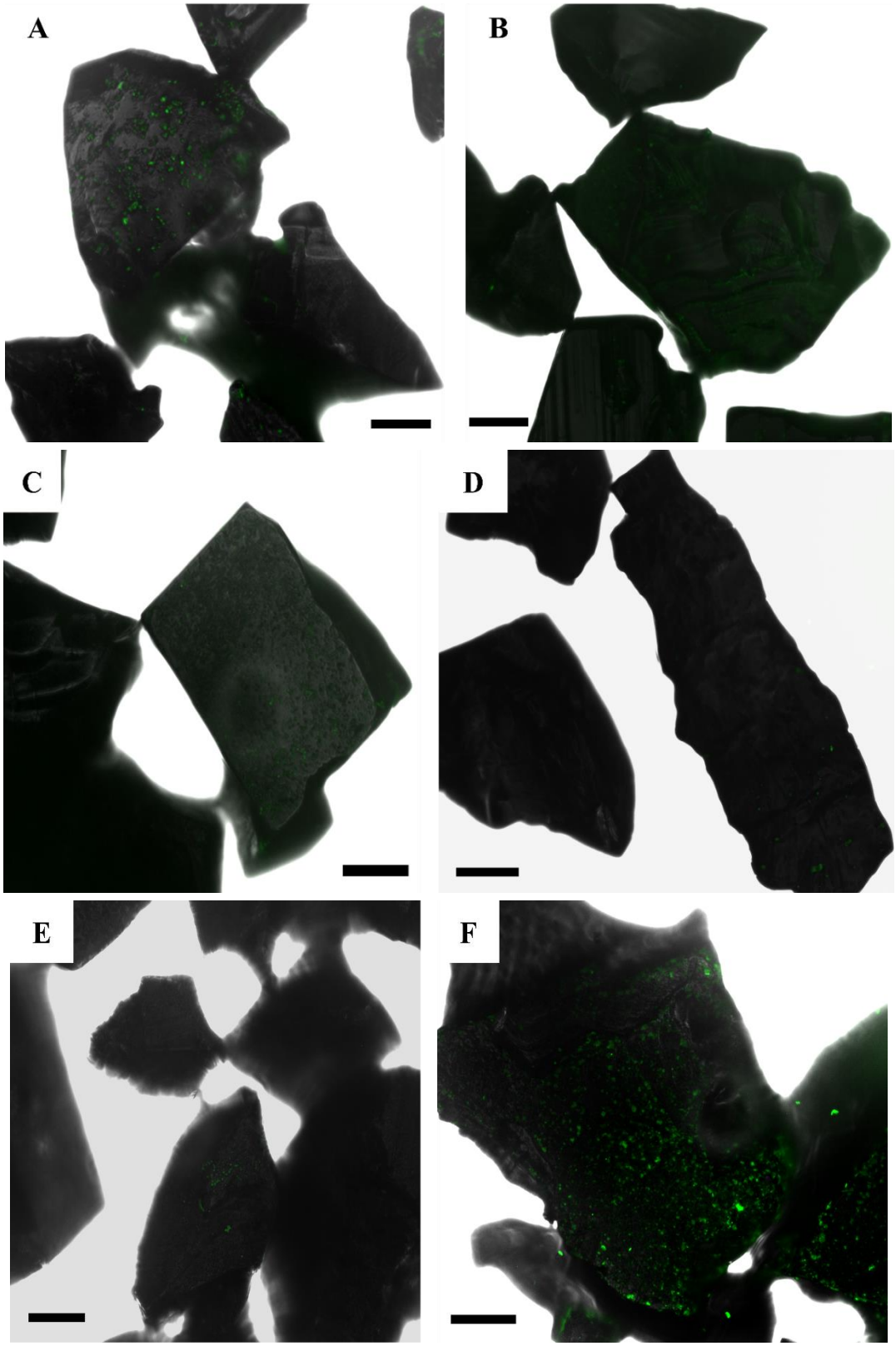

Fig. 10. Biofilms of *S. thermosulfiooxidans* on pyrite grains after 1 week of incubation with initial pH 1.5 (A) or 3.5 (B), or with 2mM $K_2S_4O_6$ (C), 2mM $Na_2O_3S_2 \cdot 5H_2O$ (D) or 1mM $FeCl_3$ (E) supplemented, or under condition of phosphate starvation (F). Scale bar, 20 µm.

Fig. 11 and 12 show development of the biofilms of *S. thermosulfidooxidans* on pyrite grains and pyrite slices under the condition of exchanging exhausted medium with fresh medium. The results demonstrate that this is the only strategy, which can enhance the biofilm formation on pyrite, since the pyrite grains or the pyrite slices were almost fully covered by the biofilms at the end of the experiments. Especially in case of pyrite slices, biofilms were shown in the form of cell clusters after 1 month of incubation. After 5 months of incubation, these cell clusters became large and connected with each other, and they almost fully covered the pyrite slices. Unlike other leaching bacteria, which form single-layered biofilms, the 3D AFM images show that the biofilms of *S. thermosulfidooxidans* have a multiply layered architecture.

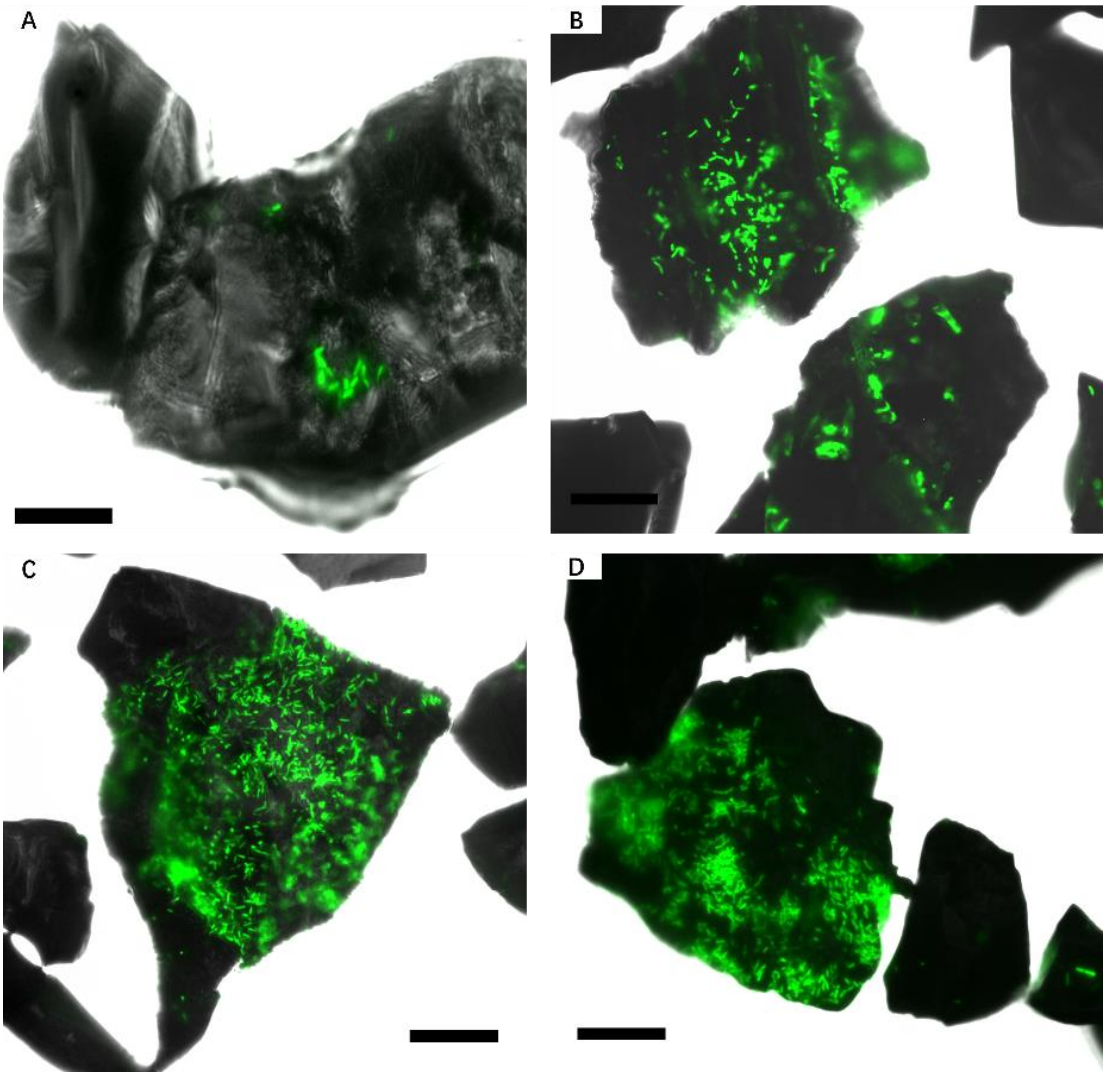

Fig. 11. Biofilms of *S. thermosulfidooxidans* on pyrite grains after 1 day (A), 20 days (B), 40 days (C) and 60 days (D) of incubation under the condition of exchanging exhausted medium with fresh medium contained 0.02% yeast extract. All the images are EFM images and green signals indicate cells. Scale bar, 20 μm.

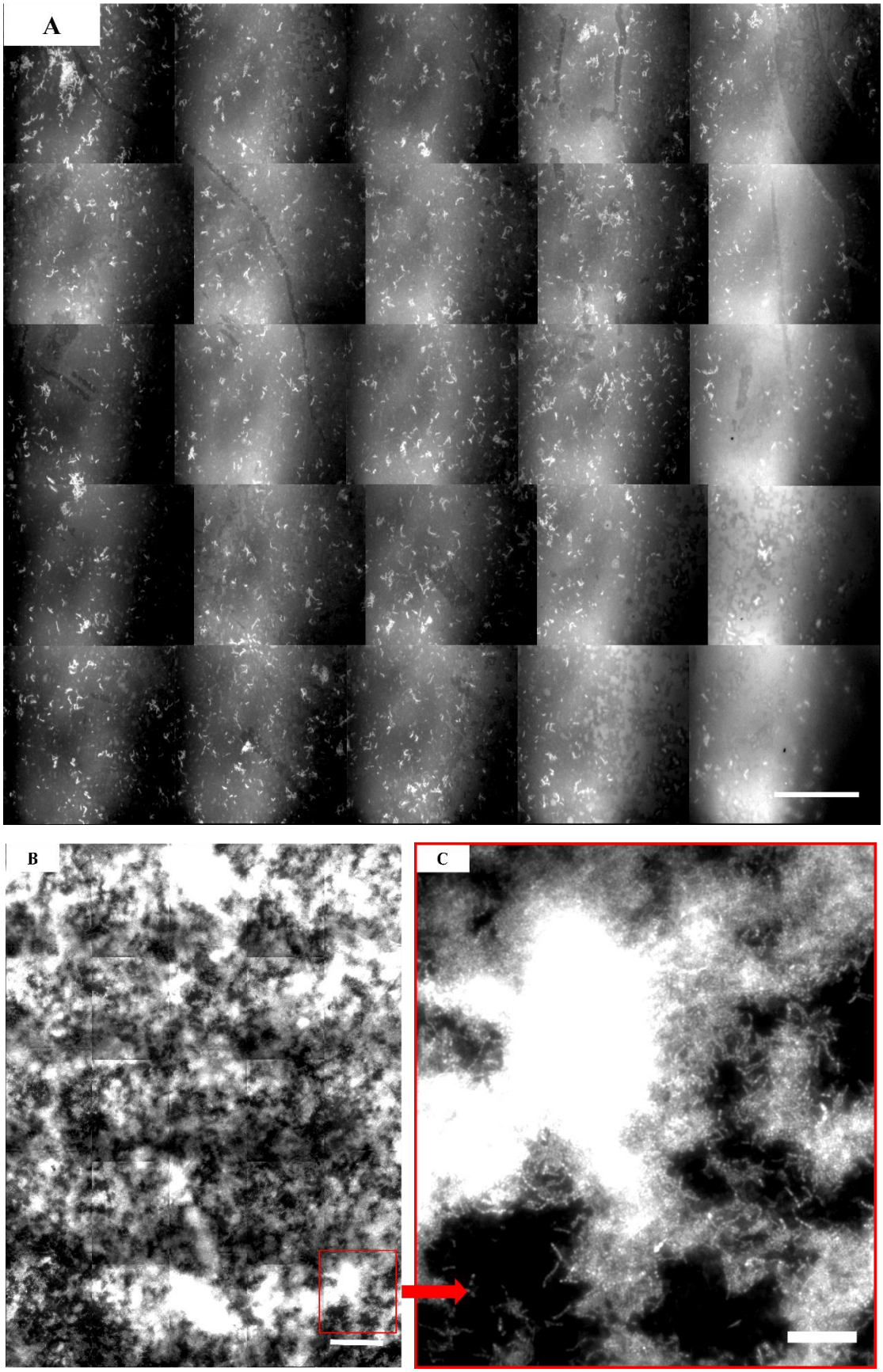
A
B
C

D

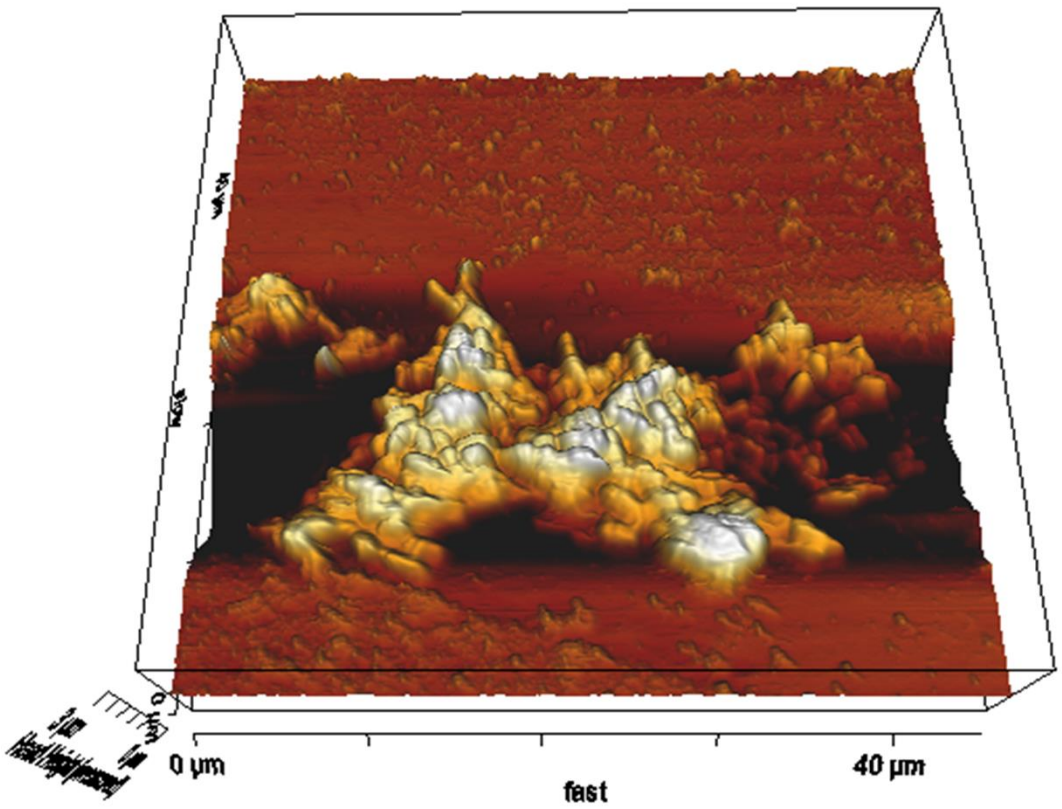

E

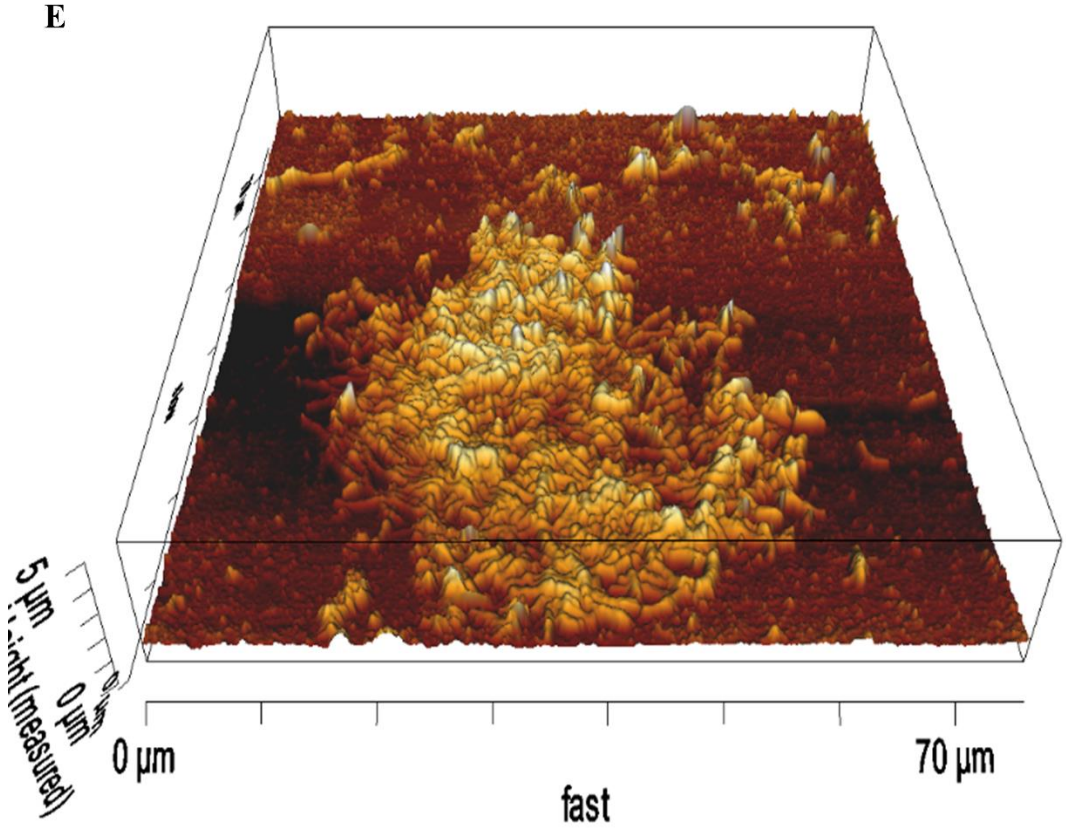

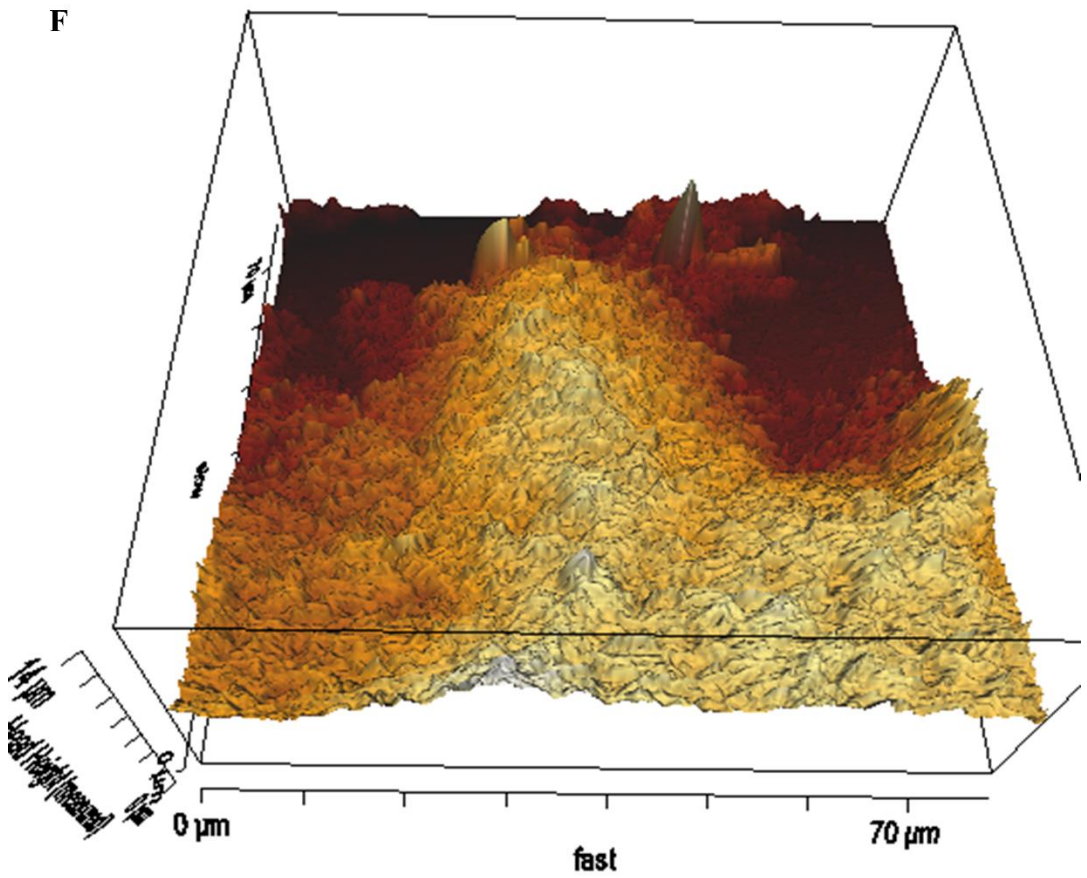

Fig. 12. Biofilms of *S. thermosulfidooxidans* on pyrite slices after 1 month (A and D), 3 months (E) and 5 months (B and F) of incubation under the condition of exchanging exhausted medium with fresh medium containing 0.02% yeast extract. C shows the area framed in B. A, B and C are EFM images and white signals indicate cells, scale bar is 20 µm. D, E and F are 3D AFM images.

4.3 Mechanical changes of cell surfaces for pyrite-grown cells of *S. thermosulfidooxidans* in transition from planktonic to biofilm growth

Fig. 13, shows the details of the morphology and topography of planktonic cells and biofilms. Several bacterial foot prints were visualized in case of a 15 days old biofilm. Obviously this was due to detachment caused by lateral forces during the scanning procedure. It is worth pointing out that the biofilms of *S. thermosulfiooxidans* were loosely or weakly attached to the pyrite surface after 15 d of incubation. Only later a more stable

attachment to the surface occured, but the reason is not clear. Many artifacts can be seen in image E of Fig. 13. Detachment of cells during scanning or slimy EPS could be the reason for the artefacts. For the pyrite surface, a layer in form of a heterogeneous film combined with particles was observed.

According to the adhesion force maps in Fig. 13 the planktonic cells or the biofilms exhibited less affinity to the AFM tip than to the substrata surfaces. However, some light points along edges of the biofilms can be noticed. A similar result was reported by Fang et al. [80], whose data indicate that the adhesion forces at the cell-substratum periphery are 25% higher than those on the cell surface. Accumulation of EPS at the cell-substratum periphery to enhance bacterial adhesion to the surface could account for the finding [81].

The Young's modulus maps shown in Fig. 13 demonstrate that biofilms can be distinguished well from the substrata due to their different stiffness values. As the biofilms develop, the difference in stiffness of the biofilms and the surfaces decreased, suggesting mechanical changes took place on the pyrite surface. At the beginning, the pyrite surface was stiffer than the biofilms, but after 5 months of incubation it became softer than the biofilms. Most likely an organic conditioning film had developed on the pyrite surface. Another information from these images is that the stiffness of the cell/biofilm surface shows heterogeneity. The heterogeneity could

be associated with stiff structures inside the biofilm/EPS-layer, since EPS are a heterogeneous mixture of polysaccharides, proteins, lipids and nucleic acids [19, 71]. Another possible reason may be that cells were heterogeneously embedded in EPS.

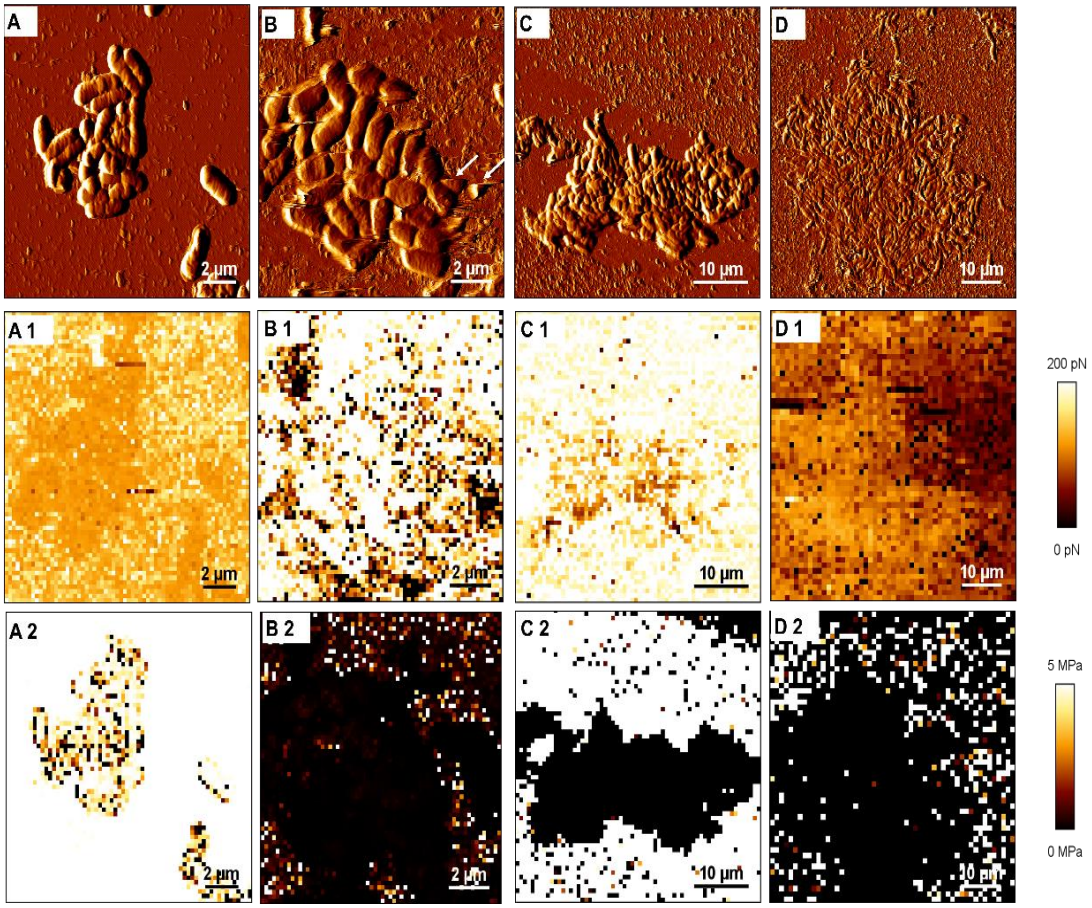

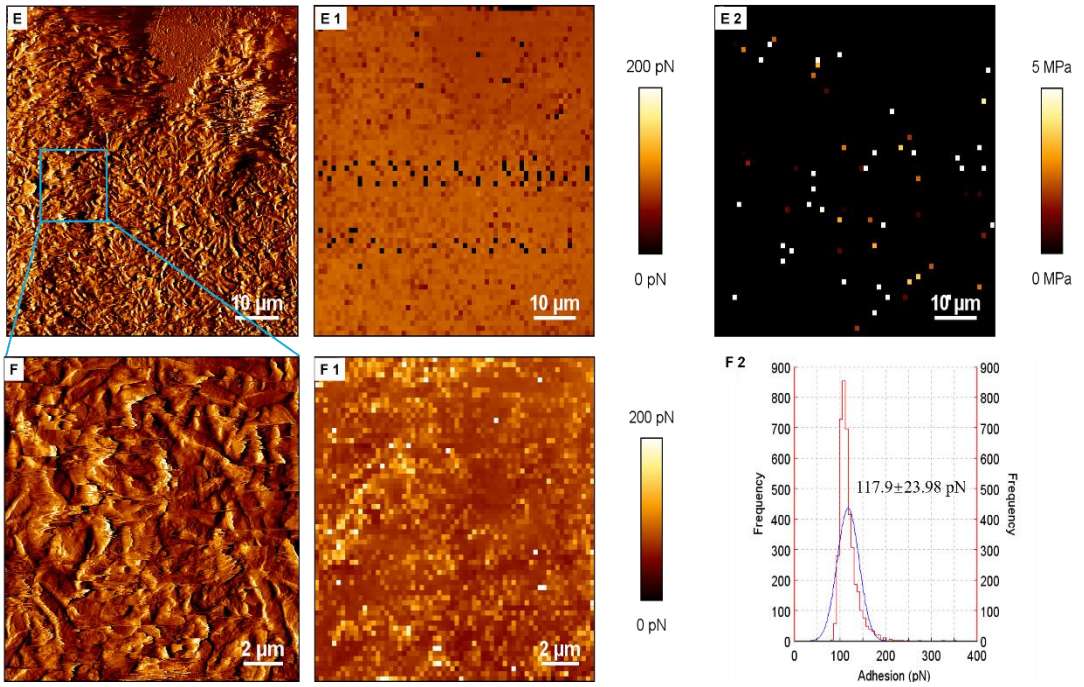

Fig. 13. Morphology, adhesiveness and stiffness of cells of *S. thermosulfidooxidans* on glass or pyrite. AFM vertical deflection images of A shows planktonic cells of *S. thermosulfidooxidans* immobilized on a glass slide; B, C, D and E show 15 d, 1, 3 and 5 months old biofilms of *S. thermosulfidooxidans* on pyrite. The arrows in B show remaining EPS of cells because of removal by scanning. A1 and A2, B1 and B2, C1 and C2, D1 and D2, as well as E1 and E2 are the force maps and Young's modulus maps of images A, B, C, D and E, respectively. Force map shows the distribution of adhesion forces between the scanned area and the AFM tip. Young's modulus map shows the distribution of stiffness. Image F is a magnification of the framed area in image E. Image F1 is the according force map. Image F2 is the histogram of all the adhesion forces measured in image F1. The blue curve in F2 shows the Gaussian fit.

Table 2 shows the statistic values for adhesiveness and stiffness of the planktonic cells as well as for the biofilm and for pyrite. It was reported that under the living conditions the adhesion forces between leaching bacteria and minerals ranged from 0.4-1 nN [32, 64]. In our study, from the planktonic to the biofilm cells, cells of *S. thermosulfiooxidans* showed a comparably low affinity to the tip and the adhesion force almost stabilized at around 120 pN. A drop in the Young's modulus values for the pyrite surface indicates that a soft film layer had formed on the pyrite

surface. To be more specific, at the beginning before interacting with bacteria the sterile pyrite surface was quite stiff with a value of 784.6±622.7 MPa. As the bioleaching process proceeded, this value showed a decrease, indicating that the pyrite surface became softer than before. After 5 months the pyrite surface (0.02±0.004 MPa) was as soft as the biofilm surface (0.02±0.01 MPa). Concerning the bacterial surfaces, they were stiffer in the planktonic state than in the form of biofilm. The huge shearing force and strike from the pyrite grains made the planktonic cells stiff to adapt their living environment. While in the case of biofilms, biofilms were grown on limited number of pyrite slices with low speed shaking, the shearing force should be much lower and there was no additional strike, thus the accumulation of EPS made the biofilms slimy and soft. It is noticeable that more than one Young's modulus for the 15 days old biofilm and the pyrite, which is because more than one peak showing in their histograms.

Table 2. Adhesion forces between a silicon nitride cantilever and planktonic cells or biofilms of *S. thermosulfidooxidans* and the respective Young's modulus values during pyrite leaching, n=8192. The data for the planktonic cells and the clean pyrite before leaching are given as "0 day".

Incubation time	Adhesion force (pN)		Young's modulus (MPa)	
	Cells/Biofilms	Pyrite surface	Cells/Biofilms	Pyrite surface
0 day	124.0±17.6	243.3±85.4	2.1±1.4	784.6±622.7
15 days	104.8±29.4	197.6±85.8	0.2±0.03, 0.04±0.02	401.5±30, 26.4±11, 0.05±0.02
1 month	122.8±27.7	150.9±24.3	0.2±0.1	218.8±172.9
2 months	130.8±27.5	118.1±74.4	0.14±0.09	60.6±27.8
3 months	103.4±15.9	78.4±12.5	1±0.7	16.6±5.9
4 months	93.4±9	242.4±271.7	1±0.5	0.9±0.5
5 months	117.9±23.9	110.5±16.2	0.02±0.01	0.02±0.004

4.4 Chemical changes of cell surfaces for pyrite-grown *S. thermosulfidooxidans* in transition from planktonic to biofilm growth

EDX spectra were used to analyse the chemical composition of the surface of biofilms and of the pyrite. The spectrum of a clean pyrite before leaching (Fig. 14 A) exhibits two elements: sulfur and iron, the constituents of pyrite (FeS_2). Fig. 14 B and C show the spectra of different surfaces chosen from a pyrite slice with a biofilm grown for 3 months. The intensive bands of oxygen and carbon in the spectrum for the biofilm indicate oxidation and organic matter (Fig. 14B-a). The spectrum for the pyrite, where the biofilm is growing, exhibits also bands for oxygen and carbon (Fig. 14B-b), but

less intensive than in case of the biofilm spectrum. Two additional sites of the pyrite surface were chosen for analysis and the results are shown in Fig. 14 C. Both spectra exhibit the bands of oxygen and carbon and in both spectra the bands are more intensive than in Fig. 14 B. This means that organic substances cover heterogeneously the pyrite surface. Both spectra, the one of the biofilm and the one of the pyrite surface, show bands for phosphate and potassium. This means that precipitates, most likely jarosites, were also formed [37]. Obviously, bioleaching with *S. thermosulfidooxidans* caused the formation of films consisting of organic and inorganic substances on the pyrite surface.

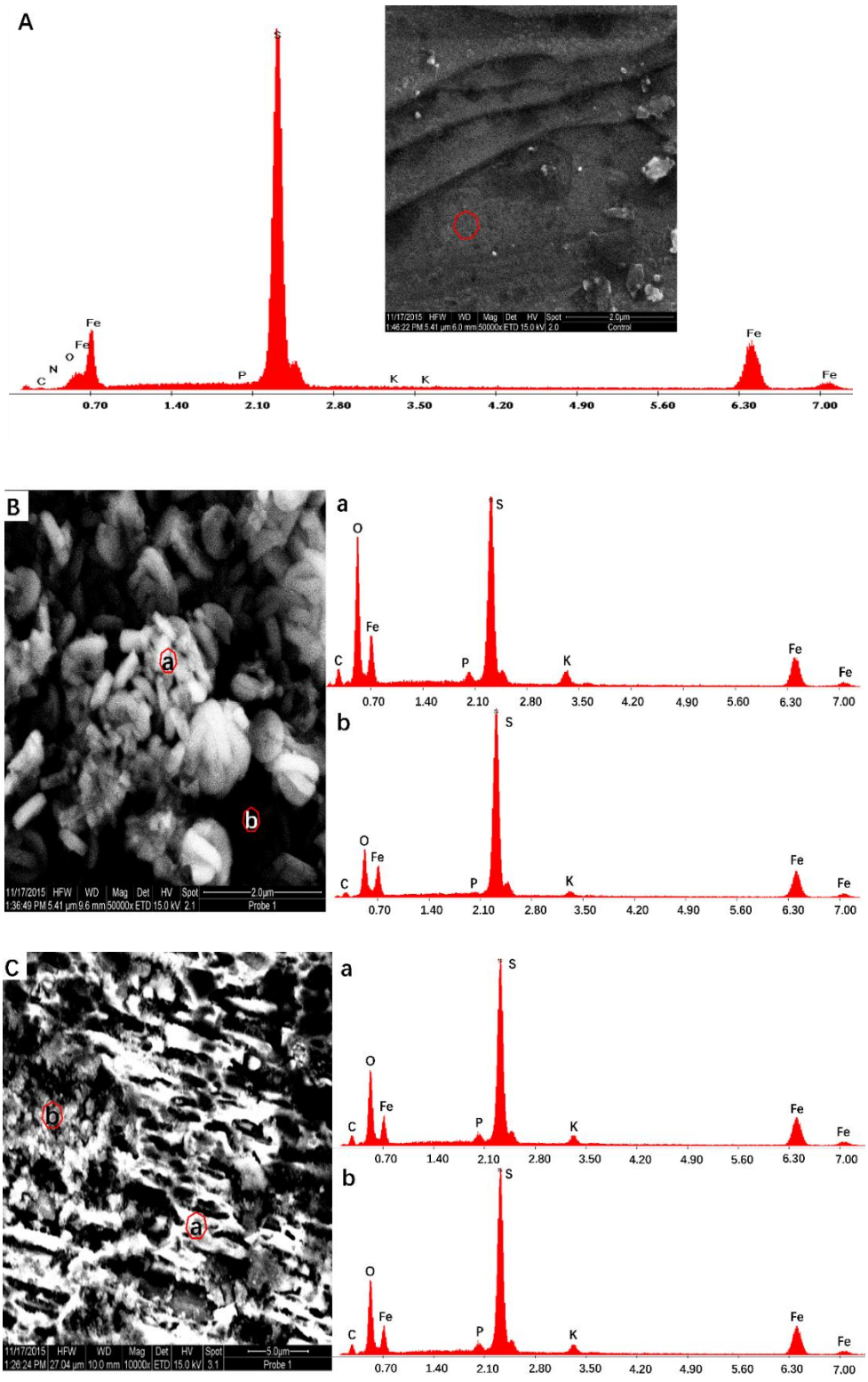

Fig. 14. EDX spectra for elemental analysis for surfaces of pyrite and of biofilm of *S. thermosulfidooxidans*. A shows a SEM image together with an EDX spectrum for a clean pyrite surface before leaching; B shows a SEM image of a 3 months old biofilm growing on pyrite and the spectra for biofilm (a) and pyrite (b); C shows a SEM image of pyrite surface after 3 months of incubation with bacteria and two spectra for pyrite. The framed area in the SEM image is the spot selected for EDX analysis.

The ATR-FTIR spectra in Fig. 15 indicate that the EPS collected from the planktonic cells of *S. thermosulfidooxidans* can be distinguished from those collected from the biofilms. The EPS collected from the planktonic cells are composed of proteins (based on the peak area centred at 1455 cm^{-1}, 1398 cm^{-1}, 1645 cm^{-1} and ~1542 cm^{-1}), lipids (the peak area centred 1380 cm^{-1}) and carbohydrates (the peak area centred at ~1114 cm^{-1}) [82, 83]. The spectrum of the EPS collected from the biofilms shows similar data, indicating that the components for the EPS collected from the biofilms also contained proteins, lipids and carbohydrates. However, conformation and/or composition of the proteins must have changed, since the typical bands for proteins, such as amide II (1542 cm^{-1}), CH_3 (1455 cm^{-1}) and CH_2 (1398 cm^{-1}), are missing. Instead, new bands are visible. The bands located at 1039 cm^{-1} and 1008 cm^{-1} arise from the vibration of a P-OFe bond [84]. Phosphodiester groups of nucleic acids in the EPS can form monodentate complexes with Fe irons on the iron-containing mineral surface to provide an energetically stable bond for further EPS or cell adhesion [85]. Thus, these bands could be unique for biofilm EPS. In addition, sulphated polysaccharides were also shown as another unique component of the biofilm EPS, due to a unique band located at 832 cm^{-1}, which is caused by C-O-S stretching vibrations [86, 87]. It indicates that bioleaching was proceeding and sulfates was formed.

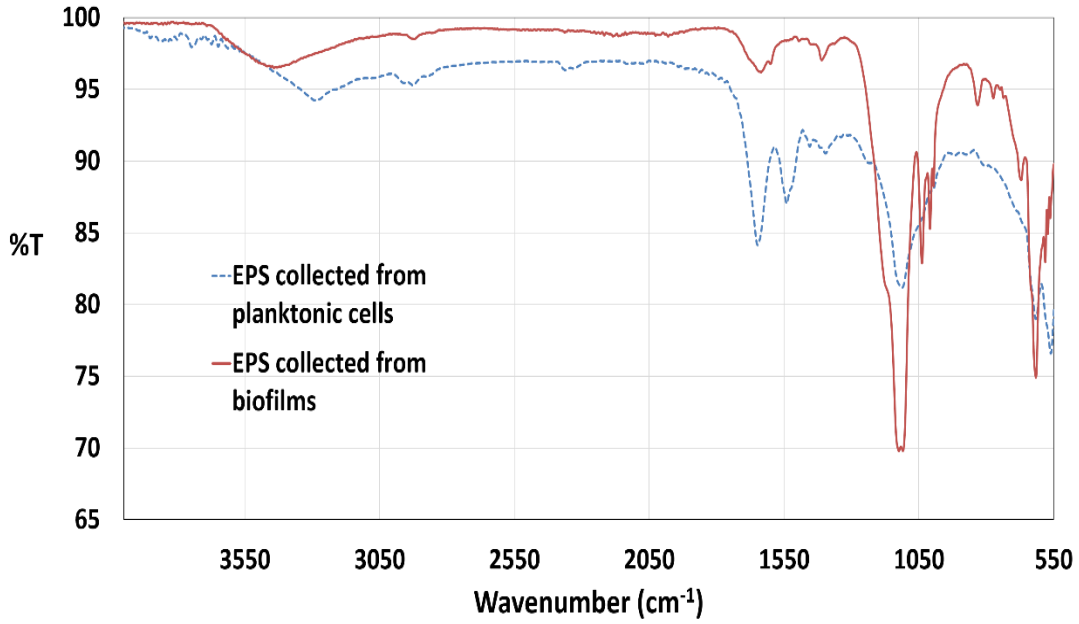

Fig. 15. ATR-FTIR spectral analysis of EPS collected from cells of *S. thermosulfidooxidans*. The blue dashed and the red solid lines show the spectra of EPS collected from pyrite-grown planktonic cells and 3 months old of biofilms of *S. thermosulfidooxidans* grown on pyrite, respectively.

In order to obtain more detailed information on the changes in the EPS composition during the process of transition from planktonic to biofilm growth, the main EPS components such as polysaccharides, proteins, humic substances and glucuronic acids were analysed by spectrophotometry. Table 3 lists the percentages of each component accounted for in total EPS. For the EPS collected from planktonic cells, proteins and polysaccharides were the two dominant constituents. A small amount of humic substances was detected, which might result of dead cells. A low amount of glucuronic acids was also found in the EPS. After attaching to the pyrite surface, the EPS constituents changed due to the adaptation of the cells to a new life style. One of the most obvious changes

was that humic substances became the dominant component. The contents of proteins and polysaccharides decreased, but they were still major constituents. The amount of glucuronic acids increased more than 10 times above the value for planktonic cells.

Table 3. Chemical composition of the EPS collected from pyrite-grown planktonic cells and 3 months old of biofilms of *S. thermosulfidooxidans* grown on pyrite. Mean values are from at least 3 parallels.

EPS collected from	EPS constituent (% of total EPS)			
	Polysaccharides	Proteins	Humic substances	Uronic acids
Planktonic cells	24±9	47±26	5±4	0.2±0.2
Biofilms	18±0.3	21±7	42±5	3±3

4.5 Evaluation of pyrite bioleaching by *S. thermosulfidooxidans* under biofilm favoring conditions

Bioleaching efficiency of *S. thermosulfidooxidans*, when the medium was regularly exchanged, was evaluated by comparing with the results of cultivation under standard conditions (without any operation). Fig. 16 A shows the cell growth and the dissolved iron ions as a function of time under standard conditions. A fluctuation of cell numbers was observed in the first 2 days, indicating cell attachment and detachment. Afterwards the cell density kept decreasing, probably related to the reduced organic nutrition. The concentration of iron ions remained constant during the first 7 days of the experiment. The largest iron leaching rate was measured between day 7 and day 18. Afterwards the iron ion concentration remained

constant again, which indicates that the bioleaching had stopped. In total 195 mg iron ions were leached within 35 days. Fig. 16 B and C show the cell density and the concentration of iron ions in the spent medium before exchanging with fresh medium, respectively. The results indicate that the cell numbers in the leachate started to decrease considerably from day 18, but the concentration of iron ions decreased only slowly. Only 4.1 mg iron ions in total were dissolved within 35 d under these conditions, whereas under the standard conditions 195 mg iron ions in total had been dissolved. It is noticeable that the bioleaching stopped under the standard conditions after 18 d, whereas bioleaching continued if the medium was constantly exchanged. The degree of oxidation also provides information about the leaching efficiency. Fig. 17 A shows surfaces of a pyrite slice after 10 months of incubation. The surfaces are corroded, since several pits can be observed. The CLSM images of the pyrite slice surfaces indicate an average depth of the pits of 25±9 µm.

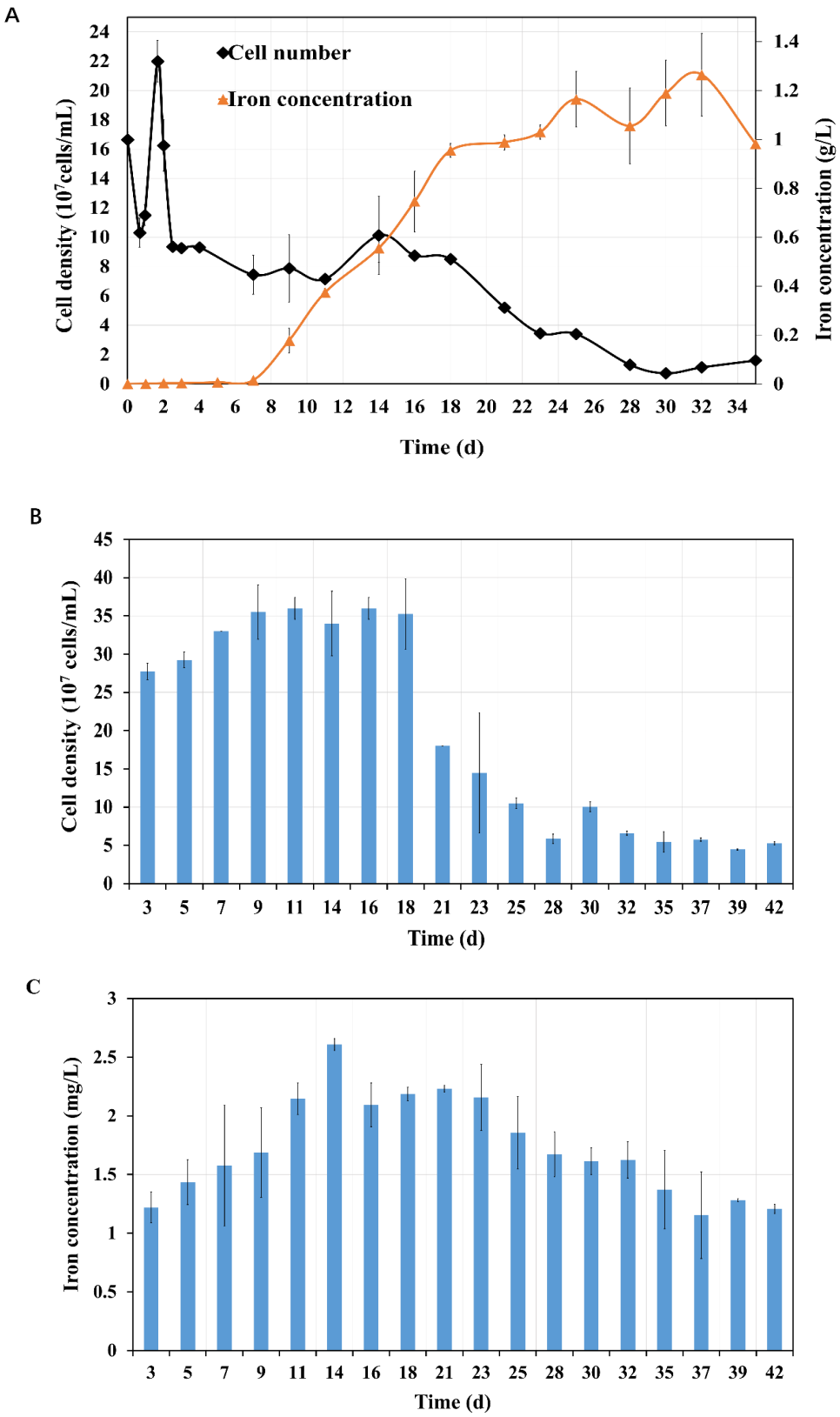

Fig. 16. Cell numbers of *S. thermosulfiooxidans* and dissolved iron ions concentration as function of time during bioleaching under standard conditions (A) or under the condition of exchanging exhausted medium with fresh medium (B and C). For the latter the data were recorded from the exhausted medium each time before discarding.

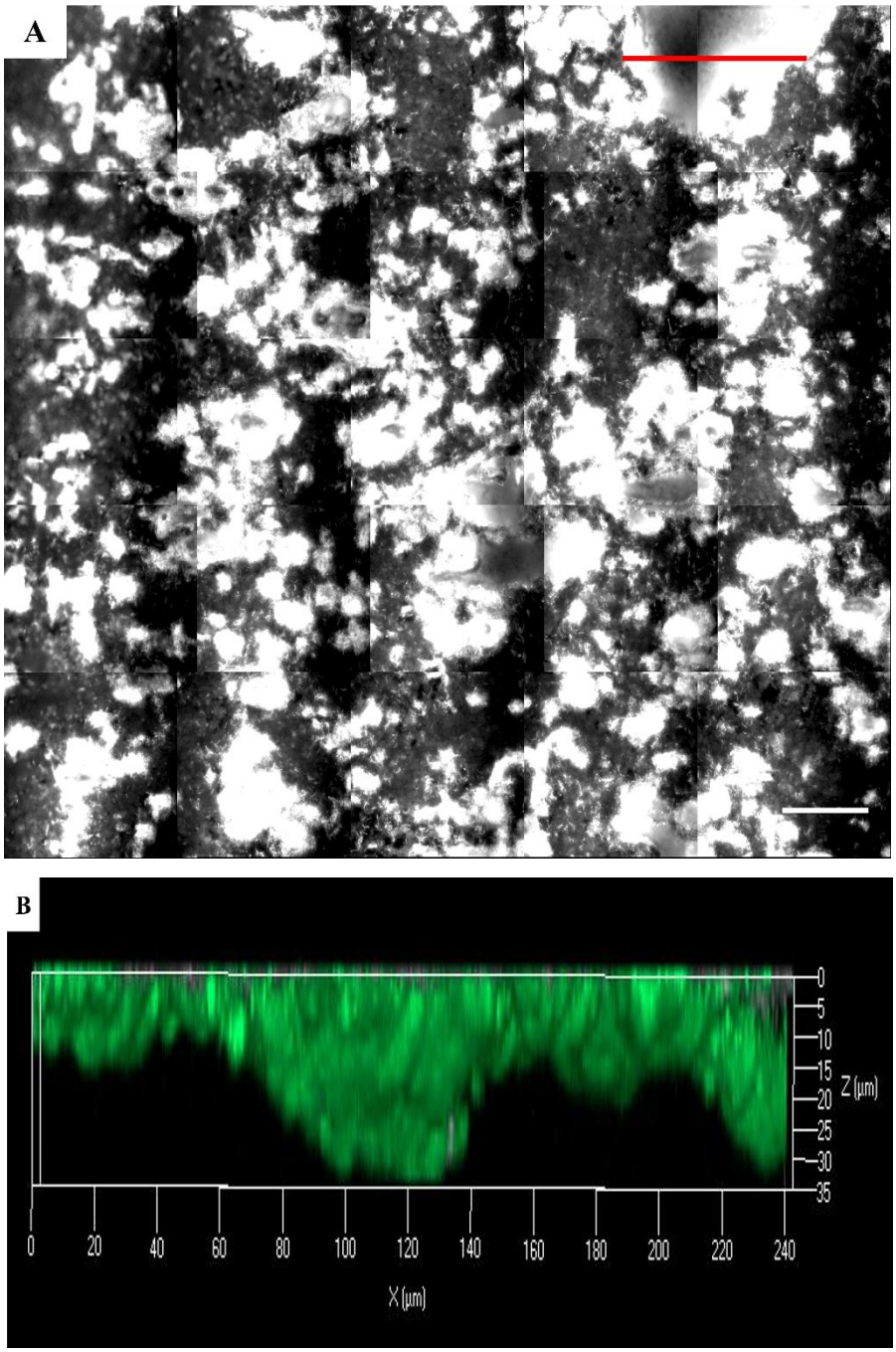

Fig. 17. EFM (A) and 3D CLSM images (B) of pyrite slices after 10 months of incubation under the condition of exchanging exhausted medium with fresh medium every 2 days. Image B is the cross-section view of surface topography in the area of image A labelled with a red line. Scale bar, 100 µm.

4.6 Adhesion to, biofilm formation on and bioleaching of pyrite by cells of *S. thermosulfidooxidans* in the presence of *L. ferriphilum*

Fig. 18 demonstrates how the number of cells attached to pyrite pre-colonized with *L. ferriphilum* changes as a function of time. Comparing with the control after 3 hours the percentage of attached cells of *S. thermosulfidooxidans* increased by around 5% if pyrite pre-colonized with living *L. ferriphilum* was used. However, the percentage decreased by approximately 5%, if the pyrite was pre-colonized with inactivated *L. ferriphilum*. Consequently, the biofilm formation by *S. thermosulfidooxidans* on pyrite in the presence of cells of *L. ferriphilum* was followed. Fig. 19 shows the biofilm formation by either a pure culture of *S. thermosulfidooxidans* or a pure culture of *L. ferriphilum* on sterile pyrite within 14 days. A pure culture of *S. thermosulfidooxidans* as does not form biofilms, but well-formed biofilms can be observed in case of *L. ferriphilum*. Fig. 20 illustrates the biofilm formation after 14 days by *S. thermosulfidooxidans* on pyrite if its occurring in the presence of *L. ferriphilum*. The cells of *S. thermosulfidooxidans* are rod-shaped, while the cells of *L. ferriphilum* are small and vibrioid-shaped, thus allowing them to be distinguished under the microscope. In all three cases after 14 days of incubation the biofilms of *S. thermosulfidooxidans* grow on pyrite. This indicates that *S. thermosulfidooxidans* can form biofilms on pyrite in the presence of *L. ferriphilum*. However, the architecture of these biofilms of *S. thermosulfidooxidans* is different. Many single cells of *S. thermosulfidooxidans* are observed on the pyrite if it is pre-colonized with

living cells of *L. ferriphilum*. In the other two cases biofilms of *S. thermosulfidooxidans* grow in the form of a colony. In all three cases physical contact between cells of *S. thermosulfidooxidans* and of *L. ferriphilum* can be observed. This is visible in the images of the EFM and the AFM (Fig. 21). The AFM images show cells of *L. ferriphilum* in colonies of *S. thermosulfidooxidans*.

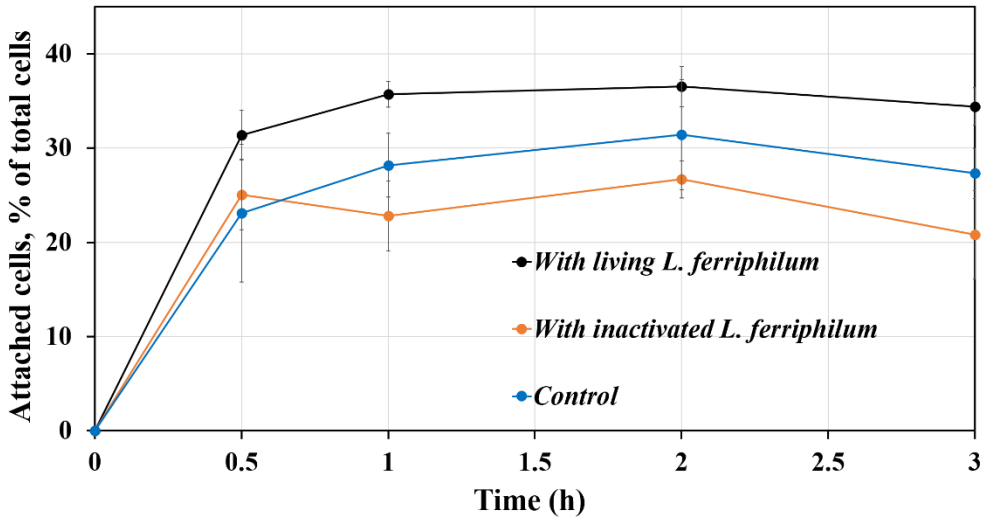

Fig. 18. Adhesion of sulfur-grown cells of *S. thermosulfidooxidans* to pyrite pre-colonized by a 1 day old biofilm of *L. ferriphilum* within 3 hours under 45°C. Sterile pyrite was used in control.

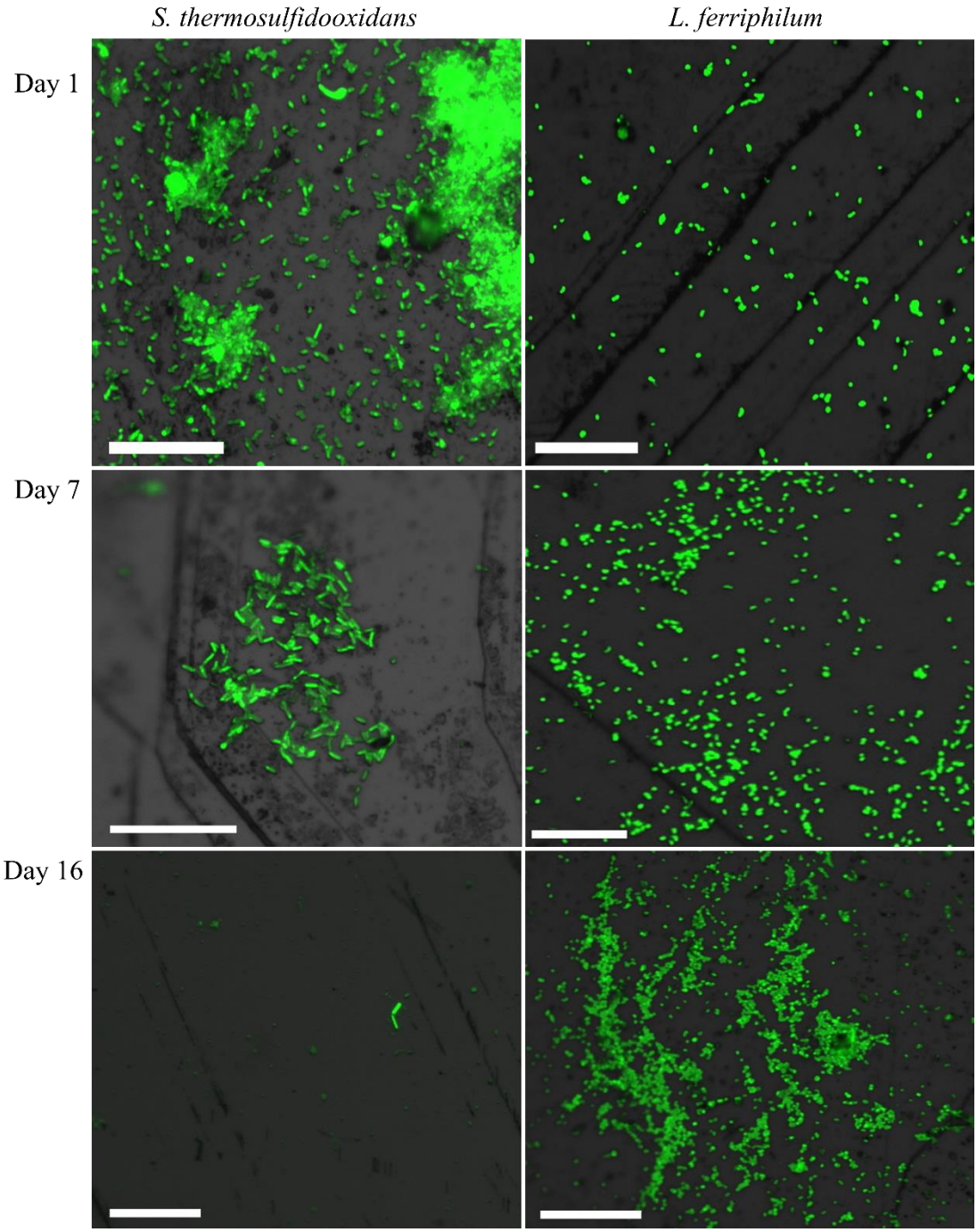

Fig. 19. EFM images show biofilm formation on pyrite slices by a pure culture of *S. thermosulfidooxidans* under 45ºC without exchanging medium or *L. ferriphilum* under 37ºC. Scale bar, 20 µm.

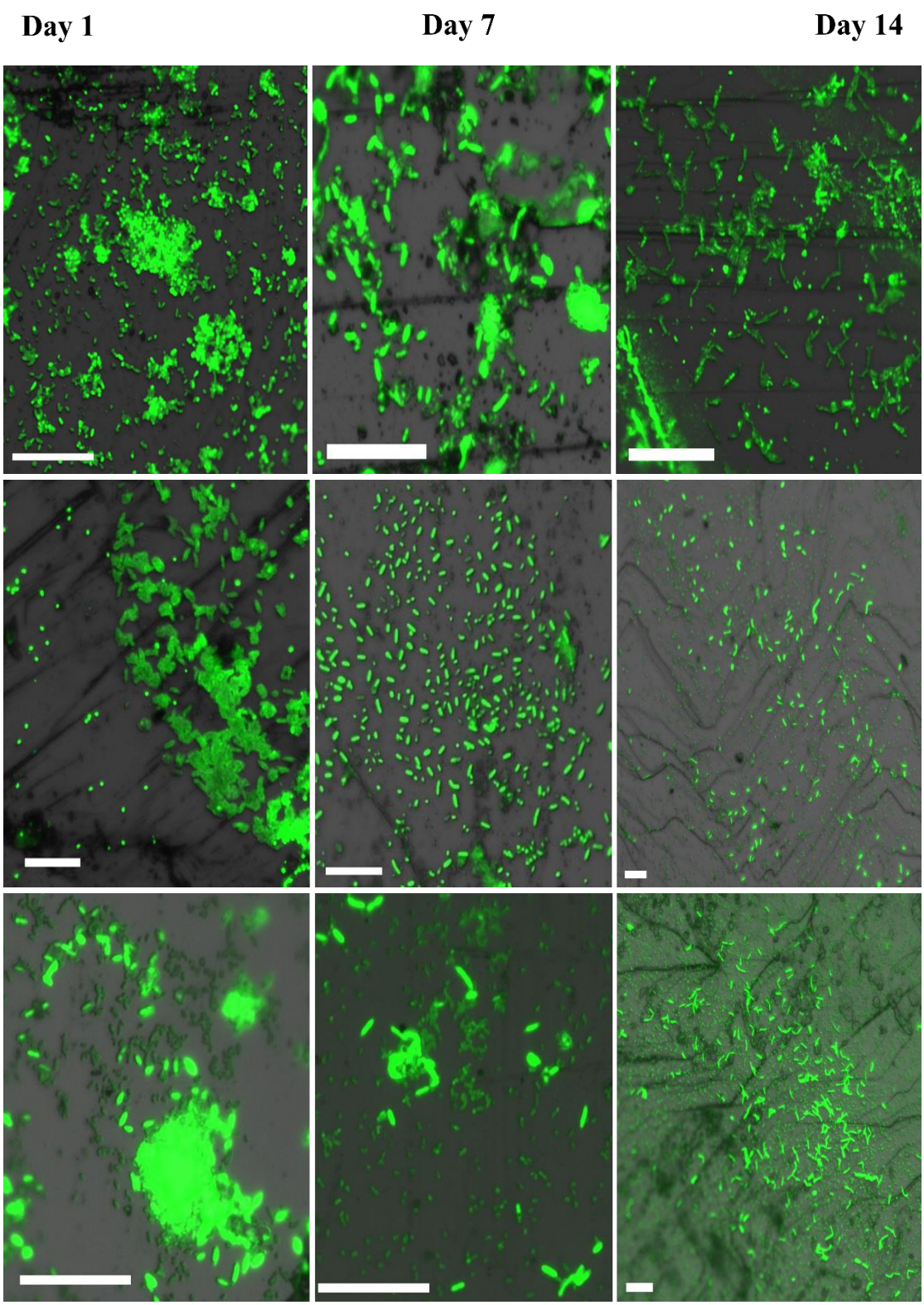

Fig. 20. Biofilm formation by cells of *S. thermosulfidooxidans* on pyrite in the presence of cells of *L. ferriphilum* under 45ºC without exchanging medium. The biofilms developed in three cases: inoculum consisting of *S. thermosulfidooxidans* and *L. ferriphilum* incubated with clean pyrite (the first row); *S. thermosulfidooxidans* incubated with pyrite pre-colonized by a 1 day old living (the second row) or inactivated (the third row) biofilm of *L. ferriphilum*. Scale bar, 20 µm.

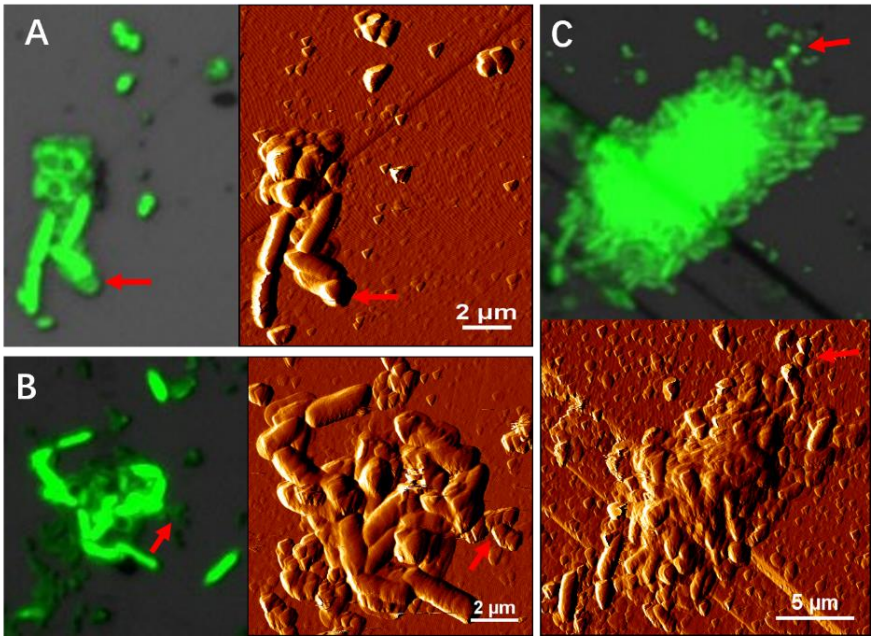

Fig. 21. AFM and EFM images show the physical contact between cells of *S. thermosulfidooxidans* and cells of *L. ferriphilum* during biofilm formation on pyrite under 45°C without exchanging medium. The biofilms developed in three cases: *S. thermosulfidooxidans* incubated with pyrite pre-colonized by 1 day old living (A) or inactivated (B) biofilm of *L. ferriphilum*; inoculum consisting of *S. thermosulfidooxidans* and *L. ferriphilum* incubated with clean pyrite (C). All the red arrows in images indicate the cells of *L. ferriphilum*. Scale bar, 20 µm.

The leaching efficiency of *S. thermosulfidooxidans* for pyrite by in the presence of cells of *L. ferriphilum* was tested. The results are shown in Fig. 22. The decreasing pH values indicates that the bioleaching was ongoing. Since *L. ferriphilum* can oxidize only ferrous iron for energy, the pH value decreased least compared to the assays with mixed cultures. After 16 days of leaching most iron had been leached by *L. ferriphilum* giving a final concentration of 1.5 g/L, followed by binary culture of *S. thermosulfidooxidans* and *L. ferriphilum* with a concentration of 1 g/L. Although in the first 14 days, lower amount of iron was leached by pure culture of *L. ferriphilum* than by binary culture of *S. thermosulfidooxidans*

and *L. ferriphilum*, at the end of the experiments the two assays leached almost the same amount of iron. No matter whether the pyrite was pre-colonized with living or inactived cells of *L. ferriphilum*, cultures of *S. thermosulfidooxidans* performed worst and only 0.5 g/L or 0.3 g/L of iron ions were detectable, respectively.

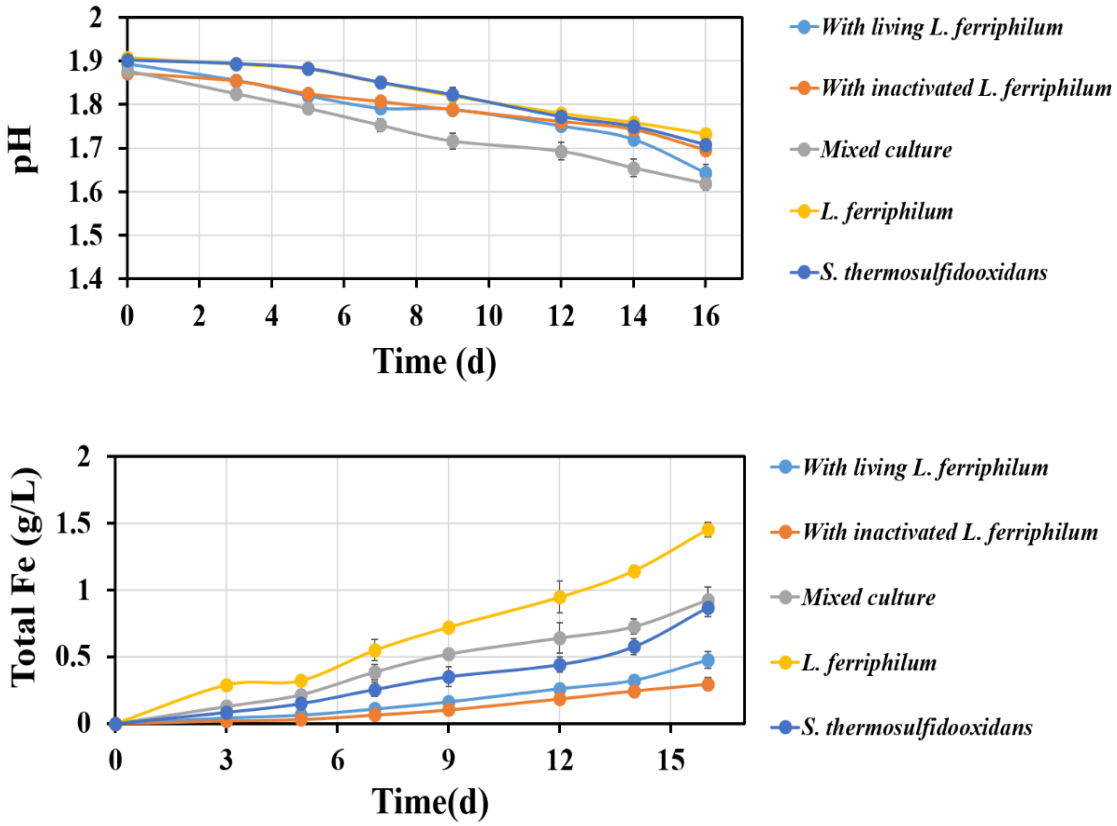

Fig. 22. Changes of pH and total iron ion concentration as a function of time during pyrite leaching by pure culture of *S. thermosulfidooxidans* or pure culture of *L. ferriphilum* or binary culture of these two under 45°C without exchanging medium. The assays contained: *S. thermosulfidooxidans* incubated with pyrite pre-colonized by 1 day old living (marked as "With living *L. ferriphilum*") or inactivated (marked as "With inactivated *L. ferriphilum*") biofilm of *L. ferriphilum*; inoculum consisting of *S. thermosulfidooxidans* and *L. ferriphilum* incubated with clean pyrite (marked as "Mixed culture"); pyrite colonized by 1 day old biofilm of *L. ferriphilum* incubated in fresh medium (marked as "*L. ferriphilum*"); *S. thermosulfidooxidans* incubated with clean pyrite (marked as "*S. thermosulfidooxidans*").

4.7 Bioleaching of pyrite by *S. thermosulfidooxidans* in pyrite leachate from a *L. ferriphilum* culture

Fig. 23 shows pyrite leaching by cells of *S. thermosulfidooxidans* with different pyrite leachates from a *L. ferriphilum* culture. Images A-E show changes of iron ion concentration, density of planktonic/biofilm cells and pH during pyrite leaching and final biofilm formation on pyrite by cells of *S. thermosulfidooxidans* in fresh medium without addition of yeast extract. These are the control experiment data. In the first 12 days the iron concentration in the leachate increased gradually to 260 mg/L. Finally 300 mg/L were measured. The final leached iron ions was totally in the form of ferrous iron. The pH of the leachate decreased also and it decreased most rapid by the first 15 days. The numbers of the planktonic cells in the leachate decreased: from the initial cell density of $1.1x10^8$ cells/mL to the final cell density of $4x10^6$ cells/mL. The number of attached biofilm cells was monitored during the leaching. The results are shown in image C. The bar chart clearly shows that the number of attached biofilm cells increased during the leaching. Finally the pyrite surfaces were colonized with $5x10^6$ cells/cm^2 (images D and E). Images F and G, H and I as well as J and K show, how each parameter changes during pyrite leaching by *S. thermosulfidooxidans*, if 3 day, 7 day or 14 day old pyrite leachate from *L. ferriphilum* is used, respectively. Here one assay was done and set as a control: ferric chloride was manually added into fresh medium. The

amount of iron ions added was equal with that detected in the pyrite leachate from *L. ferrriphilum*. Finally cells of *S. thermosulfidooxidans* were inoculated. Although three different leachates were used, similar results were obtained. 1) *S. thermosulfidooxidans* performed leaching better in the assay with an initial iron addition than in the assay with leachate only; 2) The dissolved iron occurred mostly in the form of ferrous iron; 3) The pH values of the leachate and the cell density of the planktonic cells of *S. thermosulfidooxidans* decreased during leaching; 4) The number of attached biofilm cells increased (image J).

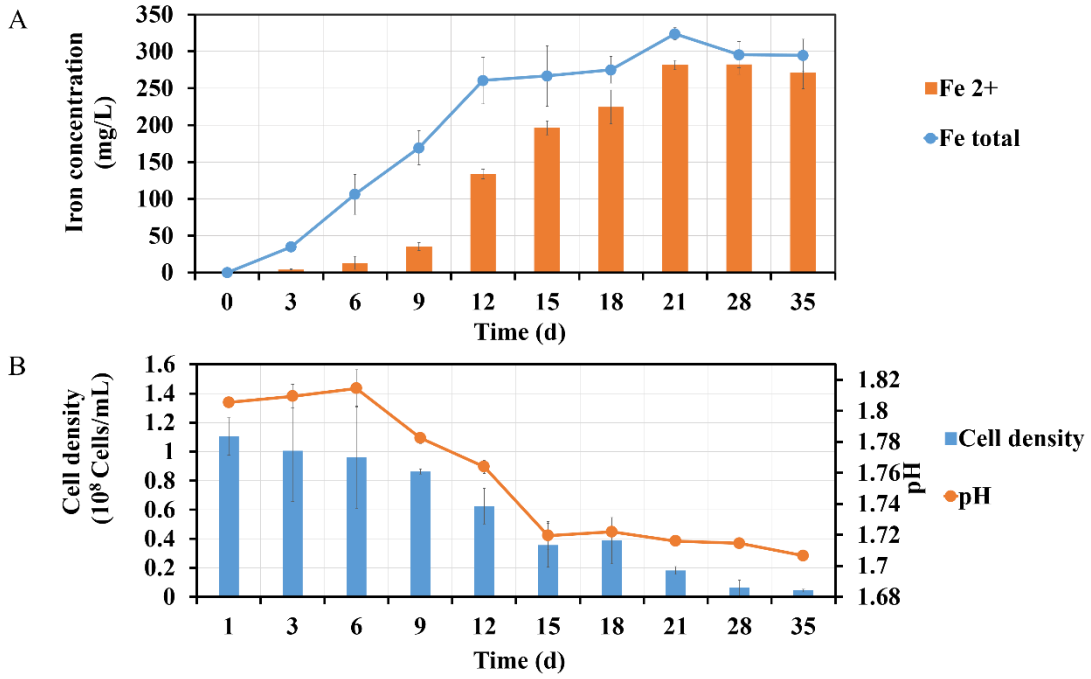

C

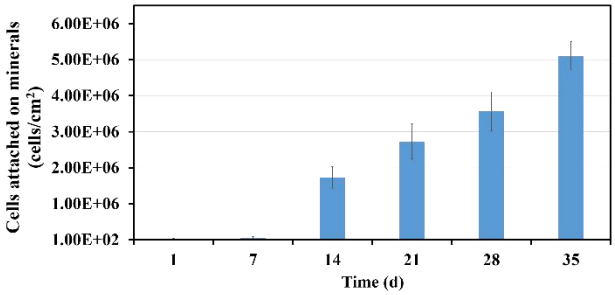
Cells attached on minerals (cells/cm²)
6.00E+06
5.00E+06
4.00E+06
3.00E+06
2.00E+06
1.00E+06
1.00E+02
1
7
14
21
28
35
Time (d)

D

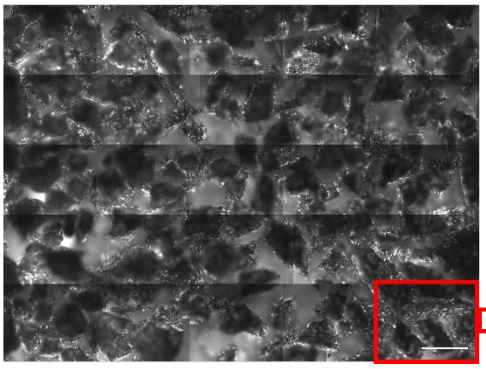

E

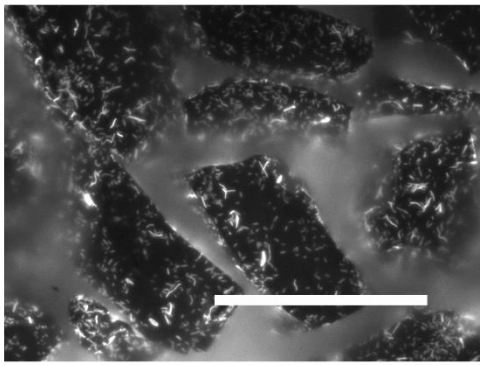

F

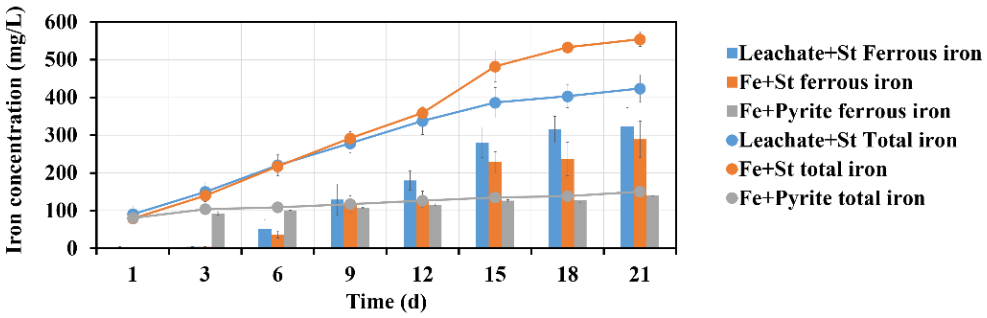
Iron concentration (mg/L)
600
500
400
300
200
100
0
1
3
6
9
12
15
18
21
Time (d)
Leachate+St Ferrous iron
Fe+St ferrous iron
Fe+Pyrite ferrous iron
Leachate+St Total iron
Fe+St total iron
Fe+Pyrite total iron

G

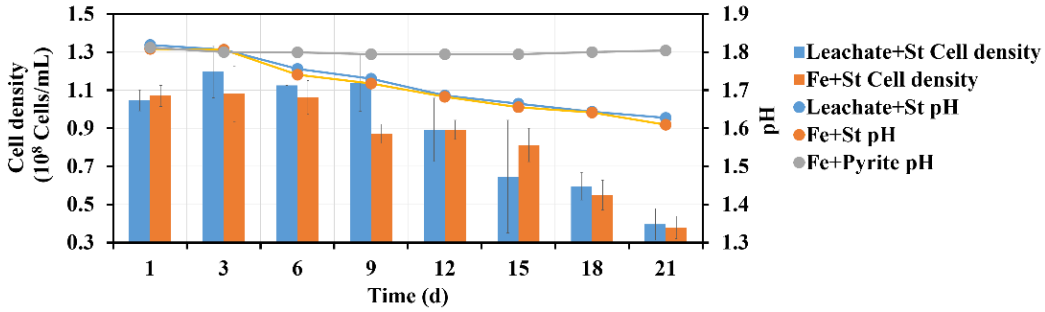
Cell density (10⁸ Cells/mL)
1.5
1.3
1.1
0.9
0.7
0.5
0.3
pH
1.9
1.8
1.7
1.6
1.5
1.4
1.3
1
3
6
9
12
15
18
21
Time (d)
Leachate+St Cell density
Fe+St Cell density
Leachate+St pH
Fe+St pH
Fe+Pyrite pH

H

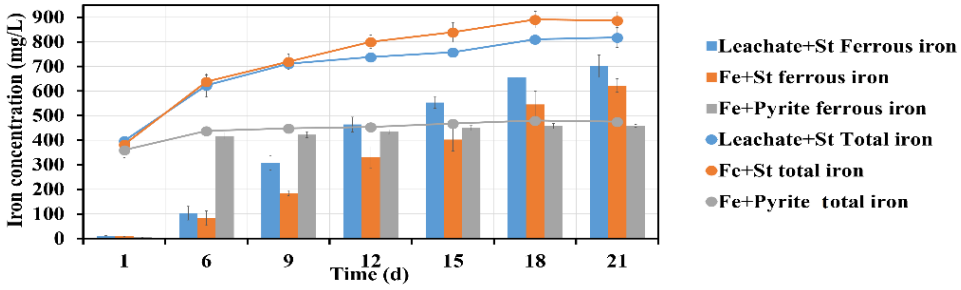
Iron concentration (mg/L)
900
800
700
600
500
400
300
200
100
0
1
6
9
12
15
18
21
Time (d)
Leachate+St Ferrous iron
Fe+St ferrous iron
Fe+Pyrite ferrous iron
Leachate+St Total iron
Fe+St total iron
Fe+Pyrite total iron

I

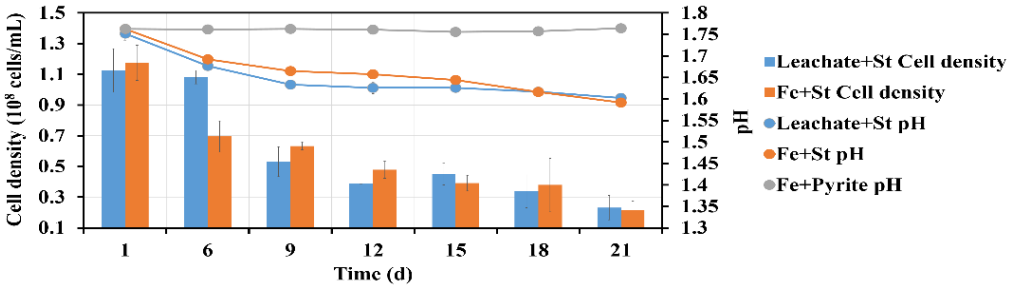
Cell density (10⁸ cells/mL)
1.5
1.3
1.1
0.9
0.7
0.5
0.3
0.1
pH
1.8
1.75
1.7
1.65
1.6
1.55
1.5
1.45
1.4
1.35
1.3
1
6
9
12
15
18
21
Time (d)
Leachate+St Cell density
Fe+St Cell density
Leachate+St pH
Fe+St pH
Fe+Pyrite pH

J

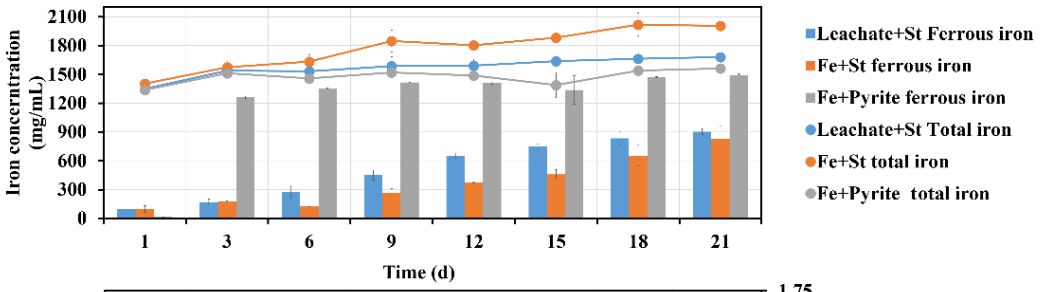
Iron concerntration (mg/mL)
2100
1800
1500
1200
900
600
300
0
1
3
6
9
12
15
18
21
Time (d)
Leachate+St Ferrous iron
Fe+St ferrous iron
Fe+Pyrite ferrous iron
Leachate+St Total iron
Fe+St total iron
Fe+Pyrite total iron

K

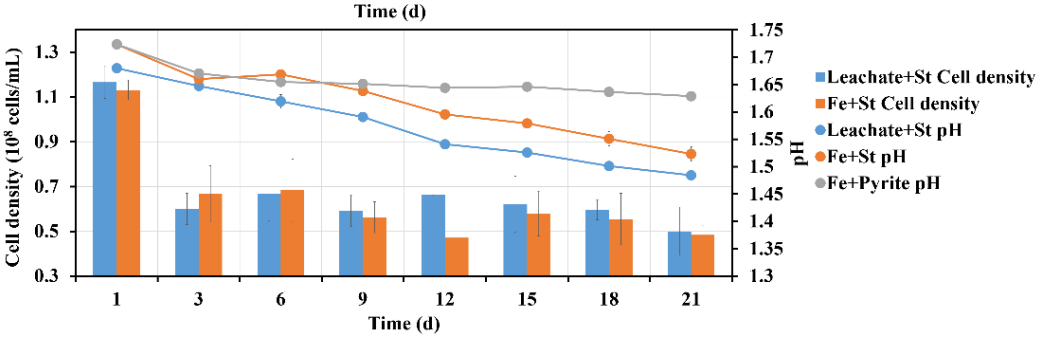
Cell density (10⁸ cells/mL)
1.3
1.1
0.9
0.7
0.5
0.3
pH
1.75
1.7
1.65
1.6
1.55
1.5
1.45
1.4
1.35
1.3
1
3
6
9
12
15
18
21
Time (d)
Leachate+St Cell density
Fe+St Cell density
Leachate+St pH
Fe+St pH
Fe+Pyrite pH

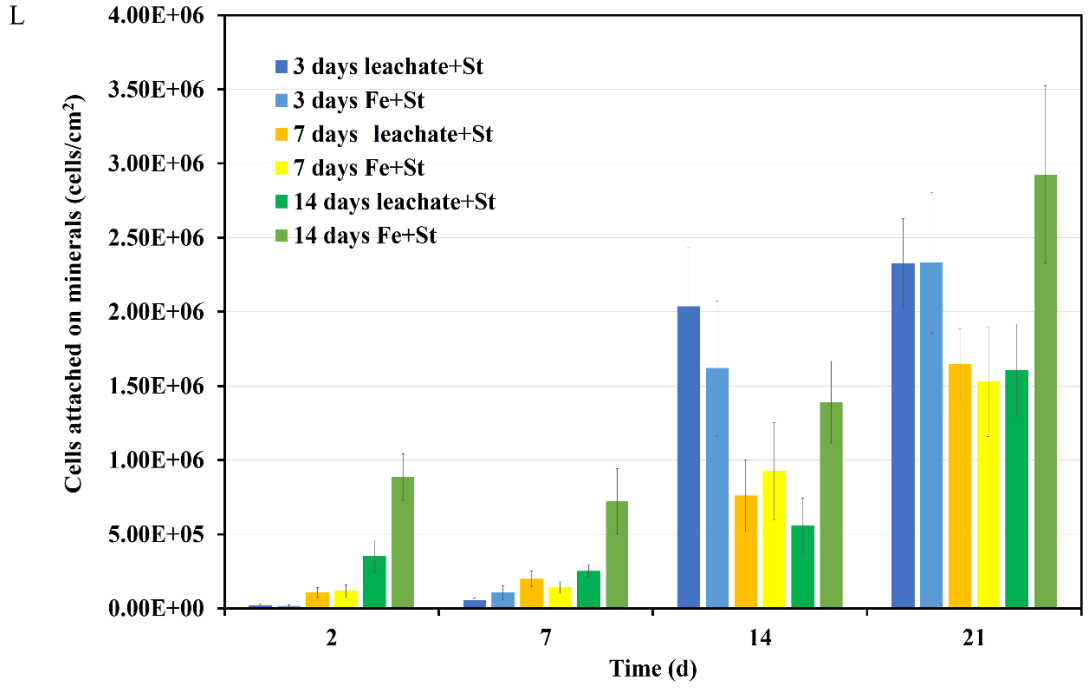

Fig. 23. Changes of iron ion concentration, density of planktonic/biofilm cells and pH during pyrite leaching by *S. thermosulfidooxidans* in MAC medium or in MAC medium with ferric iron ions added or in pyrite leachate from a *L.ferriphilum* culture. All the experiments were operated under 45°C without yeast extracts addition. A, B, C, D and E demonstrate pyrite leaching by *S. thermosulfidooxidans* in MAC medium: A and B illustrate the changes of iron ion concentration, density of planktonic cells and pH during leaching; C shows the number of biofilm cells on pyrite during leaching; D and E are EFM images showing the biofilms formed on pyrite after 35 days of leaching. Scale bar, 100 µm. Images F-K demonstrate the changes of iron ion concentration, cell density and pH during pyrite leaching by *S. thermosulfidooxidans* in 3 days (F and G), 7 days (H and I) or 14 days (J and K) pyrite leachate collected from a *L. ferriphilum* culture. Image L shows the number of biofilm cells of *S. thermosulfidooxidans* on pyrite. Leachate + St, *S. thermosulfidooxidans* performs pyrite leaching in pyrite leachate collected from *L. ferriphilum*; Fe + St, *S. thermosulfidooxidans* performs pyrite leaching in MAC medium with initial addition of same amount of iron ions detected in the pyrite leachate collected from *L. ferriphilum*; Fe + pyrite, pyrite leaching in MAC medium only with initial addition of same amount of iron detected in the pyrite leachate collected from *L. ferriphilum*.

4.8 Biofilm formation on sulfur by *S. thermosulfidooxidans* and mechanical changes of cell surfaces in transition from planktonic to biofilm growth

Information on the morphology of sulfur-grown planktonic cells of *S. thermosulfidooxidans* and their biofilm cells on sulfur slices as well as information on mechanical properties of their surfaces is shown in Fig. 24. Image A shows immobilized planktonic cells on a glass slide after incubation in basic MAC medium without any substrata for 4 hours. The cells adhere to the glass slides in form of a cluster. Images B, C and D show a typical progress of biofilm formation. After a reversible adhesion, the bacteria started to attach on the surfaces irreversibly by EPS (Fig. 24 B). Then more EPS produced to help the bacteria to firmly attach on the surfaces and they were proliferating (Fig. 24 C and D). It is noticed that *S. thermosulfidooxidans* could easily colonize on sulfur surface and no extra operation was needed to enhance the biofilm formation, which is different from the case that growing with pyrite. During the process the surface properties of the cells changed, which is shown in the adhesion force maps and Young's modulus maps.

The values for adhesion force in the charts indicate that the adhesiveness of the biofilm surfaces changes with prolonged incubation time. After 4 hours of incubation the interaction between the biofilm surface and silicon nitride cantilevers were weaker than those between the sulfur surface and the cantilever. Later on, the interaction between the biofilm surface and the cantilever increased gradually as the colour for the biofilms in image C1 becomes lighter than B1. After 5 days of incubation the interactions were

much larger than at beginning. The Young's modulus map images illustrate that the elasticity of the cell surfaces also changed. Planktonic cells were soft, which is indicated by black colour in image A2. The cell surfaces increased stiffness after transition to biofilm growth (Fig. 24 B2). The stiffness kept increasing during the biofilm formation as the colour indicated (Fig. 24 C2 and D2). Table 4 summarizes the values for adhesion force and Young's modulus. The data show that the adhesion forces between the cells and the cantilever decreased, in case cells of *S. thermosulfidooxidans* changed from planktonic to biofilm growth. However, afterwards the adhesion forces increased again in the course of biofilm formation. The Young's modulus values increased constantly demonstrating that cellular stiffness increased in the process of biofilm formation.

Table 4 Adhesion forces between a silicon nitride cantilever and planktonic cells or biofilms of *S. thermosulfidooxidans* and Young's modulus values for the cells during growth on sulfur, n=8192. The data for the planktonic cells are given as "0 day".

Incubation time	Adhesion force (pN)	Young's modulus (MPa)
0 day	57.9±15.2	0.2±0.08
4 hours	13.5±2.2	0.3±0.2
2 days	21.1±5.5	0.8±0.4
5 days	124.4±13.9	2.3±1.4

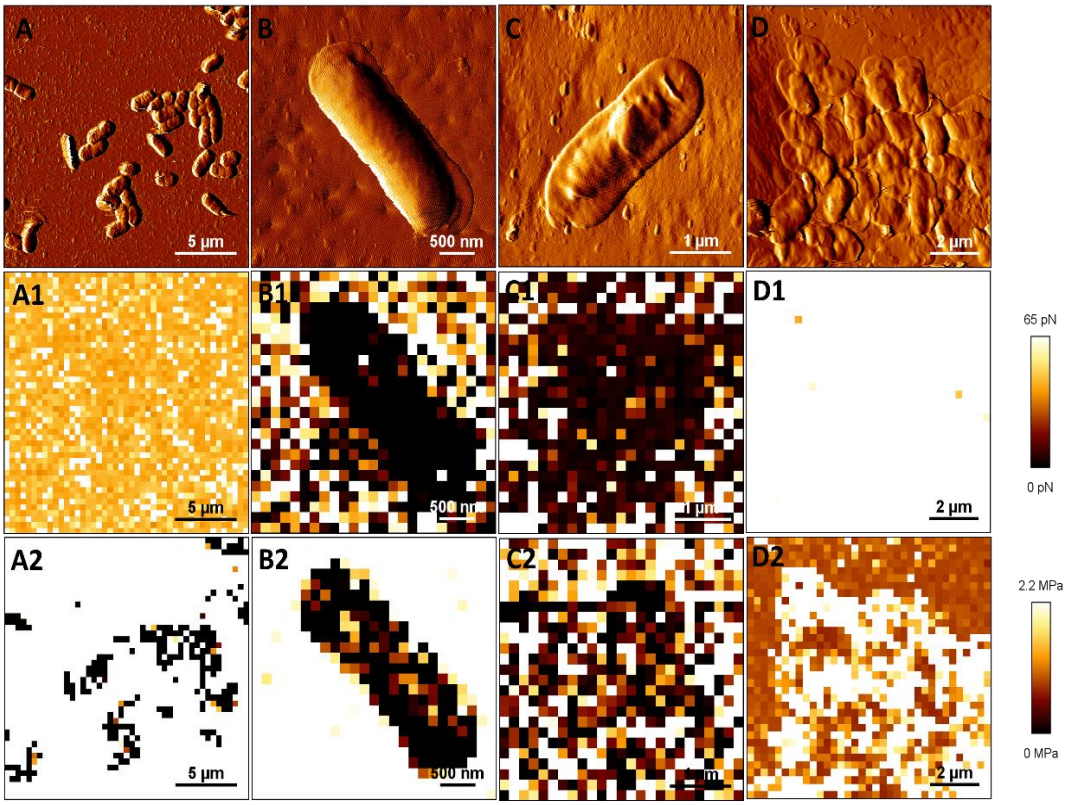

Fig. 24. Morphology, adhesiveness and stiffness of cells of *S. thermosulfidooxidans* on glass or sulfur. A-D are AFM vertical deflection images. A shows planktonic cells of *S. thermosulfidooxidans* immobilized on a glass slide; B, C, D and E show 4 hours, 2 and 5 days old cells of *S. thermosulfidooxidans* on sulfur. A1 and A2, B1 and B2, C1 and C2, D1 and D2 are the force maps and Young's modulus maps of images A, B, C and D, respectively. Force map shows the distribution of adhesion forces between the scanned area and the AFM tip. Young's modulus map shows the distribution of stiffness.

4.7 Chemical changes of cell surfaces for sulfur-grown *S. thermosulfidooxidans* in transition from planktonic to biofilm growth

The composition of EPS from sulfur-grown planktonic or biofilm cells was analysed by ATR-FTIR. The results are shown in Fig. 25. The spectra indicate that the EPS of the planktonic cells are composed mainly of proteins (based on the peak area centred at 1645 cm^{-1}, 1542 cm^{-1}, 1455 cm^{-1} and 1398 cm^{-1}) and polysaccharides (peak area centred at around 1114 cm^{-1}) [82]. A peak centred at 671 cm^{-1} indicates that also thiosulfate occurs

in the EPS [88]. The spectrum for the EPS of sulfur-grown biofilm cells is quite different. There are five distinguishable peaks. The peaks related to proteins centred at 1645 cm^{-1} and 1398 cm^{-1} are small. The peaks representing polysaccharides centred at 1114 cm^{-1}, 1038 cm^{-1} and 996 cm^{-1} are well formed and dominated [34, 35]. The peaks in the region between 1200 and 900 cm^{-1} may have been caused also by the stretching vibrations of phosphate in or on the cell [36, 37]. Based on the FTIR data, we chose the main EPS components as indicators and analysed the chemical composition by spectrophotometry. The results are presented in Table 5. 67.7% of the total EPS collected from planktonic cells could be analysed, but only 31% of total EPS collected from biofilm cells were analysable. For the EPS from planktonic cells proteins are the dominant components followed by polysaccharides. Also low amounts of humic substances are found but uronic acids are not detectable. For the EPS from biofilm cells polysaccharides and humic substances become dominant with 16% or 12%, respectively. The proteins decreased to 2% only. However, uronic acids were present with 1%.

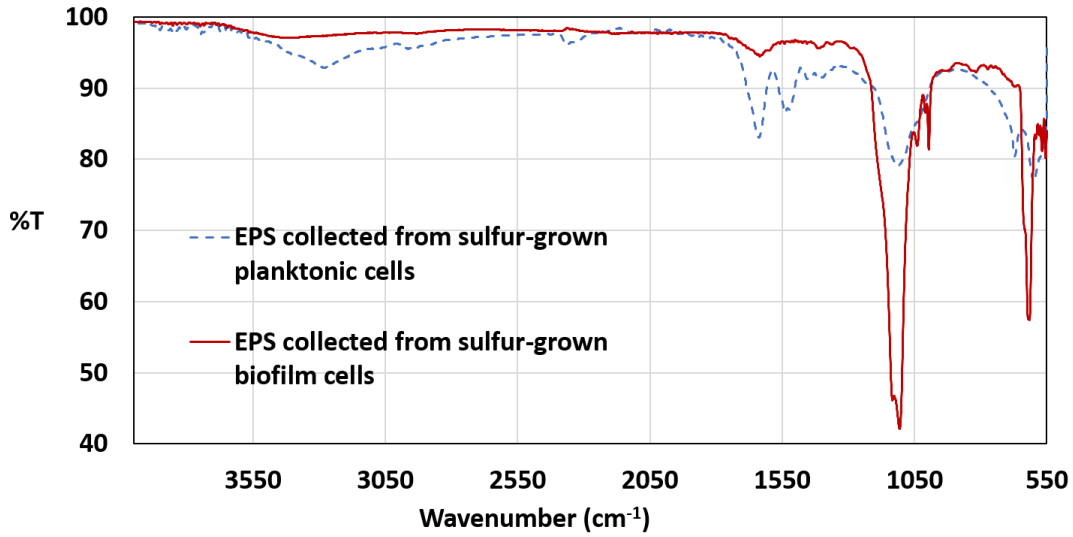

Fig. 25. ATR-FTIR spectral analysis of EPS collected from sulfur-grown planktonic/biofilm cells of *S. thermosulfidooxidans*. The blue dashed and the red solid lines show the spectra of EPS collected from planktonic cells and biofilms of *S. thermosulfidooxidans*, respectively.

Table 5 Chemical composition of the EPS collected from sulfur-grown planktonic/biofilm cells of *S. thermosulfidooxidans*. Mean values are from at least 3 parallels.

EPS collected from	EPS constituent (% of total EPS)			
	Polysaccharides	Proteins	Humic substances	Uronic acids
Sulfur-grown planktonic cells	14±4	53±18	0.7±0.5	b.d.
Sulfur-grown biofilm cells	16±5	2±1	12±5	1±0.04

b.d., below detection limit

4.8 Quantification of adhesion forces between cells of *S. thermosulfidooxidans* and substrata by AFM: cantilevers with mineral tips

Due to their construction mineral probes cannot be used for image scanning in the normal mode, but only in the force mapping mode. Images are

produced as matrices of force-distance curves. Consequently, the more force measurements one produces, the more details one can obtain, but also the more time is needed. Thus, it is crucial to find a method, which allows to firmly immobilize planktonic bacteria on a substratum to withstand the long-time measuring. Three methods were tested and the results are shown in Fig. 26. Images A, B and C show cells of *S. thermosulfidooxidans* immobilized on a glass slide by glutaraldehyde, poly-L-lysine (PLL) and polyethyleneimine (PEI), respectively. In all cases the cells could be immobilized. However, with glutaraldehyde the surfaces of the cells were denatured, since no rod-shaped cells are visible in Fig. 26 A. Both PLL and PEI performed well, but PEI is preferable, since the glass slide was covered fully with cells, whereas with PLL the glass slide was not fully covered. The magnified images (Fig. 26 D, E and F) prove that the glass slide is fully covered by multiple layered cells.

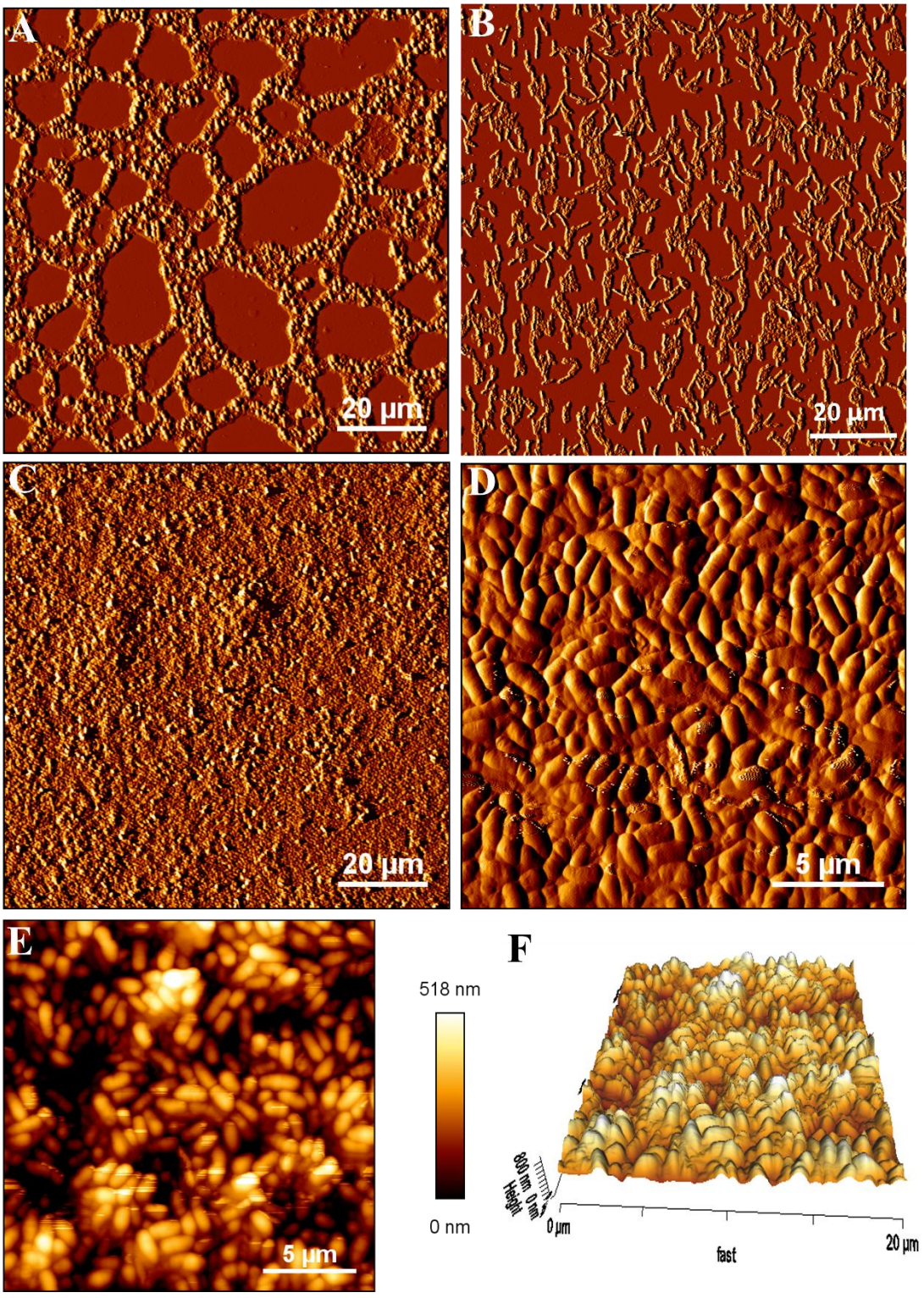

Fig. 26. AFM images of pyrite-grown planktonic cells of *S. thermosulfidooxidans* immobilized on glass slides by glutaraldehyde (A), PLL (B) or PEI (C). D is a magnified image of C. E and F are height and 3D images of D, respectively.

Fig. 27 A shows an AFM height image of pyrite-grown planktonic cells of *S. thermosulfidooxidans* immobilized on a glass slide by PEI, which was recorded by a pyrite-modified cantilever. Although individual bacteria cannot be distinguished well because of the low amount of pixels, the fully colonized surface and a rough morphology of the cells are visible. Fig. 27 B is the respective adhesion force map, which shows the distribution of the adhesion forces between the pyrite probe and the immobilized cells in the selected area. The histogram of adhesion forces (Fig. 27 C) is obtained from 8192 force curves from two independent experiments. It indicates that the adhesion forces between pyrite cantilever and pyrite-grown planktonic cells range from 1.6 to 4.1 nN. The Gaussian fit determines the maximum at 2.6±0.3 nN. Dense biofilm cells of *S. thermosulfidooxidans* on pyrite can be seen in Fig. 28 A, an AFM height image (100 x 100 µm) scanned with a silicon nitride probe. Fig. 28 B is a height map image (50 x 50 µm) acquired by the pyrite probe. It shows the framed area in Fig. 28 A. Fig. 28 C and D are the height map image and the adhesion force map image of the selected area framed in B. The adhesion forces between the pyrite cantilever and the biofilm cells range from 55 to 175 pN. The Gaussian fit gives a maximum at 77.3±7.1 pN.

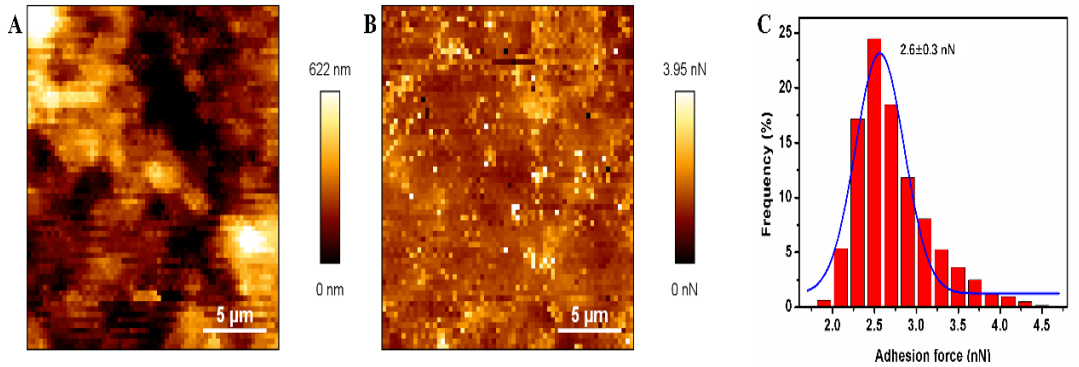

Fig. 27. AFM height map (A), adhesion force map (B) and adhesion force histogram image (C) of pyrite-grown planktonic cells of *S. thermosulfidooxidans* immobilized on glass surfaces, mapped by a pyrite tip in MAC medium, pH 2.5. The adhesion force histogram (n=8192) reveals a distribution of adhesion forces with maximum at 2.6±0.3 nN, as determined by a Gaussian fit.

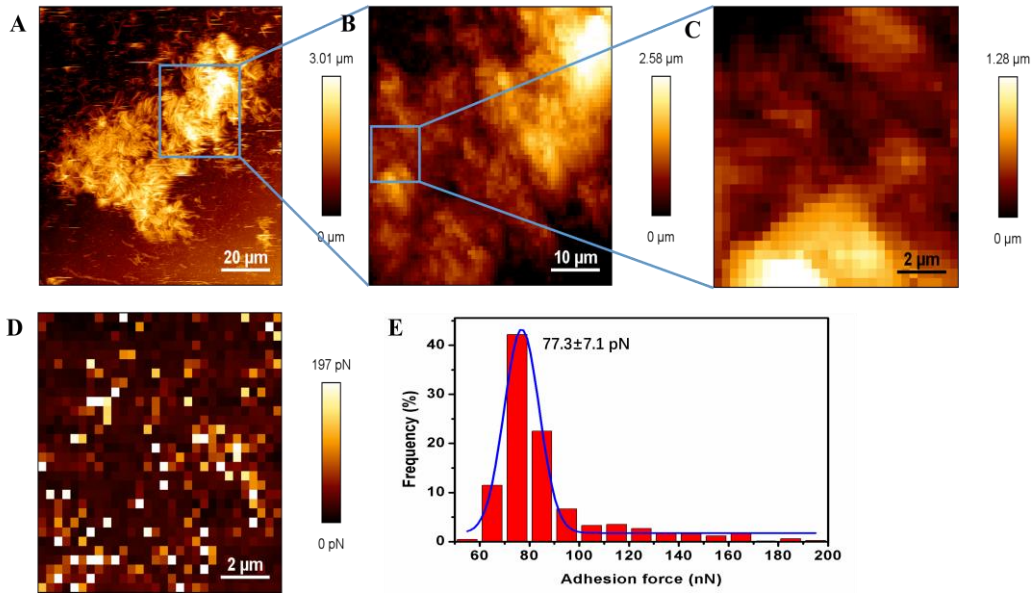

Fig. 28. AFM height map (A), adhesion force map (B) and adhesion force histogram image (C) of biofilm cells of *S. thermosulfidooxidans* grown on pyrite, mapped by a pyrite tip in MAC medium, pH 2.5. The adhesion force histogram (n=8192) reveals a distribution of adhesion forces with maximum at 77.3±7.1 pN, as determined by a Gaussian fit.

Since the pyrite probes functioned well with both planktonic cells and biofilm cells, chalcopyrite probes were also tested. Adhesion forces between silicon nitride cantilevers and cells were measured as control. Table 6 lists the adhesion forces between differently pregrown cells of *S. thermosulfidooxidans* and differently modified cantilever tips. The data

indicate that both pyrite- and sulfur-grown planktonic cells were more adhesive to pyrite tips, with adhesion forces of 2.7 and 2.2 nN, than to chalcopyrite or silicon nitride tips with adhesion forces of 0.13 or 0.12 and 0.06 nN. The adhesion forces between the biofilm cells and the three types of tips were low and more or less in the same range.

Table 6 Adhesion forces in nN between cells of *S. thermosulfidooxidans* and different substrata measured by AFM in MAC medium, pH 2.5, n=8192.

Adhesion force (nN)	Pyrite-grown planktonic cells	Sulfur-grown planktonic cells	Pyrite-grown biofilm cells	Sulfur-grown biofilm cells
Pyrite tip	2.7±0.4	2.2±0.3	0.10±0.07	0.08±0.03
Chalcopyrite tip	0.13±0.1	0.13±0.07	0.09±0.04	0.05±0.004; 0.02±0.002
Silicon nitride tip	0.12±0.02	0.06±0.02	0.02±0.01	0.02±0.01

5. Discussion

Adhesion to, biofilm formation on and bioleaching of pyrite. Bacterial biofilms are formed by adhesion of individual planktonic cells to a surface. This is a complex and highly regulated developmental process. Motility is required for this process [25, 26, 89]. Planktonic cells may initiate interactions with a surface in response to various signals such as nutrients. Motility enables planktonic cells to swim towards nutrients associated with a surface or towards signals generated by attached cells. In addition, there may be kinds of repulsive forces between planktonic cells and a surface and motility can help the cells to overcome it, thereby reaching the surface. After attachment motility may be required to spread daughter-cells of the attached cells along the surface. In our study, sulfobacilli are used for biofilm formation. However, these are non-motile acidophiles. This may in part account for their poor capability to adhere to and subsequently to form a biofilm on pyrite. Because of this lack of motility, cells of *S. thermosulfidooxidans* can only attach to pyrite surfaces by accident, passively, e.g. by convection or turbulences. In addition, not all sites are suitable for attachment and further colonization, because only at imperfections of the mineral surface, where the crystal structure can be easily destroyed [5, 90], nutrients are available. Cell detachment will occur, which leads to a poor biofilm formation. Biofilms in form of cell clusters were observed, when *S. thermosulfidooxidans* was incubated with pyrite

slices. When cells were incubated with a limited number of pyrite slices at a reduced shaking speed, large flat surfaces and reduced shearing forces provided a chance to facilitate their attachment to the surface. Using a genetic technique Pratt and Kolter obtained motility-defective mutants of *E. coli*. They found that these mutants attached poorly to the substratum, and the few cells that did attach were often located in small dense clusters [26]. Such behaviour like poor adhesion to pyrite and initial biofilm formation in the form of cell clusters was also observed for *S. thermosulfidooxidans*. Obviously, the lack of motility is a major reason for poor adhesion and biofilm formation.

However, no matter whether in AMD environments or in industrial bioleaching heaps, cells of *S. thermosulfidooxidans* are always detectable either in planktonic or biofilm growth [91, 92]. The culturing environment in lab is different from that in wild field, which should be the major reason for its poor cultivation in lab. Thus, the original culturing method applied for *S. thermosulfidooxidans* needs to be considered. Several possible factors were considered including pH and extra energy sources and so on. We varied the initial pH of its growth medium from original 2.5 to 1.5 or 3.5, since pH can regulate sporulation and even changes of one unit of pH can cause an increased sporulation [93]. Furthermore, in case of *S. thermosulfidooxidans*, if the pH of the growth medium is varied in the range of 1.0-3.0, the ferrous ion oxidation rate becomes affected. Best

oxidation of ferrous ion occurs around pH 1.4 [94]. We supplemented an extra energy source available under open leaching conditions such as potassium tetrathionate or sodium thiosulfate, because a recent study indicates that not planktonic but biofilm cells contribute to pyrite dissolution within the first 4-5 days after inoculation [95]. Probably the "poor" biofilms of *S. thermosulfidooxidans* on pyrite grains cannot oxidize pyrite well. The limited energy source might result in starvation, triggering sporulation or dormancy. We tried to initiate adhesion of *S. thermosulfidooxidans* to pyrite by adding ferric iron ions to or by removing phosphorus from their growth medium. Ferric ions play a role in bacterial adhesion, because ferric ion-glucuronic acid complexation in EPS provides a positive charge on the cell surface, thereby inducing the cells to adhere to negatively charged pyrite surfaces via electrostatic attract forces [5, 96]. Referring to phosphorus, it is a very important element for organisms. A limitation can increase attachment in case of *Agrobacterium tumefaciens* to polyvinyl chloride [97]. Bellenberg et al. also describes that growth under phosphate starvation results in an enhancement of EPS production and well-formed biofilms of *A. ferrooxidans* on pyrite [46]. However, none of the listed methods showed a positive effect on biofilm formation by *S. thermosulfidooxidans*. The possible reason is that not energy source nor environmental adjustment but certain essential nutrients are needed. According to our results without any operation the cells of *S.*

thermosulfidooxidans remained on the pyrite surfaces during the first week of incubation, then cell detachment occurred. This detachment must be related with the depletion of certain essential nutrients. The limited nutrients under the lab conditions can only be from yeast extracts which are available at first and then are depleted by the cells. Thus, we supplied yeast extracts after five days, but the result was not as expected. There were reddish precipitates observed after one week of bioleaching, which was related with the decreased cell density. To remove these precipitates and other potential harmful substances seems to be important. To exchange the spent medium with fresh medium containing yeast extracts each two days should be the best and the easiest method. The results turned out that by exchanging the spent medium with fresh medium each two days caused a seriously enhanced biofilm formation. Obviously, firstly yeast extracts facilitate the growth of *S. thermosulfidooxidans*. However, there is no data showing which compound in the yeast extracts can facilitate its growth. Vitamins in the yeast extracts might play an important role, but a slow growth of *S. thermosulfidooxidans* with vitamins made the tests difficult to follow. Besides providing vitamins yeast extracts may also provide carbon source for their growth. Sulfobacilli have a mixotrophic metabolism using Fe^{2+}, S^0, $S_4O_6^{2-}$, $S_2O_3^{2-}$ and sulfide minerals in the presence of low amounts of organic compounds. The purely autotrophic or heterotrophic growth is poor. Secondly, removal of spent medium means removal of harmful

factors in the growth medium. The pyrite leachate is harmful for leaching microorganisms for its high concentration of metal ions and low pH. Furthermore, during biofilm formation AFM and SEM/EDX were used to analyse the mechanical and chemical changes of cell surfaces and pyrite surfaces. Even with regularly exchanging medium, films formed on pyrite surfaces composed of organic substances and inorganic salts (most likely jarosites) [39]. It has been reported that the extensive jarosite precipitation on pyrite surfaces can effectively prevent the bacterial contact with the solid substratum [98]. Thus, the salt precipitates on pyrite surfaces might perform as a passivation layer blocking pyrite. The inorganic precipitates can also cover the cell surfaces preventing the cells from oxidizing the ferrous ions, there is data showing that the growth of the cells of *S. thermosulfidooxidans* YN22 on ferrous ion can be remarkably inhibited when the content of jarosite precipitate in their growth medium is over 4 g/L [99]. What's more, removal of planktonic cells might keep attached cells active, because a high cell density may trigger sporulation and the formation of persister cells [100].

The regular medium exchange caused *S. thermosulfidooxidans* to leach pyrite well. Bioleaching experiments with pyrite grains were run for one year. In this case finally the pyrite grains were oxidized completely. The pyrite slice surfaces were also badly corroded after 10 months of bioleaching indicated by several etch pits. The CLSM images indicate an

average pit depth of 25 µm. It is reported that pits with an average depth of 320 nm were observed after 4 months of leaching by *A. ferrooxidans* [101]. Obviously *S. thermosulfidooxidans* produces much deeper pits than *A. ferrooxidans*.

Thus, it can be concluded that a lack of motility accounts for the poor adhesion by cells of *S. thermosulfidooxidans* to pyrite, while depletion of organic supplements and essential nutrients and production of inorganic precipitates caused the cell detachment.

Effect of *L. ferriphilum* on adhesion to, biofilm formation on and bioleaching of pyrite by *S. thermosulfidooxidans*. In this work the performance of *S. thermosulfidooxidans* during pyrite leaching was analysed in the presence of *L. ferriphilum*. The presence of *L. ferriphilum* seems to help *S. thermosulfidooxidans* to colonize pyrite. A similar result was reported by Noël et al. [30] for *A. caldus* and *L. ferriphilum*. In their study they also found that *A. caldus* cannot attach to pyrite on its own, but needs a pre-colonization by *L. ferriphilum* for attachment. In our case however, the enhanced biofilm formation did not help to increase bioleaching, since in the presence of *L. ferriphilum S. thermosulfidooxidans* exhibited a worse bioleaching of pyrite than the pure culture of *L. ferriphilum.* A similar result has been published by Okibe et al. [102]. They found pyrite oxidation was less effective in case of a mixed

culture of *Leptospirillum* MT6 and *Acidimicrobium ferrooxidans* ICP than by pure culture of *Leptospirillum* MT6 alone. These authors considered a competition for the same energy source as one possible reason. However, in our study pyrite oxidation was even less effective by *S. thermosulfidooxidans* and inactived *L. ferriphilum* cells than by the pure culture of *S. thermosulfidooxidans* meaning even without competition. The reason is not clear, but some indications may be derived from the results of the experiments with addition leachate. *S. thermosulfidooxidans* was expected to oxidize pyrite better in the pyrite leachate from a *L. ferriphilum* culture than in the fresh medium without yeast extracts but with equal amount of total iron, since organic substances in the leachate might support the growth of *S. thermosulfidooxidans*. However, the results show that pyrite oxidation by *S. thermosulfidooxidans* in the pyrite leachate was less effective. Thus, it can be concluded that some substances produced by *L. ferriphilum* could have inhibited the activity of *S. thermosulfidooxidans*.

Quantification of adhesion forces by pyrite/chalcopyrite modified probes. The characterization and quantification of the real interactions between cells/biofilms and substrata under physiological conditions is a serious challenge. Here we used for the first time for force mapping by the AFM pyrite/chalcopyrite modified cantilevers. In this way we are able to test the interactions between the substrata and living cells under fully non-

biased conditions, since we do not need to denature bacteria. Especially if one is comparing our technique with the currently used cell probes (immobilized cells on a cantilever), our mineral probe has decisive serious advantages. Firstly, we immobilize a mineral grain (the substratum) on a tip-less cantilever, which means no modification to cells and is more easy and practical. A cell probe requires that the cell is firmly immobilized on the cantilever to prevent cell detachment during force measurement. To achieve this goal, the classic way is to immobilize a cell on a cantilever first by PEI and then by glutaraldehyde to enhance the fixation [62]. However, the use of glutaraldehyde leads to cell surface denaturation and cell death [103]. Beaussart et al. [104] also noticed the disadvantages of glutaraldehyde and optimized the immobilization procedure by choosing polydopamine as an adhesive instead of a combination of PEI and glutaraldehyde. Dopamine can self-polymerize to form surface-adherent polydopamine films on a substratum in an alkaline solution. The polydopamine-coated surface subsequently reacts with thiols and amines via Michael addition or Schiff base reactions to immobilize organics [105]. Thus, the polydopamine immobilizes cells via covalent interactions and the cell surface properties become modified. In addition to the problem of the denaturation of the cell surface to prepare a cell probe according to the protocol of Beaussart at least two steps are needed: first to immobilize a silica microsphere on a cantilever and then to immobilize a single cell on

this microsphere. This two-step procedure carries a high risk of contamination for the cantilever and may change its sensitivity and spring constant. After cell immobilization additional steps have to be implemented to guarantee that the cell is properly positioned and to ensure that the immobilized cell remains alive. Additionally, destruction of the EPS structure of this single cell during a repeated force scanning will become a serious problem. Secondly, we immobilize cells on a glass slide, which eliminates the possibility of cell detachment during scanning. PEI, with a high concentration of amino groups, is used to create a positively charged surface promoting an irreversible adhesion of cells [106]. Cells, immobilized via this ionic interaction (and perhaps hydrophobic forces) but without denaturing of the cell surface, can be scanned in the normal mode without facing the problem of cell detachment, if a low scan rate and loaded force are applied. Last but not the least, our method can provide real adhesion information between substratum and biofilm and, to the best of our knowledge, until now there are no other similar reports indicating such a possibility. A slight disadvantage of these pyrite probes is the fact that they cannot be used for topographic scanning. The height information of the biofilms can be recorded simultaneously during the force measurement. The height image gives a rough morphological and topographical overview for the biofilms. It is sufficient to ensure that adhesion forces are measured between biofilm cells and substratum (on the cantilever).

Adhesion between *S. thermosulfidooxidans* and pyrite or chalcopyrite.

Bacterial adhesion is mediated by a multitude of specific and nonspecific forces, which are associated with the constituents of the bacterial surface. Ohmura investigated the adhesion of iron-grown cells of *A. ferrooxidans* to the four minerals pyrite, quartz, chalcopyrite and galena. The results showed that the cells selectively adhered to pyrite and chalcopyrite by a strong interaction other than the physical interaction of hydrophobic force [28]. The strong interaction resulted from iron atoms interacting with the protein aporusticyanin, which is located on the cell surface. Aporusticyanin acts as a mineral-specific receptor for the adhesion of *A. ferrooxidans* to pyrite [107]. By applying optical trapping techniques they found that aporusticyanin was abundant in iron-grown cells of *A. ferrooxidans*, causing them to adhere to pyrite with greater forces (>5.2 pN) than sulfur-grown cells (~3.6 pN). However, an addition of soluble ferrous ions weakened the adhesion between the iron-grown cells and pyrite. These results are consistent with their hypothesis that bacterial adhesion was mediated by specific bonds between cellular components and ferrous ions on the surface of pyrite [108]. In fact, iron atoms are widely found to be important for mediating bacterial adhesion because they can interact specifically with kinds of extracellular biomolecules and made contributions to bacterial adhesion. Omoike reported that phosphodiesters in the EPS could form inner-sphere complexes with Fe-centres on a

goethite surface, thereby providing an energetically stable bond for *Pseudomonas aeruginosa* or *Bacillus subtilis* to adhere to a goethite surface [85]. Parikh and Chorover added evidence that both terminal phosphate/phosphonate and phosphodiester, either excreted from the cell or present as surface biomolecules, are involved in bacterial adhesion to iron containing substrata through formation of inner-sphere Fe-phosphate/phosphonate complexes [109]. The formation of inner-sphere Fe-phosphate/phosphonate complexes was observed also during the growth of biofilms of *S. thermosulfidooxidans* on pyrite surfaces. It is also reported that outer membrane cytochromes from *Shewanella oneidensis* form a specific and stable bond with iron oxide surfaces for a transfer of electrons [110]. Refering to our study, the minerals pyrite (FeS_2) and chalcopyrite ($FeCuS_2$) both contain iron atoms, but have a different crystal structure. Pyrite is an iron (II) disulfide with a NaCl-type structure. The S_2^{2-} groups are situated at the cube centre and the midpoints of the cube edges. The Fe^{2+} atoms are located at the corners and the face centres [111]. The tetragonal unit cell of chalcopyrite is twice as large as the unit cell of pyrite. Each sulfur atom is closely surrounded by four metal atoms, two copper atoms and two iron atoms, which are located at the corners of a nearly regular tetrahedron. Thus, each metal atom is similarly surrounded by four sulfur atoms [112]. Stereochemical evidence shows that chalcopyrite exists in a strong covalently-bonded configuration, which has

an ionic state between $Cu^{2+}Fe^{2+}S^{2-}_2$ and $Cu^{+}Fe^{3+}S^{2-}_2$ [113, 114]. The number of iron atoms within one lattice of pyrite is higher than the one for chalcopyrite. If comparing one unit area, the number of iron atoms of pyrite is twice as high as in chalcopyrite. Thus, it is possible that the iron ionic state and the amount can be a reason for the initially reduced affinity of *S. thermosulfidooxidans* cells to chalcopyrite. Also a considerably decreased protein content in the biofilm EPS may be related with the low adhesion forces. This is possibly an indication that proteins play an important role in the initial adhesion of these bacteria. Combining our findings with the studies mentioned above, it seems likely that proteins, similar to aporusticyanin, may specifically bind with ferrous iron ions to induce initial bacterial adhesion on ferrous iron-containing minerals. After the initial contact both terminal phosphate/phosphonate and phosphodiester then started to complex iron atoms, and outer membrane cytochrome might also form stable bond with pyrite/chalcopyrite surface to transfer electrons by oxidizing ferrous iron. Consequently, the adhesion gets strengthened.

Besides specific forces, non-specific forces such as hydrophobic interactions and electrostatic interactions also contribute to bacterial adhesion. Both pyrite and chalcopyrite are reported to be quite hydrophobic minerals with a contact angle of 64° measured against with water [32, 33]. However, hydrophobic forces seem to dominate attachment only in case of sulfur-grown acidophiles. A treatment with a surface-active

detergent caused detachment of sulfur-grown cells of *A. ferrooxidans* from pyrite by 82%, while it removed iron-grown cells only by 26% [108]. Gehrke also described that hydrophobic forces dominate in the adhesion of sulfur-grown cells of *A. ferrooxidans* to pyrite [7]. Thus, hydrophobic interactions play in some cases an important role in bacterial adhesion. This can be quantified in experiments with a hydrophobic (CH_3 modified) tip [115]. Alsteens quantified the hydrophobic forces between a hydrophobic tip and germinated Aspergillus fumigatus spores with a magnitude of 4273 pN [116]. Their force-distance curves are very similar with the curves recorded in this work for sulfur-grown planktonic/biofilm cells using chalcopyrite/pyrite tips.

It can be concluded that the adhesion of the cells of *S. thermosulfidooxidans* to minerals exhibits selectivity. This selectivity can be quantified as adhesion force. The higher the force is, the more cells adhere. The adhesion is mediated via bacterial EPS and protein in EPS might play an important role in adhesion.

6. Reference

[1] T. Rohwerder, T. Gehrke, K. Kinzler, W. Sand, Bioleaching review part A, Applied microbiology and biotechnology, 63 (2003) 239-248.

[2] A.R. Colmer, M. Hinkle, The role of microorganisms in acid mine drainage: a preliminary report, Science, 106 (1947) 253-256.

[3] K.L. Temple, A.R. Colmer, The autotrophic oxidation of iron by a new bacterium: Thiobacillus ferrooxidans, Journal of bacteriology, 62 (1951) 605-611.

[4] D. Lundgren, M. Silver, Ore leaching by bacteria, Annual reviews in microbiology, 34 (1980) 263-283.

[5] W. Sand, T. Gehrke, P.-G. Jozsa, A. Schippers, (Bio) chemistry of bacterial leaching—direct vs. indirect bioleaching, Hydrometallurgy, 59 (2001) 159-175.

[6] M. Vera, A. Schippers, W. Sand, Progress in bioleaching: fundamentals and mechanisms of bacterial metal sulfide oxidation—part A, Applied microbiology and biotechnology, 97 (2013) 7529-7541.

[7] T. Gehrke, J. Telegdi, D. Thierry, W. Sand, Importance of extracellular polymeric substances from *Thiobacillus ferrooxidans* for bioleaching, Applied and environmental microbiology, 64 (1998) 2743-2747.

[8] A. Schippers, W. Sand, Bacterial leaching of metal sulfides proceeds by two indirect mechanisms via thiosulfate or via polysulfides and sulfur, Applied and environmental microbiology, 65 (1999) 319-321.

[9] W. Sand, T. Gerke, R. Hallmann, A. Schippers, Sulfur chemistry, biofilm, and the (in) direct attack mechanism—a critical evaluation of bacterial leaching, Applied microbiology and biotechnology, 43 (1995) 961-966.

[10] P.C. Singer, W. Stumm, Acidic mine drainage: the rate-determining step, Science, 167 (1970) 1121-1123.

[11] D.E. Rawlings, Heavy metal mining using microbes 1, Annual reviews in microbiology, 56 (2002) 65-91.

[12] D.B. Johnson, Biodiversity and ecology of acidophilic microorganisms, FEMS microbiology ecology, 27 (1998) 307-317.

[13] R. Golovacheva, G. Karavaĭko, *Sulfobacillus*, a new genus of thermophilic sporulating bacteria, Mikrobiologiia, 47 (1978) 815-822.

[14] P.R. Norris, D.A. Clark, J.P. Owen, S. Waterhouse, Characteristics of *Sulfobacillus acidophilus* sp. nov. and other moderately thermophilic mineral-sulphide-oxidizing bacteria, Microbiology, 142 (1996) 775-783.

[15] I.A. Tsaplina, T.F. Kondrat'eva, V.I. Duda, N.E. Suzina, V.S. Melamud, G.I. Karavaiko, *Sulfobacillus thermotolerans* sp. nov., a thermotolerant, chemolithotrophic bacterium, International journal of systematic and evolutionary microbiology, 56 (2006) 1039-1042.

[16] V. Melamud, T. Pivovarova, T. Tourova, T. Kolganova, G. Osipov, A. Lysenko, T. Kondrat'eva, G. Karavaiko, *Sulfobacillus sibiricus* sp. nov., a new moderately thermophilic bacterium, Microbiology, 72 (2003) 605-612.

[17] D.B. Johnson, C. Joulian, P. d'Hugues, K.B. Hallberg, *Sulfobacillus benefaciens* sp. nov., an acidophilic facultative anaerobic Firmicute isolated from mineral bioleaching operations, Extremophiles, 12 (2008) 789-798.

[18] D.E. Rawlings, D.B. Johnson, The microbiology of biomining: development and optimization of mineral-oxidizing microbial consortia, Microbiology, 153 (2007) 315-324.

[19] H.-C. Flemming, J. Wingender, The biofilm matrix, Nature reviews microbiology, 8 (2010) 623-633.

[20] H.-C. Flemming, Biofilms and environmental protection, Water science and technology, 27 (1993) 1-10.

[21] J.W. Costerton, Z. Lewandowski, D.E. Caldwell, D.R. Korber, H.M. Lappin-Scott, Microbial biofilms, Annual reviews in microbiology, 49 (1995) 711-745.

[22] C. Dahlberg, C. Linberg, V.L. Torsvik, M. Hermansson, Conjugative plasmids isolated from bacteria in marine environments show various degrees of homology to each other and are not closely related to well-characterized plasmids, Applied and environmental microbiology, 63 (1997) 4692-4697.

[23] P. Stoodley, K. Sauer, D. Davies, J.W. Costerton, Biofilms as complex differentiated communities, Annual reviews in microbiology, 56 (2002) 187-209.

[24] H.J. Busscher, W. Norde, H.C. Van Der Mei, Specific molecular recognition and nonspecific contributions to bacterial interaction forces, Applied and environmental microbiology, 74 (2008) 2559-2564.

[25] G.A. O'Toole, R. Kolter, Flagellar and twitching motility are necessary for *Pseudomonas aeruginosa* biofilm development, Molecular microbiology, 30 (1998) 295-304.

[26] L.A. Pratt, R. Kolter, Genetic analysis of *Escherichia coli* biofilm formation: roles of flagella, motility, chemotaxis and type I pili, Molecular microbiology, 30 (1998) 285-293.

[27] D. Monroe, Looking for chinks in the armor of bacterial biofilms, Plos biology, 5 (2007) 2458-2461.

[28] N. Ohmura, K. Kitamura, H. Saiki, Selective adhesion of *Thiobacillus ferrooxidans* to pyrite, Applied and environmental microbiology, 59 (1993) 4044-4050.

[29] M.A. Ghauri, N. Okibe, D.B. Johnson, Attachment of acidophilic bacteria to solid surfaces: The significance of species and strain variations, Hydrometallurgy, 85 (2007) 72-80.

[30] N. Noël, B. Florian, W. Sand, AFM & EFM study on attachment of acidophilic leaching organisms, Hydrometallurgy, 104 (2010) 370-375.

[31] S. Bellenberg, M. Díaz, N. Noël, W. Sand, A. Poetsch, N. Guiliani, M. Vera, Biofilm formation, communication and interactions of leaching bacteria during colonization of pyrite and sulfur surfaces, Research in

microbiology, 165 (2014) 773-781.

[32] J. Zhu, Q. Li, W. Jiao, H. Jiang, W. Sand, J. Xia, X. Liu, W. Qin, G. Qiu, Y. Hu, Adhesion forces between cells of *Acidithiobacillus ferrooxidans*, *Acidithiobacillus thiooxidans* or *Leptospirillum ferrooxidans* and chalcopyrite, Colloids and surfaces B: Biointerfaces, 94 (2012) 95-100.

[33] M. Diao, E. Taran, S. Mahler, T.A. Nguyen, A.V. Nguyen, Quantifying adhesion of acidophilic bioleaching bacteria to silica and pyrite by atomic force microscopy with a bacterial probe, Colloids and surfaces B: Biointerfaces, 115 (2014) 229-236.

[34] J. Zhu, Q. Wang, S. Zhou, Q. Li, M. Gan, H. Jiang, W. Qin, X. Liu, Y. Hu, G. Qiu, Insights into the relation between adhesion force and chalcopyrite-bioleaching by *Acidithiobacillus ferrooxidans,* Colloids and surfaces B: Biointerfaces, 126 (2015) 351-357.

[35] Q. Li, Q. Wang, J. Zhu, S. Zhou, M. Gan, H. Jiang, W. Sand, Effect of Extracellular Polymeric Substances on Surface Properties and Attachment Behavior of *Acidithiobacillus ferrooxidans*, Minerals, 6 (2016) 100-100.

[36] K.J. Edwards, M.O. Schrenk, R. Hamers, J.F. Banfield, Microbial oxidation of pyrite: experiments using microorganisms from an extreme acidic environment, American mineralogist, 83 (1998) 1444-1453.

[37] K. Harneit, A. Göksel, D. Kock, J.-H. Klock, T. Gehrke, W. Sand, Adhesion to metal sulfide surfaces by cells of *Acidithiobacillus ferrooxidans*, *Acidithiobacillus thiooxidans* and *Leptospirillum*

ferrooxidans, Hydrometallurgy, 83 (2006) 245-254.

[38] K.J. Edwards, P.L. Bond, J.F. Banfield, Characteristics of attachment and growth of *Thiobacillus caldus* on sulphide minerals: a chemotactic response to sulphur minerals?, Environmental microbiology, 2 (2000) 324-332.

[39] T. Becker, N. Gorham, D. Shiers, H. Watling, In situ imaging of *Sulfobacillus thermosulfidooxidans* on pyrite under conditions of variable pH using tapping mode atomic force microscopy, Process biochemistry, 46 (2011) 966-976.

[40] C. Farah, M. Vera, D. Morin, D. Haras, C.A. Jerez, N. Guiliani, Evidence for a functional quorum-sensing type AI-1 system in the extremophilic bacterium *Acidithiobacillus ferrooxidans*, Applied and environmental microbiology, 71 (2005) 7033-7040.

[41] L.M. Ruiz, S. Valenzuela, M. Castro, A. Gonzalez, M. Frezza, L. Soulère, T. Rohwerder, Y. Queneau, A. Doutheau, W. Sand, AHL communication is a widespread phenomenon in biomining bacteria and seems to be involved in mineral-adhesion efficiency, Hydrometallurgy, 94 (2008) 133-137.

[42] A. González, S. Bellenberg, S. Mamani, L. Ruiz, A. Echeverría, L. Soulère, A. Doutheau, C. Demergasso, W. Sand, Y. Queneau, AHL signaling molecules with a large acyl chain enhance biofilm formation on sulfur and metal sulfides by the bioleaching bacterium *Acidithiobacillus*

ferrooxidans, Applied microbiology and biotechnology, 97 (2013) 3729-3737.

[43] P.L. Bond, G.K. Druschel, J.F. Banfield, Comparison of acid mine drainage microbial communities in physically and geochemically distinct ecosystems, Applied and environmental microbiology, 66 (2000) 4962-4971.

[44] G.W. Tyson, J. Chapman, P. Hugenholtz, E.E. Allen, R.J. Ram, P.M. Richardson, V.V. Solovyev, E.M. Rubin, D.S. Rokhsar, J.F. Banfield, Community structure and metabolism through reconstruction of microbial genomes from the environment, Nature, 428 (2004) 37-43.

[45] W. Zeng, S. Tan, M. Chen, G. Qiu, Detection and analysis of attached microorganisms on the mineral surface during bioleaching of pure chalcopyrite with moderate thermophiles, Hydrometallurgy, 106 (2011) 46-50.

[46] S. Bellenberg, C.-F. Leon-Morales, W. Sand, M. Vera, Visualization of capsular polysaccharide induction in *Acidithiobacillus ferrooxidans*, Hydrometallurgy, 129 (2012) 82-89.

[47] R. Zhang, T. Neu, S. Bellenberg, U. Kuhlicke, W. Sand, M. Vera, Use of lectins to in situ visualize glycoconjugates of extracellular polymeric substances in acidophilic archaeal biofilms, Microbial biotechnology, 8 (2015) 448-461.

[48] G. Binnig, C.F. Quate, C. Gerber, Atomic force microscope, Physical

review letters, 56 (1986) 930-933.

[49] Y.F. Dufrene, Using nanotechniques to explore microbial surfaces, Nature reviews microbiology, 2 (2004) 451-460.

[50] B. Drake, C. Prater, A. Weisenhorn, S. Gould, T. Albrecht, Imaging crystals, polymers, and processes in water with the atomic force microscope, Science, 243 (1989) 1586-1589.

[51] D. Müller, F.A. Schabert, G. Büldt, A. Engel, Imaging purple membranes in aqueous solutions at sub-nanometer resolution by atomic force microscopy, Biophysical journal, 68 (1995) 1681-1686.

[52] F.A. Schabert, C. Henn, A. Engel, Native *Escherichia coli* OmpF porin surfaces probed by atomic force microscopy, Science, 268 (1995) 92-94.

[53] I.B. Beech, J.R. Smith, A.A. Steele, I. Penegar, S.A. Campbell, The use of atomic force microscopy for studying interactions of bacterial biofilms with surfaces, Colloids and surfaces B: Biointerfaces, 23 (2002) 231-247.

[54] Y.F. Dufrêne, C.J. Boonaert, P.A. Gerin, M. Asther, P.G. Rouxhet, Direct probing of the surface ultrastructure and molecular interactions of dormant and germinating spores of *Phanerochaete chrysosporium*, Journal of bacteriology, 181 (1999) 5350-5354.

[55] F. Ahimou, A. Touhami, Y.F. Dufrêne, Real-time imaging of the surface topography of living yeast cells by atomic force microscopy, Yeast, 20 (2003) 25-30.

[56] H. Yamashita, A. Taoka, T. Uchihashi, T. Asano, T. Ando, Y. Fukumori, Single-molecule imaging on living bacterial cell surface by high-speed AFM, Journal of molecular biology, 422 (2012) 300-309.

[57] M. Van Der Hofstadt, M. Hüttener, A. Juárez, G. Gomila, Nanoscale imaging of the growth and division of bacterial cells on planar substrates with the atomic force microscope, Ultramicroscopy, 154 (2015) 29-36.

[58] P.J. Bremer, G.G. Geese, B. Drake, Atomic force microscopy examination of the topography of a hydrated bacterial biofilm on a copper surface, Current microbiology, 24 (1992) 223-230.

[59] W.F. Heinz, J.H. Hoh, Spatially resolved force spectroscopy of biological surfaces using the atomic force microscope, Trends in biotechnology, 17 (1999) 143-150.

[60] A. Weisenhorn, P. Hansma, T. Albrecht, C. Quate, Forces in atomic force microscopy in air and water, Applied physics letters, 54 (1989) 2651-2653.

[61] Y.F. Dufrene, Sticky microbes: forces in microbial cell adhesion, Trends in microbiology, 23 (2015) 376-382.

[62] A. Razatos, Y.-L. Ong, M.M. Sharma, G. Georgiou, Molecular determinants of bacterial adhesion monitored by atomic force microscopy, Proceedings of the National Academy of Sciences, 95 (1998) 11059-11064.

[63] M. Chandraprabha, P. Somasundaran, K. Natarajan, Modeling and analysis of nanoscale interaction forces between *Acidithiobacillus*

ferrooxidans and AFM tip, Colloids and Surfaces B: Biointerfaces, 75 (2010) 310-318.

[64] S.K. Lower, M.F. Hochella, T.J. Beveridge, Bacterial recognition of mineral surfaces: nanoscale interactions between *Shewanella* and α-FeOOH, Science, 292 (2001) 1360-1363.

[65] E. Thormann, A.C. Simonsen, L.K. Nielsen, O.G. Mouritsen, Ligand–receptor interactions and membrane structure investigated by AFM and time-resolved fluorescence microscopy, Journal of molecular recognition, 20 (2007) 554-560.

[66] D. Alsteens, H. Trabelsi, P. Soumillion, Y.F. Dufrene, Multiparametric atomic force microscopy imaging of single bacteriophages extruding from living bacteria, Nature communications, 4 (2013) 2926-2933.

[67] A.F. Guedes, F.A. Carvalho, I. Malho, N. Lousada, L. Sargento, N.C. Santos, Atomic force microscopy as a tool to evaluate the risk of cardiovascular diseases in patients, Nature nanotechnology, 11 (2016) 687-692.

[68] Y.F. Dufrêne, T. Ando, R. Garcia, D. Alsteens, D. Martinez-Martin, A. Engel, C. Gerber, D.J. Müller, Imaging modes of atomic force microscopy for application in molecular and cell biology, Nature nanotechnology, 12 (2017) 295-307.

[69] F. Gaboriaud, Y.F. Dufrêne, Atomic force microscopy of microbial cells: application to nanomechanical properties, surface forces and

molecular recognition forces, Colloids and surfaces B: Biointerfaces, 54 (2007) 10-19.

[70] A. Cerf, J.-C. Cau, C. Vieu, E. Dague, Nanomechanical properties of dead or alive single-patterned bacteria, Langmuir, 25 (2009) 5731-5736.

[71] G. Longo, L.M. Rio, C. Roduit, A. Trampuz, A. Bizzini, G. Dietler, S. Kasas, Force volume and stiffness tomography investigation on the dynamics of stiff material under bacterial membranes, Journal of molecular recognition, 25 (2012) 278-284.

[72] A.-A. Ungureanu, I. Benilova, O. Krylychkina, D. Braeken, B. De Strooper, C. Van Haesendonck, C.G. Dotti, C. Bartic, Amyloid beta oligomers induce neuronal elasticity changes in age-dependent manner: a force spectroscopy study on living hippocampal neurons, Scientific reports, 6 (2016) 25841-25841.

[73] M.E. Mackintosh, Nitrogen fixation by *Thiobacillus ferrooxidans*, Microbiology, 105 (1978) 215-218.

[74] C.O. Moses, D.K. Nordstrom, J.S. Herman, A.L. Mills, Aqueous pyrite oxidation by dissolved oxygen and by ferric iron, Geochimica et Cosmochimica Acta, 51 (1987) 1561-1571.

[75] H. Tamura, K. Goto, T. Yotsuyanagi, M. Nagayama, Spectrophotometric determination of iron (II) with 1, 10-phenanthroline in the presence of large amounts of iron (III), Talanta, 21 (1974) 314-318.

[76] M. Dubois, K.A. Gilles, J.K. Hamilton, P. Rebers, F. Smith,

Colorimetric method for determination of sugars and related substances, Analytical chemistry, 28 (1956) 350-356.

[77] B. Fr, T. Griebe, P. Nielsen, Enzymatic activity in the activated-sludge floc matrix, Applied microbiology and biotechnology, 43 (1995) 755-761.

[78] N. Blumenkrantz, G. Asboe-Hansen, New method for quantitative determination of uronic acids, Analytical biochemistry, 54 (1973) 484-489.

[79] S. Mangold, K. Harneit, T. Rohwerder, G. Claus, W. Sand, Novel combination of atomic force microscopy and epifluorescence microscopy for visualization of leaching bacteria on pyrite, Applied and environmental microbiology, 74 (2008) 410-415.

[80] H.H. Fang, K.-Y. Chan, L.-C. Xu, Quantification of bacterial adhesion forces using atomic force microscopy (AFM), Journal of microbiological Methods, 40 (2000) 89-97.

[81] P. Vandevivere, D.L. Kirchman, Attachment stimulates exopolysaccharide synthesis by a bacterium, Applied and environmental microbiology, 59 (1993) 3280-3286.

[82] H.L. Casal, D.G. Cameron, I.C. Smith, H.H. Mantsch, Acholeplasma laidlawii membranes: a Fourier transform infrared study of the influence of protein on lipid organization and dynamics, Biochemistry, 19 (1980) 444-451.

[83] H.M. Al-Qadiri, M. Lin, A.G. Cavinato, B.A. Rasco, Fourier transform infrared spectroscopy, detection and identification of

Escherichia coli O157: H7 and *Alicyclobacillus* strains in apple juice, International journal of food microbiology, 111 (2006) 73-80.

[84] B.C. Barja, M.I. Tejedor-Tejedor, M.A. Anderson, Complexation of methylphosphonic acid with the surface of goethite particles in aqueous solution, Langmuir, 15 (1999) 2316-2321.

[85] A. Omoike, J. Chorover, K.D. Kwon, J.D. Kubicki, Adhesion of bacterial exopolymers to α-FeOOH: Inner-sphere complexation of phosphodiester groups, Langmuir, 20 (2004) 11108-11114.

[86] S. Orr, Infra-red spectroscopic studies of some polysaccharides, Biochimica et biophysica acta, 14 (1954) 173-181.

[87] M.B. Mathews, Isomeric chondroitin sulphates, Nature, 181 (1958) 421-422.

[88] M. Descostes, C. Beaucaire, F. Mercier, S. Savoye, J. Sow, P. Zuddas, Effect of carbonate ions on pyrite (FeS_2) dissolution, Bulletin de la Société géologique de France, 173 (2002) 265-270.

[89] G.A. O'toole, R. Kolter, Initiation of biofilm formation in *Pseudomonas fluorescens* WCS365 proceeds via multiple, convergent signalling pathways: a genetic analysis, Molecular microbiology, 28 (1998) 449-461.

[90] K.J. Edwards, P.L. Bond, J.F. Banfield, Characteristics of attachment and growth of *Thiobacillus caldus* on sulphide minerals: a chemotactic response to sulphur minerals?, Environmental microbiology, 2 (2000) 324-

332.

[91] L.-x. Chen, L.-n. Huang, C. Méndez-García, J.-l. Kuang, Z.-s. Hua, J. Liu, W.-s. Shu, Microbial communities, processes and functions in acid mine drainage ecosystems, Current opinion in biotechnology, 38 (2016) 150-158.

[92] M. Acosta, P. Galleguillos, Y. Ghorbani, P. Tapia, Y. Contador, A. Velásquez, C. Espoz, C. Pinilla, C. Demergasso, Variation in microbial community from predominantly mesophilic to thermotolerant and moderately thermophilic species in an industrial copper heap bioleaching operation, Hydrometallurgy, 150 (2014) 281-289.

[93] S. Yazdany, K. Lashkari, Effect of pH on sporulation of *Bacillus stearothermophilus*, Applied microbiology, 30 (1975) 1-3.

[94] H. Watling, F. Perrot, D. Shiers, Comparison of selected characteristics of *Sulfobacillus* species and review of their occurrence in acidic and bioleaching environments, Hydrometallurgy, 93 (2008) 57-65.

[95] S. Bellenberg, R. Barthen, M. Boretska, R. Zhang, W. Sand, M. Vera, Manipulation of pyrite colonization and leaching by iron-oxidizing *Acidithiobacillus* species, Applied microbiology and biotechnology, 99 (2015) 1435-1449.

[96] R.C. Blake, E.A. Shute, G.T. Howard, Solubilization of minerals by bacteria: electrophoretic mobility of *Thiobacillus ferrooxidans* in the presence of iron, pyrite, and sulfur, Applied and environmental

microbiology, 60 (1994) 3349-3357.

[97] J. Xu, J. Kim, T. Danhorn, P.M. Merritt, C. Fuqua, Phosphorus limitation increases attachment in Agrobacterium tumefaciens and reveals a conditional functional redundancy in adhesin biosynthesis, Research in microbiology, 163 (2012) 674-684.

[98] P. Hiltunen, A. Vuorinen, P. Rehtijärvi, O.H. Tuovinen, Bacterial pyrite oxidation: release of iron and scanning electron microscopic observations, Hydrometallurgy, 7 (1981) 147-157.

[99] J.-n. Ding, G. Jian, X.-l. Wu, C.-g. Zhang, D.-z. Wang, G.-z. Qiu, Jarosite-type precipitates mediated by YN22, *Sulfobacillus thermosulfidooxidans*, and their influences on strain, Transactions of nonferrous metals society of China, 17 (2007) 1038-1044.

[100] J. Errington, Regulation of endospore formation in *Bacillus subtilis*, Nature reviews microbiology, 1 (2003) 117-126.

[101] D. Pace, R. Mielke, G. Southam, T. Porter, Scanning force microscopy studies of the colonization and growth of *A. ferrooxidans* on the surface of pyrite minerals, Scanning, 27 (2005) 136-140.

[102] N. Okibe, D.B. Johnson, Biooxidation of pyrite by defined mixed cultures of moderately thermophilic acidophiles in pH-controlled bioreactors: Significance of microbial interactions, Biotechnology and bioengineering, 87 (2004) 574-583.

[103] V. Vadillo-Rodriguez, H.J. Busscher, W. Norde, J. De Vries, R.J.

Dijkstra, I. Stokroos, H.C. Van Der Mei, Comparison of atomic force microscopy interaction forces between bacteria and silicon nitride substrata for three commonly used immobilization methods, Applied and environmental microbiology, 70 (2004) 5441-5446.

[104] A. Beaussart, S. El-Kirat-Chatel, R.M.A. Sullan, D. Alsteens, P. Herman, S. Derclaye, Y.F. Dufrêne, Quantifying the forces guiding microbial cell adhesion using single-cell force spectroscopy, Nature protocols, 9 (2014) 1049-1055.

[105] H. Lee, S.M. Dellatore, W.M. Miller, P.B. Messersmith, Mussel-inspired surface chemistry for multifunctional coatings, science, 318 (2007) 426-430.

[106] S. D'souza, J. Melo, A. Deshpande, G. Nadkarni, Immobilization of yeast cells by adhesion to glass surface using polyethylenimine, Biotechnology letters, 8 (1986) 643-648.

[107] R. Blake, N. Ohmura, *Thiobacillus ferrooxidans* binds specifically to iron atoms at the exposed edge of the pyrite crystal lattice, Process metallurgy, 9 (1999) 663-672.

[108] R.C. Blake, K. Sasaki, N. Ohmura, Does aporusticyanin mediate the adhesion of *Thiobacillus ferrooxidans* to pyrite?, Hydrometallurgy, 59 (2001) 357-372.

[109] S.J. Parikh, J. Chorover, ATR-FTIR spectroscopy reveals bond formation during bacterial adhesion to iron oxide, Langmuir, 22 (2006)

8492-8500.

[110] B.H. Lower, L. Shi, R. Yongsunthon, T.C. Droubay, D.E. McCready, S.K. Lower, Specific bonds between an iron oxide surface and outer membrane cytochromes MtrC and OmcA from *Shewanella oneidensis* MR-1, Journal of bacteriology, 189 (2007) 4944-4952.

[111] D. Rickard, G.W. Luther, Chemistry of iron sulfides, Chemical reviews, 107 (2007) 514-562.

[112] L. Pauling, L. Brockway, The crystal structure of chalcopyrite $CuFeS_2$, Zeitschrift für Kristallographie-Crystalline Materials, 82 (1932) 188-194.

[113] S. Hall, J. Stewart, The crystal structure refinement of chalcopyrite, $CuFeS_2$, Acta crystallographica section B: Structural crystallography and crystal chemistry, 29 (1973) 579-585.

[114] P. Sainctavit, J. Petiau, A. Flank, J. Ringeissen, S. Lewonczuk, XANES in chalcopyrites semiconductors: $CuFeS_2$, $CuGaS_2$, $CuInSe_2$, Physica B: Condensed matter, 158 (1989) 623-624.

[115] D. Alsteens, E. Dague, P.G. Rouxhet, A.R. Baulard, Y.F. Dufrêne, Direct measurement of hydrophobic forces on cell surfaces using AFM, Langmuir, 23 (2007) 11977-11979.

[116] D. Alsteens, V. Dupres, S. Yunus, J.-P. Latgé, J.r.J. Heinisch, Y.F. Dufrêne, High-resolution imaging of chemical and biological sites on living cells using peak force tapping atomic force microscopy, Langmuir,

28 (2012) 16738-16744.

Acknowledgements

When I was a child, I always tried to do something to prove the things written in the Children's Encyclopaedias, such as washing the pathway an ant just passed by to see whether it would lose its way back home. It seems like the start of my way to science looking backwards twenty years later. Now I am at the end of my PhD study here in Germany and I know I am not at the end of the science. However, the experience of PhD study here must be an important step on my way to science. During the four years study I have never been desperate and frustrated. However, thanks to these failure and frustration, because only with them I can be who I am today. I will be more confident and brave on my way to science in the future. At the end of this journey here I would like to thank the important people who helped and supported me on my way.

First of all, appreciation, from my bottom of my heart, to my supervisor, Prof. Dr. Wolfgang Sand. Thanks for his invitation in Changsha six years ago. Thanks for providing me the opportunity to study here. Without him I could never go so close to science. Without his knowledge and wisdom, I could never accomplish any scientific research I have done here. Without his encouragement and support, I could never taste any success I have won here.

At the same time I would like to express my sincere gratitude to Prof. Dr. Rainer Meckenstock. Thanks for the permission to stay in his working

group to finish my thesis, and for all the warm invitations to his group activities.

High tribute shall be paid to China Scholarship Council for financing my PhD study in Germany.

I would like to thank Prof. Dr. Bettina Siebers for her kindly reviewing my thesis and her readiness to be my co-adviser.

I am greatly indebted to Dr. Tilman Gehrke for his every time lifesaving help and support. He is a superman in our lab. He is super busy and he must be super tired, but each time he is still willing to help me and give me advice and feedback to my questions. I am deeply grateful for all the things he did for me.

I appreciate the cooperation with Dr. Thomas Becker who provided me the amazing modified cantilevers and helpful suggestions in paper work.

I would like to say thanks to all the people from AG Sand: thanks to Dr. Beate Agnes Krok for every scientific discussion, help and encouragement. Without her kind help my life here would be more than difficult; thanks to Petra for her supports and every happy conversation; thanks to Dr. Ruiyong Zhang for his help when I first arrived here; thanks to Christian and Natascha for the happy hours we had in the office; thanks to Friede, Yutong, Jing, Nova, Dieu and Jens for all the time we have spent together in the lab.

I also want to say thanks to all my colleagues in Biofilm Centre from the

groups of Prof. Dr. Meckenstock, Prof. Dr. Siebers and Prof. Dr. Flemming for the positive learning environment.

Special thanks should go to my friends Yuhong, Xiaoxiao, Lu, Xinping, Mao, Jincheng and Hao for every cheerful encouragement and enthusiastic help.

At last I am deeply indebted to my parents and my twin sister for their endless support and love.

Curriculum Vitae

The biography is not included in the online version for reasons of data protection.

The biography is not included in the online version for reasons of data protection.

List of Publications

1. **Q. Li**, W. Sand; Mechanical and chemical studies on EPS from *Sulfobacillus thermosulfidooxidans*: from planktonic to biofilm cells; Colloids and Surfaces B: Biointerfaces, 2017, 153, 34-40.

2. **Q. Li**, W. Sand, R. Zhang; Enhancement of Biofilm Formation on Pyrite by *Sulfobacillus thermosulfidooxidans*; Minerals; 2016, 6(3), 71.

3. **Q. Li**, Q. Wang, J. Zhu, S. Zhou, M. Gan, H. Jiang, W. Sand; Effect of Extracellular Polymeric Substances on Surface Properties and Attachment Behavior of *Acidithiobacillus ferrooxidans*; Minerals, 2016, 6(4), 100.

4. J. Liu, **Q. Li**, W. Sand, R. Zhang; Influence of *Sulfobacillus thermosulfidooxidans* on Initial Attachment and Pyrite Leaching by Thermoacidophilic Archaeon *Acidianus* sp. DSM 29099; Minerals, 2016, 6(3), 76.

5. J. Zhu, Q. Wang, S. Zhou, **Q. Li**, M. Gan, H. Jiang, W. Qin, X. Liu, Y. Hu, G. Qiu; Insights into the relation between adhesion force and chalcopyrite-bioleaching by *Acidithiobacillus ferrooxidans*; Colloids and Surfaces B: Biointerfaces, 2015, 126, 351-357.

6. S. Zhou, M. Gan, J. Zhu, **Q. Li**, S. Qi, B. Yang, X. Liu; Catalytic effect of light illumination on bioleaching of chalcopyrite; Bioresource Technology, 2015, 182, 345-352.

7. R. Zhang, T. R. Neu, Y. Zhang, S. Bellenberg, U. Kuhlicke, **Q. Li**, W. Sand, M. Vera; Visualization and analysis of EPS glycoconjugates of the

thermoacidophilic archaeon *Sulfolobus metallicus*. Applied Microbiology and Biotechnology, 2015. 99(17): p. 7343-7356.

8. J. Zhu, J. Zhang, **Q. Li**, T. Han, Y. Hu, X. Liu, W. Qin, L. Chai, G. Qiu; Bioleaching of heavy metals from contaminated alkaline sediment by auto- and heterotrophic bacteria in stirred tank reactor; Transactions of Nonferrous Metals Society of China, 2014, 24(9), 2969-2975.

9. J. Zhu, J. Zhang, **Q. Li**, T. Han, J. Xie, Y. Hu, L. Chai; Phylogenetic analysis of bacterial community composition in sediment contaminated with multiple heavy metals from the Xiangjiang River in China; Marine Pollution Bulletin, 2013, 70(1), 134-139.

10. J. Zhu, **Q. Li**, W. Jiao, W. Sand, J. Xia, X. Liu, W. Qin, G. Qiu, Y. Hu, L. Chai; Adhesion forces between cells of *Acidithiobacillus ferrooxidans*, *Acidithiobacillus thiooxidans* or *Leptospirillum ferrooxidans* and chalcopyrite; Colloids and Surfaces B: Biointerfaces, 2012, 94, 95-100.

11. J. Zhu, W. Jiao, **Q. Li**, X. Liu, W. Qin, G. Qiu, Y. Hu, L. Chai; Investigation of energy gene expressions and community structures of free and attached acidophilic bacteria in chalcopyrite bioleaching; Journal of Industrial Microbiology & Biotechnology, 2012, 39(12), 1833-1840.

Deklaration

Hiermit versichere ich, dass ich die vorliegende Arbeit mit dem Titel

„Extracellular polymeric substances involved adhesion and biofilm formation by *Sulfobacillus thermosulfidooxidans*"

selbst verfasst und keine außer den angegebenen Hilfsmitteln und Quellen benutzt habe, und dass die Arbeit in dieser oder ähnlicher Form noch bei keiner anderen Universität eingereicht wurde.

Essen, im August 2017

QIAN LI